



**UNIVERSITY OF NAIROBI
FACULTY OF ENGINEERING
DEPARTMENT OF ENVIRONMENTAL AND BIOSYSTEMS ENGINEERING**

**Optimization of Evaporative Cooling Chamber using Computational Fluid Dynamics for
Storage of Fruits and Vegetables**

By

**George P. Fayiah-Tumbay
(F56/12014/2018)**

**A thesis submitted in partial fulfillment for the degree of Master of Science in
Environmental and Biosystems Engineering in the Department of Environmental and
Biosystems Engineering in the University of Nairobi**

December 11, 2021

DECLARATION


This thesis is my original work and has not been presented for a degree in any other university.

Signature: 

Date: 11/12/2021

George P. Fayiah-Tumbay (F56/12014/2018)

This thesis has been submitted for examination with our approval as university supervisors.

Signature: 

Date: 14/12/2021

Dr. (Eng.) Duncan O. Mbuge
*Department of Environmental and
Biosystems Engineering,
University of Nairobi.*

Signature: 

Date: 14/12/2021


Professor Urbanus N. Mutwiwa
*Jomo Kenyatta University of Agriculture and
Technology*

Signature: 


Date: 14/12/2021

Mr. Januarius O. Agullo
*Department of Environmental and Biosystems
Engineering,
University of Nairobi.*

DECLARATION OF ORIGINALITY

Name of student: George P. Fayiah-Tumbay 
Reference No: F56/12014/2018
College: Architecture and Engineering
Faculty/School/Institute: Engineering
Department: Environmental and Biosystems Engineering
Course Name: MSc in Environmental and Biosystems Engineering
Title of work: Optimization of Evaporative Cooling Chamber using Computational Fluid Dynamics for Storage of Fruits and Vegetables

- i. I understand what plagiarism is and I am aware of the University policy in this regard.
- ii. I declare that this thesis is my original work and has not been submitted elsewhere for examination, award of a degree or publication. Where other works or my own work has been used, this has properly been acknowledged and referenced in accordance with the University of Nairobi's requirements.
- iii. I have not sought or used the services of any professional agencies to produce this work.
- iv. I have not allowed and shall not allow anyone to copy my work with the intention of submitting it as his/her work.
- v. I understand that any false claim in respect of this work shall result in disciplinary action in accordance with University of Nairobi anti-plagiarism policy.


Signature: _____
Candidate

Date: 11/12/2021

DEDICATION

To my family and friends

For their prayers and support during this study.

I wish you God's blessings.

ACKNOWLEDGEMENT

Foremost, I am grateful to the almighty God for His Grace and Mercy upon us during these difficult times of our human existence. I would like to express my gratitude to my supervisors: Dr. (Eng) Duncan O Mbuge, Prof. Urbanus N. Mutwiwa, and Mr. Januarius O. Agullofor giving me the opportunity, guidance, and encouragement to work on this project. Working under your supervision inspired and allowed me to explore my potential. It was truly a challenging but rewarding experience working under your supervision.

I acknowledge the Jomo Kenyatta University of Agriculture and Technology for allowing me to use their facilities for this project. In addition, I would like to acknowledge the overwhelming support from the members of staff of the Department of Environmental and Biosystems Engineering, University of Nairobi and the Department Agricultural and Biosystems Engineering, JKUAT.

I would like to express my very special gratitude to my family; Hawa Kumba Tumbay (mother), Setta Sia Tumbay (sister), and Dr. James K. Sowah Jr. (brother) for their unlimited support and patience all through my studies. To my friends; Solo B. Gbayor, Trokon G. Smith, Amos M. Kollie, and Joseph S. Bundoo; I say thank you for your moral and financial support. To the Lofa County Community College, I remain grateful for granting me a study leave. Finally, I am thankful to my postgraduate colleagues at the Department of Environmental and Biosystems Engineering, University of Nairobi.

May the sufficient Grace of our Lord Jesus Christ be with us all!

TABLE OF CONTENTS

DECLARATION	i
DECLARATION OF ORIGINALITY	ii
Turnitin Originality Report	iii
M.Sc. THESIS By George P Fayiah-Tumbay	iii
DEDICATION	xiii
ACKNOWLEDGEMENT	xiv
TABLE OF CONTENTS	xv
LIST OF TABLES	xix
LIST OF FIGURES	xx
LIST OF ABBREVIATIONS	xxiii
LIST OF SYMBOLS	xxv
ABSTRACT	xxix
CHAPTER ONE	1
INTRODUCTION	1
1.1 Background	1
1.2 Problem statement.....	4
1.3 Research justification.....	5
1.4 Overall objective	5
1.4.1 Specific objective	5
1.5 Research questions.....	6
1.6 Scope and limitation of the study.....	6
1.7 Thesis layout	7
CHAPTER TWO	8
LITERATURE REVIEW	8
2.1 Postharvest losses of fruits and vegetables	8
2.1.1 Reasons that derive postharvest losses in fresh produce.....	8
2.2 History of evaporative cooling.....	9
2.3 Factors affecting evaporative cooling	10
2.4 Cooling technologies used in storage of fruits and vegetables	11
2.4.1 CoolBot™ – Air condition cooling system.....	12

2.4.2 Mechanical refrigeration	12
2.4.3 Advances, cooling pad, and energy conservation in evaporative cooling system	13
2.4.4 Convective cooling	17
2.4.5 Evapotranspiration cooling	20
2.4.6 Hydro-cooling	21
2.4.7 Vacuum cooling	21
2.5 Computational Fluid Dynamics modelling	22
2.6 Computational Fluid Dynamics Modelling Procedure	25
2.6.1 Governing equations of fluid mechanics.....	25
2.7 Research gaps from the review of literature	26
CHAPTER THREE	28
THEORETICAL FRAMEWORK	28
3.1 Principle of evaporative cooling	28
3.2 Computational Fluid Dynamics modelling	28
3.2.1 Simulation procedure	29
3.3 Governing equations for the simulation of evaporative cooling chamber	30
3.3.1 Heat and mass transfer equations.....	30
3.3.2 Governing equations for fluid flow simulation.....	32
3.3.3 Airflow, heat, and mass transfer modelling	39
3.4 Energy conservation in evaporative chamber	42
3.5 Convective cooling	42
3.6 Evapotranspiration cooling	45
CHAPTER FOUR.....	47
MATERIALS AND METHODS	47
4.1 Research area	47
4.2 Experimental setup.....	47
4.2.1 Capacity of the storage chamber	48
4.2.2 Fan capacity calculation.....	49
4.2.3 The evaporative cooling chamber	49
4.2.4 Design of the solar power system	53
4.3 Data collection from the physical model	53
4.3.1 Solar radiation.....	54

4.3.2 Wind speed.....	54
4.3.3 Temperature and relative humidity	54
4.3.4Data collection	55
4.3.5Saturation efficiency	56
4.3.6 Performance of the cooling chamber	57
4.4 Mathematical modeling	57
4.4.1 Heat transfer Analysis.....	58
4.4.2 Computational Fluid Dynamics Simulation.....	58
4.5 The choice of turbulence model for simulation of the storage chamber	60
4.5.1 Model boundary conditions	61
4.5.2 Convergence criteria	62
4.6 Solving discretized governing equations	62
4.7Post-processing	63
4.8 Validation of the results	63
4.9 Optimization of the storage chamber	63
4.10 Data analysis	63
CHAPTER FIVE	65
RESULTS AND DISCUSSION	65
5.1 Performance of the storage chamber.....	65
5.1.1 The cooling chamber with natural convection	68
5.1.2 Performance evaluation of convective cooling applied to the cooler	69
5.1.3 Performance evaluation of the cooling chamber with evaporative cooling applied	71
5.1.4 Performance evaluation of evapotranspiration cooling.....	74
5.1.5 Performance evaluation of the cooling chamber with combined cooling	76
5.1.6 Comparisons between the cooling methods.....	78
5.2 Computational fluid dynamics modelling.....	81
5.2.1 The domain mesh.....	81
5.2.2 The result mesh independence study.....	81
5.3Temperature predictions	82
5.4Model validation	83
5.4.1 Natural cooling Vs.Model temperature.....	84
5.4.2 Convection cooling Vs.Model temperature	85

5.4.3 Evaporative cooling Vs.Model temperature	85
5.4.4 Evapotranspiration cooling Vs.Model temperature	86
5.4.5 Combined cooling Vs Model Temperature.....	87
5.5 Storage optimization	87
5.5.1 Optimum pumice pad thickness	88
CHAPTER SIX	89
CONCLUSIONS AND RECOMMENDATIONS.....	89
6.1 Conclusion	89
6.2 Recommendations.....	91
6.3Future work.....	91
References.....	92

LIST OF TABLES

TABLE 2.1 DIFFERENT MATERIALS USED AS COOLING PAD FOR EVAPORATIVE COOLING	16
TABLE 2.2 SUMMARY ON LITERATURE SURVEY FOR COOLING PAD MATERIALS	16
TABLE 5.1 MESH INDEPENDENCE TEST AND RESULTS	81
TABLE 5.2 EXPERIMENTAL TEMPERATURE AND PREDICTED TEMPERATURE AT 30 MINUTES INTERVAL FROM 8AM TO 6PM	83
TABLE 5.3 STORAGE OPTIMIZATION BASED ON PAD THICKNESS.....	88

LIST OF FIGURES

FIGURE 3.1 THE MAIN STAGES IN COMPUTATIONAL FLUID DYNAMICS SIMULATION.....	29
FIGURE 3.2 SIMULATION PROCEDURES IN ANSYS FLUENT	30
Figure 4.1 The map of Kenya showing the study area (Musa and Odera, 2015)	47
FIGURE 4.2 PHOTOGRAPHIC VIEWS OF THE EVAPORATIVE COOLING SYSTEM	51
FIGURE 4.3 SCHEMATIC DIAGRAM OF THE COOLING SYSTEM	51
FIGURE 4.4 SCHEMATIC OF THE WATER DISTRIBUTION NETWORK	52
FIGURE 4.5 THE SCHEMATICS OF THE STORAGE CHAMBER IN THREE-DIMENSIONAL VIEW	52
FIGURE 4.6 SCHEMATIC OF THE POWER DISTRIBUTION NETWORK	53
FIGURE 4.7 A SCHEMATIC DIAGRAM SHOWING TEMPERATURE AND RELATIVE HUMIDITY SENSORS AT DATA COLLECTION POINTS	55
FIGURE 4.8 DATA COLLECTION POINTS FOR BOTH AMBIENT AND STORAGE CHAMBER	56
FIGURE 4.9 THE THREE-DIMENSIONAL GEOMETRY OF THE EVAPORATIVE COOLING CHAMBER	59
Figure 5.1 Plots showing average values from 8 AM – 6 PM daily for no cooling	65
FIGURE 5.2 PLOTS SHOWING AVERAGE VALUES FROM 8 AM – 6 PM DAILY FOR CONVECTIVE COOLING	66
FIGURE 5.3 PLOTS SHOWING AVERAGE VALUES FROM 8 AM – 6 PM DAILY FOR EVAPORATIVE COOLING	66
FIGURE 5.4 PLOTS SHOWING AVERAGE VALUES FROM 8 AM – 6 PM DAILY FOR EVAPOTRANSPIRATION COOLING	67
FIGURE 5.5 PLOTS SHOWING AVERAGE VALUES FROM 8 AM – 6 PM DAILY FOR COMBINED COOLING SYSTEM	67
FIGURE 5.6 TRENDS OF DAILY AVERAGES OF TEMPERATURE AND RELATIVE HUMIDITY FROM 8AM – 6PM	68

FIGURE 5.7TRENDS OF HOURLY AVERAGESOF TEMPERATURE AND RELATIVE HUMIDITY FROM 8AM - 6PM.	69
FIGURE 5.8TRENDS OF DAILY AVERAGES TEMPERATURE AND RELATIVE HUMIDITY FOR CONVECTIVE COOLING	70
FIGURE 5.9TRENDS OF HOURLY AVERAGES OFTEMPERATURE AND RELATIVE HUMIDITY FOR CONVECTIVE COOLING	71
FIGURE 5.10TRENDS OF DAILY AVERAGES OF TEMPERATURE AND RELATIVE HUMIDITY FOR EVAPORATIVE COOLING	72
FIGURE 5.11TRENDS OF HOURLY AVERAGESOFTEMPERATURE AND RELATIVE HUMIDITY FOR EVAPORATIVE COOLING	73
FIGURE 5.12 TRENDS OF DAILY AVERAGES FOR TEMPERATURE AND RELATIVE HUMIDITY FOR EVAPOTRANSPIRATION COOLING	74
FIGURE 5.13TRENDS OF HOURLY AVERAGESOFTEMPERATURE AND RELATIVE HUMIDITY FOR EVAPOTRANSPIRATION COOLING	75
FIGURE 5.14TRENDS OF DAILY AVERAGES FOR TEMPERATURE AND RELATIVE HUMIDITY FOR COMBINED COOLING	76
FIGURE 5.15TRENDS OF HOURLY AVERAGESOFTEMPERATURE AND RELATIVE HUMIDITY FOR COMBINED COOLING	77
FIGURE 5.16TRENDS OF HOURLY CHANGES FOR EACH MEASURE VARIABLE IN ALL INSTANCES.	80
FIGURE 5.17MESH SECTION OF THE COMPUTATIONAL MODEL	82
FIGURE 5.18PREDICTED MODEL TEMPERATURE PROFILE FOR STEADY STATE CONDITION	83
FIGURE 5.19COMPARISON OF AMBIENT TEMPERATURE, STORAGE TEMPERATURE, AND MODEL PREDICTED TEMPERATURE FOR NO COOLING	84

FIGURE 5.20	COMPARISON OF AMBIENT TEMPERATURE, STORAGE TEMPERATURE, AND MODEL PREDICTED TEMPERATURE FOR CONVECTION COOLING	85
FIGURE 5.21	COMPARISON FOR AMBIENT TEMPERATURE, STORAGE TEMPERATURE, AND MODEL PREDICTED TEMPERATURE FOR EVAPORATIVE COOLING	85
FIGURE 5.22	COMPARISON FOR AMBIENT TEMPERATURE, STORAGE TEMPERATURE, AND MODEL PREDICTED TEMPERATURE FOR EVAPOTRANSPIRATION COOLING	86
FIGURE 5.23	COMPARISON FOR AMBIENT TEMPERATURE, STORAGE TEMPERATURE, AND MODEL PREDICTED TEMPERATURE FOR COMBINED COOLING TECHNOLOGIES	87
FIGURE 5.24	THE PLOT SHOWING THE OPTIMUM PAD THICKNESS	88

LIST OF ABBREVIATIONS

3-D	Three-dimensional
ANSYS	Analysis System
CB-AC	CoolBot™-air conditioner
CFD	Computational Fluid Dynamics
EC	Evaporative Cooling
ECC	Evaporative Cooling Chamber
ECT	Evaporative Cooling Technology
F&V	Fruits and Vegetables
FAO	Food and Agriculture Organization
JKUAT	Jomo Kenyatta University of Agriculture and Technology
PHL	Post-harvest Losses
RH	Relative Humidity
T&RH	Temperature and Relative Humidity
K- ϵ	K-Epsilon
K- ω	K-Omega
RANS	Reynolds Average Navier-Stokes
Re	Reynolds number
RH	Relative Humidity
RNG	Re-Normalization Group
LRN	Low Reynolds Number
PHL	Post-harvest Loss
Pr	Prandtl number

SL Shelf Life

SST K- ω Shear Stress Transport K-omega

LIST OF SYMBOLS

Δ	Vapor pressure or temperature (h Pa K ⁻¹)
A	Surface area (m ²)
A _{floor}	Floor area (m ²)
A _{front}	Front side area (m ²)
A _{left}	Lift side area (m ²)
A _p	Surface area of the particle (m ²)
A _{rear}	Rear side area (m ²)
A _{right}	Right-side area (m ²)
A _{spec}	Specific surface area (m ² m ⁻³)
A _{top}	Top area (m ²)
C _{nbulk}	Concentration in the fluid bulk particle ()
C _{ns}	Concentration of species ()
C _p	Heat capacity (Jkg ⁻¹ °C ⁻¹)
C _{p,p}	Specific heat capacity of product ((Jkg ⁻¹ °C ⁻¹)
C _{pa}	Air heat capacity (Jkg ⁻¹ °C ⁻¹)
C _{pf}	Fluid heat capacity (Jkg ⁻¹ °C ⁻¹)
C _{pw}	Water heat capacity (Jkg ⁻¹ °C ⁻¹)
D	Air pressure deficit (h Pa)
D _i	Diffusivity (m ² s ⁻¹)
d _p	Length (m)
D _ω	Cross-diffusion term (m ² s ⁻¹)
F(u)	Wind speed (m s ⁻¹)

F_{capacity}	Fan capacity
g	Force of gravitation (m s^{-2})
G_k	Generation of turbulence kinetic energy due to mean velocity gradients
Gr	Grashof number ()
G_ω	Generation of ω
h	Heat transfer coefficient ($\text{W m}^{-2} \text{K}^{-1}$)
H	Enthalpy (J kg^{-1})
H_c	Height of the cooler (m)
h_{fg}	Heat of evaporation (J kg^{-1})
h_m	Mass transfer coefficient (m s^{-1})
H_r	Reaction enthalpy (kJ)
k	thermal conductivity of the material ($\text{W.m}^{-1} \text{K}^{-1}$)
$k_{cn/i}$	Convective mass-transfer coefficient (m s^{-1})
L	Surface length (m)
L_c	length of the cooler (m)
m	Evaporation moisture ($\text{kg m}^{-3} \text{s}^{-1}$)
M	Molecular mass (kg mol^{-1})
\dot{m}_k	Mass transfer ($\text{gm cm}^{-2} \text{s}^{-1}$)
m_p	Mass of particle (kg)
N_n	Mass ($\text{mol m}^{-2} \text{s}$)
Nu	Nusselt number ()
p	Pressure (Pa)
Q	Local heat flux density (W m^{-2})

q_p	Product heat of respiration (W m^{-3})
Q_R	Heat transfer rate (W)
R	Rate of reaction (s^{-1})
r_p	Product volume fraction ()
r_s and r_a	Resistance factors
RT	Gas constant ($\text{J mol}^{-1} \text{K}^{-1}$)
Sc	Schmidt number ()
S_E	Energy ($\text{m}^{-3} \text{s}^{-1}$)
SE	Saturation Efficiency (%)
Sh	Sherwood number ()
S_k and S_ω	Source terms ($\text{kg m}^{-3} \text{s}^{-1}$)
$S_{mx, my, mz}$	Source terms ($\text{m}^{-3} \text{s}^{-1}$)
T	Temperature ($^{\circ}\text{C}$ or K)
t	Time (s)
$T_1(\text{db})$	Dry bulb outdoor temperature ($^{\circ}\text{C}$)
$T_1(\text{wb})$	Wet bulb outdoor temperature ($^{\circ}\text{C}$)
$T_2(\text{db})$	Dry bulb cooler temperature ($^{\circ}\text{C}$)
T_a	Air temperature ($^{\circ}\text{C}$)
τ_{ij}	Stress (Pa)
T_p	Product temperature ($^{\circ}\text{C}$)
T_{ref}	Reference temperature ($^{\circ}\text{C}$)
U	Velocity (x, y, z, t) (m s^{-1})
V	Fluid velocity (m s^{-1})

V_C	Volume capacity ()
W_a	Molecular weight of air (kg kmol^{-1})
W_C	Width of cooler (m)
Y	Humidity ratio ()
Y_k and Y_ω	Dissipation of k and ω due to turbulence ()
β	Expansion coefficient (K^{-1})
γ	Psychometric coefficient (0.67 h Pa K^{-1})
ΔT	Surface and fluid temperature difference ($^{\circ}\text{C}$)
ΔT_m	Mean temperature difference between fluid and surface (K)
μ	Viscosity ($\text{kg m}^{-1} \text{ s}^{-1}$)
μ	Dynamic viscosity ($\text{kg m}^{-1} \text{ s}^{-1}$)
μ_t	Turbulent viscosity ()
ρ_f	Fluid density (kg m^{-3})
ρ_a^v	Density of water in vapour phase (kg m^{-3})
ρ_p^v	Density of water vapour at equilibrium (kg m^{-3})
ϕ	Heat flux (W m^{-2})
∇T	Temperature gradient (K m^{-1})
λ	Latent heat of vaporization (kJ kg^{-1})
Γ_k and Γ_ω	Effective diffusivity of k and ω ($\text{m}^2 \text{ s}^{-1}$)
ρ	Density (kg m^{-3})
ρ_{ref}	Density at reference condition (kg m^{-3})
σ_k and σ_ω	Turbulent Prandtl numbers

ABSTRACT

The rise in global temperature is affecting almost all fabrics of our society, including food security. Increase in average temperature leads to a corresponding decrease in relative humidity that affects quality and shelf life of fruits and vegetables (F&V). In Kenya, about 25-45% of total production of fruits and vegetables are wasted because of inappropriate storage facilities. This is particularly alarming amongst rural farmers. In recent years, charcoal cooling has offered hope in Kenya for storage of F&V, but is a major of Greenhouse Gas Emissions.

The primary objective of this study was to evaluate the performance of the pumice evaporative cooling chamber (ECC) with energy savings and thermal control and to develop Computational Fluid Dynamics (CFD) model to predict storage temperature.

Pumice evaporative cooling chamber of 14.58 m² capacity with convective and evapotranspiration support, powered by solar energy was designed and constructed at Jomo Kenyatta University of Agriculture and Technology (JKUAT) for the study. Temperature, relative humidity, solar radiation, and wind speed were measured for natural convection cooling, force convection cooling, evaporative cooling, evapotranspiration cooling, and combined cooling system. The data evaporative cooling was used to develop a CFD model to predict storage temperature. The cooling chamber operated on principle of evaporation to lower temperature and increased relative humidity. It was tested and evaluated under no load condition.

The three-dimensional CFD geometry was developed and used to simulate the cooling chamber with the Shear-Stress Transport (SST) k-omega model. The result was compared to experimental data and the model optimized using a single variable optimization method. The mass flow rate was optimized for maximum thermal performance and the optimum point was used to investigate optimal pad thickness.

The study showed that with no artificial influence on the cooler, the difference between ambient and storage temperature was 11.47 °C, ambient and storage relative humidity was 42.44%. The cooling pad was 83% effective. With convective cooling, the difference between ambient and storage temperature was 11.77 °C, relative humidity increased by 44.18%, and 85% efficient. The ambient and storage temperature difference was 13.64 °C, humidity increases by 64.44%, and 98.6% efficient for evaporative cooling. The ambient and storage temperature difference was 13.04 °C, humidity increases by 64.44%, and 94% efficient for evapotranspiration cooling. The ambient and storage temperature difference was 13.74 °C, humidity increases by 65.61%, and 99% efficient for combined cooling system. The Computational Fluid Dynamics predicted result was compare against experimental data with a 98% confidence for evaporative cooling. The pad thickness of 200 mm was chosen for the optimized model with 5% standard deviation at optimum water flow rate of 0.105 m³/hr.

The study provided useful guidelines for the design of evaporative cooling system with efficient energy savings for storage of F&V. If the use of this technology is adopted at a national level, it has the potential to increased shelf life, food availability, and farmer's earnings.

CHAPTER ONE

INTRODUCTION

1.1 Background

The increase in human population and the quest for better living condition is further expanding global economy. This has resulted in sharp increase in food demand and consumption, posing a serious challenge to countries meeting her sustainable development goals (Griggs et al., 2013). In Kenya, a large percentage of her population goes to bed hungry because of postharvest losses (PHL) that poses a serious threat to her food security (Arah et al.,2015). Though the impacts of food security are well known, little or nothing has been done positively to remedy the situation along the complex food chain to increase production and food availability effectively and sustainably (James and Zikankuba, 2017). Food for her population is achievable through essentially appropriate storage technologies with requisite knowledge of what to evade along the supply chain (Bradford et al., 2018).

Thermal environment control in cold rooms is vital to prolonged and maintained quality of F&V because most horticultural produce are preserved at low temperatures and high relative humidity (RH). However, achieving the required storage conditions depends mainly on mechanical refrigeration that is driven by high-energy consumption and a major source of carbon dioxide emission. The continuous carbon emission leads to a rise in temperatures that is altering atmospheric conditions and ecosystems, thereby causing global warming. Due to the impact of global warming, there are several calls for innovation in technology that might lead to the reduction in the carbon dioxide emission.

High temperature is one of the main factors that affect the shelf life of fruits and vegetables. Their quality is never better than the time of harvest as they begin to deteriorate from that

moment until they eventually die up. To keep F&V fresh and alive, they must be stored in appropriate storage facilities soon after harvest to reduce PHL. Appropriate storage facilities must be deployed all along the supply chain for both short and long-time preservation of F&V (Kumar and Kalita, 2017; Bradford et al., 2018). This is so because fresh produce contain water that keep them alive soon after harvest to reduce their post-harvest losses. This is necessary because the quality of fruits and vegetables depend on how fast they use their stored energy, and the rate of water loss (James and Zikankuba, 2017). Therefore, optimal temperature and RH should be maintained during storage (Vala et al., 2014).

Evaporative cooling and mechanical refrigeration are among some cooling methods used to preserve fruits and vegetables in Africa. Mechanical refrigeration is more popular and most widely used form of cooling along the supply chain. However, it has a high procurement and operational cost; and requires a constant supply of electricity that renders it inappropriate for rural and small-scale farmers who are mostly poor. Evaporative cooling is a simple alternative that is used to increase relative humidity and lower temperature. It is simple, eco-friendly, energy efficient and does not require technical knowledge to operate. Evaporative cooling is an ancient method used to increase relative humidity and lower temperature of a given space and it has proven to be an effective method of cooling for stored fruits and vegetables soon after harvest (Liberty et al., 2013; Islam et al., 2013). Unlike refrigeration, evaporative cooling does not release carbon dioxide, but keeps the produce in shape with quality air, and in most cases do not require external energy for operation. Although evaporative cooling has proven to be effective and efficient in fruits and vegetables preservation, little effort has been put to understand the real-time processes constantly taking place within the storage space. This is partially due to the cost of experimentation and time required in understanding such processes.

With the introduction of computer simulation in engineering, there is need to use such tools to bridge gaps in the understanding of such processes in evaporative cooling. For instance, there is a need to determine the optimum size of evaporation structures with economical and efficient materials. This project is a response to this need. Therefore, a study was carried on an evaporative cooler to determine its efficiency and optimized the system to enhance food security. In the food processing industry, CFD has been used to design optimum and energy efficient air distribution systems without compromising the food quality and shelf life (She et al., 2018; Bradford et al., 2018; Boyd 2019). CFD models are computer-aided techniques used in industry to solve fluid problems by the application of general transport equations over a controlled volume (Ambaw et al., 2013). In todayresearch effort, computers can perform numerical calculations required to simulate flows with surfaces defined by boundary conditions (ANSYS, 2019). Although modelling is often applied in mechanical cooling, some studies Point to the usage of models for evaporative cooling(Sohani et al., 2016).

The development of super computers has enhanced the work of scientists and engineers, particularly in flow simulation due to their ability to performed millions of calculations required for flow simulation. In practice, CFD is an important addition to design configuration and a substitute for complicated and difficult experiments. In today's research effort, CFD have been used to analyze different parameters regarding fluid flow (Ambaw et al., 2013; Liberty et al., 2013; Vala et al., 2014; Sohani et al., 2016;Tolesa and Workneh 2017; James and Zikankuba, 2017; She et al., 2018; Bradford et al., 2018; Boyd 2019).

1.2 Problem statement

Agricultural engineers are challenged with providing food for the ever-increasing population while at the same time maintaining a sustainable environment. The use of evaporative coolers, referred to as charcoal coolers by local farmers, is an affordable way of preserving produce. However, its environmental challenges such as deforestation, climate change and greenhouse gas emission, all of which are causes of global warming. Therefore, there is a need to discourage the use of charcoal, and search for alternative materials to enhance sustainable environment and higher returns for rural farmers(Dhakulkar et al., 2018; Dogramaci and Aydin, 2020).

The seasonal scarcity of fruits and vegetables is largely due to postharvest losses. These losses have a negative bearing on producer income, price, and availability. Countering these effects requires rebuts action that will lead to a reduction in temperature with and anincrease in RH. This can only be achieved amongst rural farmers if engineers develop improved design for local evaporative coolers. Design improvement requires knowledge about the environmental parameters affecting cooling chambers.

Several studies have been taken to understand how the evaporative cooling chamber (ECC) can be used for preservingfresh produce(Vala et al., 2019; James and Zikankuba, 2017; Tolesa, 2018; Liu et al., 2015).However, little is known when it comes to mathematical modelling of the same under Kenyan conditions.Mathematical modelling could be used to determine how the evaporative cooling system performs under specific environmental factors. This could eliminate the difficulty and time required to conduct experiment for evaporative cooling system in Kenya.

1.3 Research justification

It is difficult, expensive, and time consuming to understand and accurately measure heat and mass transfer (HMT) processes in cooling chambers. These problems can be solved by use of Computational Fluid Dynamics (CFD). CFD simulation can be used to evaluate HMT processes. CFD uses algorithms along with numerical analysis to evaluate problems associated with engineering flow (Vala et al., 2019). A CFD model once developed can be used to optimize a cooling chamber and provide a qualitative forecast.

Given the disadvantages of using charcoal in evaporative coolers, it would be appropriate to replace the charcoal with a different material. Pumice is a naturally occurring igneous rock that is formed from volcanic eruption. It is a light-coloured rock with extremely high porosity and good permeability. Unlike charcoal, use of pumice does not put additional pressure on the environment and it is abundantly available. Therefore, pumice would be a good substitute for charcoal, and could ease the environmental burden of cutting down trees for charcoal only to be used in evaporative coolers as cooling pads.

1.4 Overall objective

The overall objective of this study was to validate the efficiency of an evaporative cooling chamber with pumice padding for storage of fruits and vegetables and optimized it using Computational Fluid Dynamics.

1.4.1 Specific objective

The specific objectives were:

1. To evaluate the performance of an evaporative cooling chamber under different cooling methods (Evaporation, convection, and evapotranspiration).
2. To develop a three-dimensional (3D) Computational Fluid Dynamics model to predict temperatures inside the evaporative cooling chamber.
3. To optimize the pumice padding an evaporative cooling chamber using computational fluid dynamics.
4. To validate the simulation model against experimental data for no-load evaporative cooling.

1.5 Research questions

For the researcher to meet the specific objectives, the following questions will be answer.

1. What are the procedures involved in Computational Fluid Dynamics modeling and how effective are these models?
2. How was the storage chamber optimized?
3. Is the developed model able to predict the temperature and air distribution inside the storage chamber?

1.6 Scope and limitation of the study

The scope of this study was to evaluate the performance of an evaporative cooler with convective, and evapotranspiration cooling embedded into it. The study looked at temperature and relative humidity (RH)distribution within the storage chamber. The research focused on modelling the existing storage chamber and optimized the pad thickness using Computational Fluid Dynamics (CFD). Understanding RH and temperature distribution in evaporative chamber is key to reducing post-harvest losses.

Post-harvest loss in fruits and vegetables can be reduced by drying, value addition, processing, storage etc. This study was limited to post-harvest storage using a locally designed evaporative cooler. The CFD simulation was also limited to ANSYS WORKBENCH of Fluent student version. The optimization was limited to a single variable optimization and only the pad thickness was optimized for saturation efficiency.

1.7 Thesis layout

Chapter 1 introduces the research; it gives the background information, statement of the problem, research objectives, justification, and scope. **Chapter 2** provides a review of literature about evaporative coolers and Computational Fluid Dynamic. **Chapter 3** presents governing generic equations relevant to the study; **Chapter 4** detailed the materials and methods, the experimental setup, and CFD simulation processes. **Chapter 5** gives the data, finding, and discusses the result. **Chapter 6** concludes the research, recommendations, and further research.

CHAPTER TWO

LITERATURE REVIEW

2.1 Postharvest losses of fruits and vegetables

Fresh produce losses occur throughout the supply chain due to the use of inappropriate storage facilities and market constraints. Rosegrant et al., (2018) projected postharvest losses (PHL) of fruits and vegetables (F&V) at 25 – 50% of total production globally. The highest loss is being experienced in Africa, particularly in regions that experience high temperature and has poor infrastructural development. These losses include mechanical damage, loss in nutritional value, physiological and microbiological deterioration; all of which lead to loss in market value, thereby proportionately affecting the income of farmers and reducing the availability of fruits and vegetables. Estimates of PHL in Kenya have been reported to be as high as 50% (Kitinoja and Kader, 2015; Kituu et al., 2014; Kipruto, 2017). Therefore, there is a pressing need for appropriate postharvest technologies in order to mitigate.

2.1.1 Reasons that derive postharvest losses in fresh produce

The factors affecting postharvest losses (PHL) are mainly due to consumer behavior, and lack of adequate coordination amongst farmers and buyers (Rosegrant et al., 2018). The main reasons for PHL in Africa are environmental and social economic factors, which includes lack of finance, poor management practices, harvesting method, climatic conditions, storage facilities, value addition, marketing, and infrastructure (Kitinoja and Kader, 2015).

The environmental factors can be looked at collectively under climatic conditions to include rainfall, wind, relative humidity (RH), and temperature influence. Higher temperature reduces the shelf life of horticultural produce and quality. Fresh farm produce contain large quantity of

water that keep them alive soon after harvest, but at higher temperature and low relative humidity, the store water is fast consume. Therefore, temperature and RH affect fruits and vegetables greatly, and by controlling them can yield more return for farmers as well as providing more food for the growing population (Kitinoja and Kader 2015).

2.2 History of evaporative cooling

The history surrounding natural cooling is largely credited to the ancient Egyptians who discovered that hot-dry air become moist and cool the environment as it blows through a dampened mats or porous clay pots that contains water (Duan et al., 2012; Balogun et al 2019; Balogun and Ariahu, 2020). Greeks, Romans, and people living in India are also credited to have used evaporative cooling to cool their homes in the late 1930s. Evaporative cooling occurs naturally in streams, oceans, lakes, and on animal skin. It is an ancient innovation that is broadly classified into direct or indirect evaporation (Balogun et al., 2019).

Evaporation can either be direct (natural process) or indirect (artificial process) and can lead to temperature drop with rise in humidity. Naturally, evaporation is one of the most economical methods use for cooling a given space (Singh and Das, 2017). As the evaporation takes place, heat is simultaneously transferred from the air to water, thereby reducing temperature. Evaporative cooling (EC) is broadly classified into direct EC or EC, and sometimes the combination of the two with other cooling cycles (Duan et al., 2012, Sultan et al., 2018). Either of them is a versatile and energy efficient alternative to refrigeration and compressor-based cooling. The underlying theory of this process is the transfer of sensible heat to latent heat of vaporization that occurs when hot dry air moves over a wet porous material.

The performance of evaporative cooling chamber reduces with a rise in relative humidity and eventually stops when the air is fully saturated. The decrease in temperature using this process leads to a corresponding increase in relative humidity. Therefore, evaporative cooling process can be most effective in hot climatic zones. In the tropics, evaporation can satisfy the cooling of spaces with appropriate air ventilation that usually occurs at constant enthalpy (adiabatic cooling) in an ideal process. The minimum temperature reached during evaporation is known as the wet bulb temperature (Hasan 2012).

2.3 Factors affecting evaporative cooling

The main factors that affect evaporative cooling are temperature, humidity, air velocity and surface area (Duan et al., 2016). Therefore, cooling in an evaporative cooler is controlled by the rate of evaporation. The environmental factors that plays key role during the storage of fresh produce are temperature and relative humidity (RH) (El-Ramady et al., 2015). High RH and low storage temperature can extend produce shelf life (Singh et al., 2016). However, to achieve these conditions inside the storage chamber, high temperature and low RH is required within the surrounding. The quality of water is also an important parameter for evaporative cooling. Under optimal conditions, evaporative coolers can reduce temperature down to 10°C and above depending on the cooling system (Liberty et al., 2013).

Increase in average temperature on earth has altered atmospheric conditions and ecosystems that are causing global warming. This rise in temperature has affected many factors of our society including post-harvest losses (PHL) especially in tropical countries. This is one of the reasons evaporative coolers are considered as a promising technology to combat PHL with a minimal effect to the environment. At 100 °C, water expands and escapes into the atmosphere and its

quantity in the air is known as water vapour. The amount of water vapour present in the air within a given space expressed as the percentage of the amount needed for saturation at the same temperature is known as RH. When the relative humidity is at hundred percent, the air becomes completely saturated, and it is at this time that condensation will begin. Therefore, the rate of evaporation decreases with corresponding increase in relative humidity.

As the wind blows, it carries along water molecules present in the air, thereby causing water to expand (Boyd, 2019). This process transcends into creating more vapor that is susceptible for evaporation to occur while air continue to move. Similarly, evaporation will slow down if the humid air remains stationary. Therefore, increase in air velocity leads to an increase in evaporation because greater surface area leads to greater rate of evaporation (Carrier et al., 2016). When the surface area is increased, it allows more water molecules to escape faster and more evaporation will take place.

2.4 Cooling technologies used in storage of fruits and vegetables

Cooling technologies can reduce temperature of given space. In the case of storage chamber design for fruits and vegetables (F&V), this reduction in temperature has a corresponding effect that can lower respiratory heat production, slow ripening, minimize transpiration and microbial activity by microorganisms (Ambaw et al., 2013). Therefore, storage optimization requires proper temperature and relative humidity control inside a given space. Some cooling methods used for fruits and vegetables preservation are CoolBot™-air-conditioner, mechanical refrigeration, convective cooling, evaporative cooling, vacuum cooling, hydro cooling, and more (Ambaw et al., 2013).

2.4.1 CoolBot™ – Air condition cooling system

CoolBot™ Air Conditioner (CB-AC) is an economically advantageous cooling system to vacuum and hydro-cooling, not only for its portable nature, but also for its efficiency in maintaining produce quality (Tolesa and Workneh 2017). It is an electronic device designed to keep storage air below set point and it is considered by many as effective (Kitinoja, 2013). CB-AC has been used as assisted cold storage for potatoes in India, and for onions in Ghana with excellent result (Tolesa, 2018; Ridolfi et al., 2018). The working principle of CB-AC is that for water to evaporate, it needs latent heat of evaporation. The water that is sprayed over the pads then takes the required latent heat from atmospheric air surrounding them and cools down on losing its heat. This cooled air is blown inside the room by the exhaust fan fitted on the cooler and thus the room temperature drops making the ambiance inside comfortable. It has been established that it has low installation costs, low repair costs, electricity savings and reduced operational costs (Karithi 2016). With inadequate research tailored on fluid movements within the CB-AC, numerical simulation, and optimization, using Computational Fluid Dynamics can be an option. CB-AC cooling technology requires detail study (Tolesa and Workneh 2017).

2.4.2 Mechanical refrigeration

Mechanical refrigeration is the most common form of cooling process that is mostly used in urban areas with constant supply of electricity. The mechanical refrigerators work on the principle of absorption that is widely used in commercial installations with ammonia mostly used as refrigerant. In this technology, liquid refrigerants circulate in tubular coil, remove heat, and cool the store (She et al., 2018). Mechanical refrigerator is good for storage of fresh produce because of its uniformity in cooling. It is used in precooling devices, refrigerated vehicles,

shipping containers, refrigerated cargo, cold warehouses etc. The global population growth and the quest for development, it is expected that the demand for cooling will rise exponentially by 2050 (Goldstein et al., 2017).

However, it is associated with high procurement and operational costs; and requires technical knowledge to operate. Mechanical refrigeration affects the environment negatively through carbon dioxide and depends largely on public energy (Goldstein et al., 2017). In developing countries, constant power supply is a serious challenge in urban settlements and in rural areas where there is no electricity. Therefore, this technology is not feasible for small-scale rural farmers and processors due to costs associated with its operation (Liu et al., 2015).

2.4.3 Advances, cooling pad, and energy conservation in evaporative cooling system

Evaporation is a process through which water is converted to vapour (Vala et al. 2019). It has been successfully used for both local and industrial applications (James and Zikankuba, 2017). The effectiveness depends on relative humidity (RH) and its performance depends on ambient air, RH, permeability, and the produce surface area (Tolesa, 2018). Unlike mechanical refrigeration, evaporation is simple to operate. It saves energy in that energy is only required for the fans and water pump and in some special designs, do not require energy (Liu et al., 2015).

This method of cooling can be achieved through different designs, but most of which comprise of porous wall. The cooling pad can be charcoal, sand, clay, wood chips, coconut fiber, pumice, or other porous materials (Khond, 2011; Gunhun et al., 2007; Al-Sulaiman, 2002; Vala et al., 2016). Therefore, for this technology to achieve the desired purpose, water must be constantly supplied to keep the cooling pad wet. Cooling occurs when hot dry air pass through the wet pad and subsequently convert the sensible heat to latent heat (Liberty et al., 2013).

Kitinoja (2013) carried out a study on storage chamber in hot and dry climate. In his analysis, the storage chamber was able to reduce the cooled space temperature by 10 °C during morning hours and by 25 °C during midday compared to ambient temperature and relative humidity (T&RH). The relative humidity (RH) of the cooled space air was raised by 90%. His findings show that optimum T&RH are dependent on harvest season, location, time of the day and weather conditions. However, Kitinoja (2013) did not offer any solution on how to improve the storage chamber that could narrow the gap in the temperature variation within the cooled space from morning to noon. Roy and Pal (1989) designed a low-cost evaporative cooler from local materials and got a good result with temperature dropping while RH increased to 90 percent. In their study, they show that as the water evaporates, heat energy is removed from the cooled space and transferred to the environment. They concluded that the cooling effect of an evaporative chamber is largely controlled by environmental factors.

James and Zikankuba (2017) demonstrated that high temperature are major causes for rapid quality deterioration of freshly harvested produce. Fruits and vegetables contain huge quantities of water that keep them alive after harvest; a condition that depends on how fast they use their stored energy and rate of water loss. Therefore, temperature and relative humidity should be maintained at optimum levels during storage (Vala et al. 2019). The evaporation rate depend on high temperature, and due this reason, temperate climatic zones are more suitable for the application of this technology. Similarly, in temperate climatic zones, the humidity is naturally low, thereby presenting a unique opportunity for evaporation. Other factors include permeability, velocity, and surface area.

2.4.3.1 Advances in evaporative cooling technology

Several researchers have made tremendous efforts to the development of storage chambers for fresh produce. Roy and Pal (1989) designed a low-cost evaporative cooler using locally available materials. In their findings, there was a considerable decrease in temperature of the given space. Mordi and Olorunda, (2003) conducted a study on evaporative cooling chamber for tomato storage and reported that the storage temperature was reduced by 8.2 °C, and relative humidity increase by 36.6%; thereby increasing the tomato shelf life by seven days. Kitinoja (2013) reported that evaporative cooling technology can reduce temperature in hot, dry climate by 25°C, and improving the relative humidity to 90%. Manyozo et al (2018) investigated the effectiveness and performance of evaporative cooling chambers for tomato storage in Malawi during the rainy and dry seasons using charcoal cooler, brakes evaporative cooler, and pot in pot evaporative cooler. They reported better results in all cases during the dry season as the shelf life of the stored tomatoes was increased by seven dayson an average. They reported that unlike mechanical refrigeration systems, evaporative cooler is simple to operate and good in preserving tomatoes.

2.4.3.2 Some materials used as cooling pad in evaporative cooling

Several factors are responsible for the efficiency of the evaporative cooling (EC) process. These factors include surface area, pad thickness, perforation size, air flow rate (FR), inlet relative humidity (RH), water volume FR, inlet temperature, and so on (Shahali et al., 2016). Amongst these parameters, the cooler performance depends on the cooling pad material. Cooling pad material should have the following characteristics: good water flow rate, water absorbing and holding qualities, high porosity, less costly, good thermal conductivity, noncorrosive, light weight, and easily available(Al-Sulaiman, 2002; Khond, 2011; Vala et al., 2016). The quest for

improving the efficiency of evaporative cooler to reduce cost has prompted many researchers to work on the development of novel pad materials (EM Ahmed et al., 2011). Table 2.1 present different materials that are consider for evaporative cooling, and Tab. 2.2 summarized the review of literature,

Table 2.1 Different materials used as cooling pad for evaporative cooling

Cooling pad materials				
Organic-based	Metal-based	Plastic-based	Natural fiber-based	Stone-based
Aspen pad	Porous metal plate	PVC	Coconut coir	Bulk charcoal
Khus pad	Metal mesh	Corrugated plastic sheet	Eucalyptus	Volcanic ash
Rice husk	Metallic foam		Palash	Porous ceramic
Celdek pad	Metal wool		Jute	Roof brick
Kraft paper			Cotton	
			Luffa	

Table 2.2 Summary on literature survey for cooling pad materials

No	Source	Cooling pad material(s) used	Observations contained
1	Khond, (2011)	wood wool----- coconut coir----- Khus ----- Stainless steel wire mesh-----	Water consumption rate by pads at constant fan speed were: 0.24 l/m 0.134 l/m 0.21 l/m 0.066 l/m
2	Gunhan et al., (2007)	Coarse and fine pumice stones, volcanic tuff, greenhouse shading nets and Celdek	They reported the following: Celdek pad exhibited 30-Pa pressure drop and approximately 80% cooling efficiency for 150 mm pad thickness, and was the best pad. But authors concluded that further investigations were needed to optimize the particle size, pad thickness and static pressure.
3		Celdek-----	Average temperature drop and saturation efficiency for each pad were: 8 °C and 92.20%

	Vala et al., (2016)	Aspen----- Coconut coir ----- Wood shavings -----	9.75 °C and 90.70% 3.5 °C and 67.42% 3.25 °C and 65.83%
4	Al-Sulaiman, (2002)	Jute----- Luffa----- Aspen (commercial)-- Date palm fibers-----	The order of efficiency and material degradation based on grams of salt deposited per gram of dry fibers were: 62.1% and 4.8% 55.1% and 37.25% 49.9% and 82% 38.9% and 27.3% They concluded that luffa had an overall advantage and jute was a viable material if treated for degradation.

2.4.3.3 Energy conservation in evaporative chamber

The theory behind the energy conservation equation of cooling systems can be categorized as energy transfer from produce to fluid (Nahor et al. 2005). Due to respiration heat of the produce, energy and heat configuration between fruits and vegetables interface, condensation and evaporation occurs as the temperature and energy gradient becomes the driving force (Nahor et al., 2005).

2.4.4 Convective cooling

The theory of heat transfer can best be described as an operation that occurs repeatedly as heat is spontaneously transferred between bodies. During storage, the unsteady-state heat transfer occurs as temperature changes. Conversely, a steady-state heat transfer occurred when temperatures do not change. This process can be categorized as conduction, radiation, or convection. Convective cooling is a heat transfer process that occurred because of fluid motion either naturally or by the application of force. During forced convection, fluid movement is influenced by external forces.

Depending on the extent of the applied force, the flow can be either laminar or turbulent. In the case of turbulence, cold and hot air can be perfectly mixed with grater drop in pressure and flow rate. Therefore, forced convective cooling from any produce surface is a function of velocity magnitude. Heat transfer coefficients from produce surfaces can be empirically predicted through dimensional analysis.

Equation 3.20 can be used to calculate the correlation coefficient of the forced convection cooling.

$$Nu = a \cdot (Re)^b \cdot (Pr)^c \quad (2.1)$$

where:

a, b, and c are constants

Nu is the Nusselt number

Re is the Reynolds number()

Pr is the Prandtl number ()

However, to account for all the parameters described above, Eq. 3.21, 3.22, 3.23, and 3.24 must be considered:

$$Re = \rho \cdot v \cdot L / \mu \quad (2.2)$$

$$Gr = \beta \cdot g \cdot \nabla T \cdot \rho^2 \cdot L^3 / \mu^2 \quad (2.3)$$

$$Pr = C_p \cdot \mu / k \quad (2.4)$$

$$Nu = h \cdot L / k \quad (2.5)$$

where:

Re is the Reynolds number

ρ is the fluid density (kg m^{-3})

V is the fluid velocity (m s^{-1})

L is the surface length (m)

μ is the dynamic viscosity ($\text{kg s}^{-1}\text{m}^{-1}$)

β is the expansion coefficient (K^{-1})

g is the force of gravitation (m s^{-2})

ΔT is the surface and fluid temperature difference ($^{\circ}\text{C}$)

C_p is the heat capacity ($\text{kJ kg}^{-1}\text{C}^{-1}$)

K is the thermal conductivity ($\text{W m}^{-1}\text{C}^{-1}$)

h is the heat transfer coefficient ($\text{Wm}^{-2}\text{C}^{-1}$)

To calculate thermal resistance in heat transfer network, Eq. 3.25 is considered.

$$\mathbf{A} = \mathbf{1}/(\mathbf{h} \cdot \mathbf{A}) \quad (2.6)$$

where:

A is the surface area (m^2)

h is the heat transfer coefficient ($\text{Wm}^{-2}\text{C}^{-1}$)

2.4.5 Evapotranspiration cooling

The Penman equation is mostly used to determine the rate of evapotranspiration due to plant canopy and requires data for light intensity, temperature, humidity, wind speed and surface characteristics. Monteith concept is credited for introducing bulk surface resistance that describes the resistance of vapour flow through the transpiring crop and evaporating soil surface (Allen et al., 1998). The resistance factors are control by vapour pressure, solar radiation, leaf's temperature, canopy water, vegetation height, etc. These factors can be combined to get the general Penman-Monteith equation, Eq, 3.26 (Schymanski and Or, 2017).

$$E = \frac{\Delta}{\Delta\gamma} \frac{R_n}{\lambda} + \frac{\gamma}{\Delta + \gamma} F(u) D \quad (2.7)$$

where:

E is the rate of evapotranspiration ($mm\ t^{-1}$)

Δ is the vapor pressure or temperature ($h\ Pa\ K^{-1}$)

λ is the latent heat of vaporization ($2460\ KJ\ kg^{-1}$)

γ is the psychometric coefficient ($0.67\ h\ Pa\ K^{-1}$)

R_n net radiation at the crop surface [$MJ\ m^{-2}\ day^{-1}$]

D is the air pressure deficit ($h.Pa$)

$F(u)$ is the wind speed ($m\ Day^{-1}$)

The psychometric coefficient can be calculated from Eq. 3.27.

$$\gamma = \gamma \left(1 + \frac{r_s}{r_a}\right) \quad (2.8)$$

where:

r_s and r_a are resistance factors

The time varying changes in real life situation makes it nearly impossible to get surface resistance from a field data. However, it is universally accepted that the surface resistance for water is zero but must be computed analytically for any other surfaces characterized by evapotranspiration if the resistance factors are known. Therefore, Food and Agriculture Organization suggested the use of reference crop height of 0.12 m, with standard velocity, temperature, and humidity at 2 m.

2.4.6 Hydro-cooling

Hydrocooling is a process used to preserve fruits and vegetables immediately after harvest with cold water. The cooling done by either spraying or immersion into cold water to remove heat, remnants of dirt and other microorganisms. The conduction of heat from solid to liquid is faster than solid to gas (Sena et al., 2019; de Oliveira et al., 2019; Alves et al., 2019; Franca et al., 2015). Therefore, cooling of produce with cold water does happen swiftly with no loss in weight, as the produce is flooded with water that is continuously circulating. When the produce is elated about pack chamber, it slots in hydro-cooler that provides fast and uniform cooling (Franca et al., 2015). However, the cooling time is relatively lower than other pre-cooling methods (Elsisi et al., 2020).

2.4.7 Vacuum cooling

This method is widely considered as one of the fastest ways to preserve some produce. The system is made of a chamber, pump, and a condenser. The produce to be cooled is loaded and the system put to work, but the evaporated water from the produce must be removed constantly to

prevent condensation. The temperature reduction right after harvest is a fundamental requirement for fruits and vegetables preservation (Cheng et al., 2015). Vacuum cooling is used in industry to reduce the time required to cool fruits and vegetables, extend produce life, and maintain quality. In contrast to conventional cooling methods, vacuum cooling provides fast cooling (Ding et al., 2014). Agricultural and food products are cooled by subjecting them to a deep vacuum, which increases the efficiency of the moisture evaporation by reducing the pressure and decreasing the temperature. However, it is not suitable when applied to fruits and vegetables due to its functional principles. Vacuum-cooled products exhibit undesirable weight loss because more moisture is evaporated in vacuum chambers compared to other conventional cooling methods (Cheng et al., 2015). This weight loss is the main defect of vacuum cooling technology because it can lead to increased economic losses when widely applied during the postharvest process.

2.5 Computational Fluid Dynamics modelling

The branch of fluid mechanics that utilizes the numerical method and data structures to analyze and solve problems relating to fluid flow is called computational fluid dynamics (CFD). CFD models are computer-aided techniques used in the industry due to the complex nature of industrial fluid flow and transport problems to solve fluid problems by the application of general transport equations over a controlled volume (Ambaw et al., 2013). Computers are used to perform numerical calculations required to simulate flows with surfaces defined by boundary conditions. Although modelling is often applied in mechanical cooling, some studies point to the usage of models for evaporative cooling (EC). Models are valuable tools for solving problems of fluid flow in storage chamber and are cardinal in industry due to the complex nature of industrial fluid flow and problems of transport (Sohani et al., 2016).

Computer usage in computational and simulation work has increased tenfold in engineering flow analysis (Yadav and Bhagoia, 2013; Dhande and Pande, 2018). In practice, CFD is perfect and wonderful addition to problem solving. CFD has been used by many researchers to study and analyzed fluid, heat, and mass, and shows its potential for analyzing fluid flow (Zhang et al., 2010; Luo et al., 2014; Montazeri et al., 2015; Yanhua et al., 2017; Misra and Ghosh, 2018; Mishra and Aharwal, 2018).

Zhang et al., (2010) used CFD to study and analyze velocity of air and temperature distribution in evaporative cooling system. Their analysis, however, did not address the issue of relative humidity and mass flow rate regarding the storage of fruits and vegetables. Luo et al., (2014) developed a neural network that predicted the performance of an evaporative cooler for different operational situation. Their finding was like experimental data and recommended that the model can be used to predict the performance of an evaporative cooler.

Montazeri et al., (2015) studied the potential and performance of buildings cooled with water spray using Lagrangian-Eulerian technique for evaporative cooling with a nozzle design and obtained an organized assessment of the system that agreed with experimental results. They were privileged to analyze several physical parameters by mist spray. Their systematic approach allowed them to analyze several key factors with nozzle configuration, relative humidity ratio, air temperature, air velocity, water temperature, and water droplet size at inlet. Although, they validated these physical parameters against the experimental data using CFD, their analysis was only applied to selected boundary conditions. Therefore, there is a need for a comprehensive study on both inlet and outlet physical parameters.

Yanhua et al., (2017) investigated heat transfer in a zero-energy evaporative cooler and reported that a chamber size of 0.6 m, the filter size of 0.075 m, and a load of 30 kg saw an acceptable

result. The numerical results were like experimental data, and they concluded that numerical simulation could be applied in evaporative cooling chamber to predict the distribution of velocity, temperature, and relative humidity.

Misra and Ghosh, (2018) developed a CFD model that was used to simulate the greenhouse cooling system that was designed with a fanpad-cooling system. They modeled the temperature and air velocity distribution, and the results were compared with experimental data. Their model result was like experimental data, and they recommended the model to be used to predict temperature and velocity in any fan-pad-cooling greenhouse.

Mishra and Aharwal (2018) conducted a review on the selection of turbulence model for CFD analysis of airflow and various aspects of the models with respect to their application within a cold storage. They reported that CFD could predict turbulent flow through any of the three turbulence models: Direct Numerical Simulation (DNS), Large Eddy Simulation (LES) or Detached Eddy Simulation (DES) and Reynolds – Averaged Navier – Stokes (RANS). These models (DNS, LES and DES) provided results that were like experimental values, but required skills, time, and large computational capacity. They concluded that due to these challenges, most of the authors chose RANS model for cold storage simulation. Finally, their finding was that RANS eddy viscosity models with two equation turbulence model, and a three-dimensional geometry for modelling can predict airflow in a well-designed and constructed cold storage chamber.

Vala et al., (2019) carried out a validation of evaporative cooling system using CFD analysis and developed a mathematical model for predicting temperature, velocity, and humidity distribution in an evaporative cooling chamber. The model results and experimental results were similar, which demonstrated that it could be successfully applied for predicting storage chamber

conditions. However, there is a need to replicate such findings in different regions and countries. Therefore, conceptual examination of evaporative cooler is vital for enlightening heat and mass transfer laws and for forecasting outputs under various circumstances for numerical simulation (She et al., 2017).

2.6 Computational Fluid Dynamics Modelling Procedure

The quest for modelling airflow using computational fluid dynamics (CFD) has gained a lot of interest in recent years due to its accuracy in handling the complex air flow and heat transfer processes. Research shows that finite volume method is mostly preferred in CFD simulation because it conserved mass directly and its flexibility in industrial application (Defraeye 2014; Yanhua et al., 2017). The simulation of any fluid problem that can be solved numerically is possible with computational fluid dynamics. However, this simulation process is segmented into three primary stages: Pre-processing, Solving, and Post-processing (Tolesa 2018; Mishra and Aharwal, 2018).

2.6.1 Governing equations of fluid mechanics

The equations of fluid flow and heat transfer are mathematical manipulation of conservation laws of fluid mechanics. They are continuity equation (which explicitly defines the rate at which mass enters and leaves the system, along with its accumulation); the momentum equation (the mathematical formulation that defines the conservation of momentum entering and leaving a control volume); and energy equation (the mathematical formulation of the statement of the conservation of energy principle).

The flow field can best be described by two formulations: the Eulerian and Lagrangian representations. The Eulerian representation describes the flow field with functions of space and time; while the Lagrangian representation on the other hand describes the flow field following individual fluid elements in the flow (Taira et al., 2017; Kajishima and Taira 2017). The equations of fluid flow and heat transfer are mathematical manipulation of conservation laws of fluid mechanics.

2.7 Research gaps from the review of literature

The literature survey shows that there are some related studies on the operation and design of evaporative coolers, but how relevant parameters influence the cooling process and temperature distribution in the chamber has rarely been thoroughly investigated. Therefore, further studies are needed to evaluate the effect of parameter combinations to utilize them efficiently for various situations in the design and operation. From the literature review, the following specific conclusions were noticed:

1. That evaporative cooling is an effective method of preserving fresh produce that can be explored to reduced postharvest losses. This has the potential to alleviate the challenges facing the local fruits and vegetables farmers. Most fresh produce are climacteric, highly perishable, and if proper preservation techniques are not put in place, there might be food insecurity, especially in developing countries (Kitinoja and Kader, 2015).
2. That the evaporative cooling performed excellently on many occasions. However, other factors that improved efficiency include water, air movement and surface area. Fresh produce are widely consumed, nutritious, and fragile and are of economic importance (Bergougnoux, 2014). Although, production is high, several researchers have reported

postharvest losses. Therefore, appropriate postharvest technologies for fruits and vegetables are indispensable.

3. That low storage temperature and high storage relative humidity are the most important factors that influence the produce shelf life and quality.

4. That CFD models can predict storage temperature and relative humidity.

CHAPTER THREE

THEORETICAL FRAMEWORK

3.1 Principle of evaporative cooling

Evaporation can either be direct (natural process) or indirect (artificial process) and can lead to temperature drop with rise in humidity. Naturally, evaporation is one of the most economical methods use for cooling a given space (Singh and Das, 2017). As the evaporation takes place, heat is simultaneously transferred from the air to water, thereby reducing temperature. Evaporative cooling (EC) is broadly classified into direct EC or EC, and sometimes the combination of the two with other cooling cycles (Duan et al., 2012, Sultan et al., 2018). Either of them is a versatile and energy efficient alternative to refrigeration and compressor-based cooling. The underlying theory of this process is the transfer of sensible heat to latent heat of vaporization that occurs when hot dry air moves over a wet porous material.

The performance of evaporative cooling chamber reduces with a rise in relative humidity and eventually stops when the air is fully saturated. The decrease in temperature using this process leads to a corresponding increase in relative humidity. Therefore, evaporative cooling process can be most effective in hot climatic zones. In the tropics, evaporation can satisfy the cooling of spaces with appropriate air ventilation that usually occurs at constant enthalpy (adiabatic cooling) in an ideal process. The minimum temperature reached during evaporation is known as the wet bulb temperature (Hasan 2012).

3.2 Computational Fluid Dynamics modelling

Computational Fluid Dynamics (CFD) models are computer-aided techniques used in industry to solve flow problems by the application of general transport equations over a controlled volume

(Ambaw et al., 2013). CFD is perfect for solving problems of airflow, heat, and mass transfer in an evaporative cooling storage chamber (Sohani et al., 2016). It has been used by many researchers to show its potential in analyzing fluid flow and heat transfer problems; Fig. 3.1 and 3.2 (Zhang et al., 2010).

3.2.1 Simulation procedure

The three-dimensional steady state turbulence model is usually solved using the Shear-Stress-Transport (SST) $k-\omega$ model because of its reasonable computational time and accuracy compared to other turbulence models (ANSYS 2019). The simulation process is divided into three main stages as shown in Fig. 3.1 and 3.2.

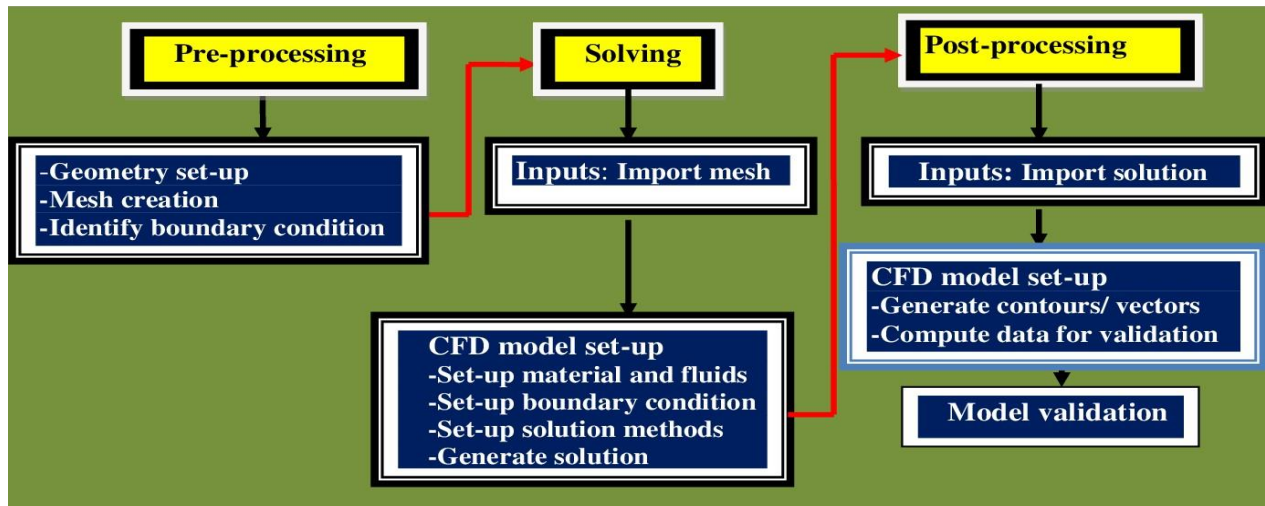


Figure 3.1 The main stages in computational fluid dynamics simulation

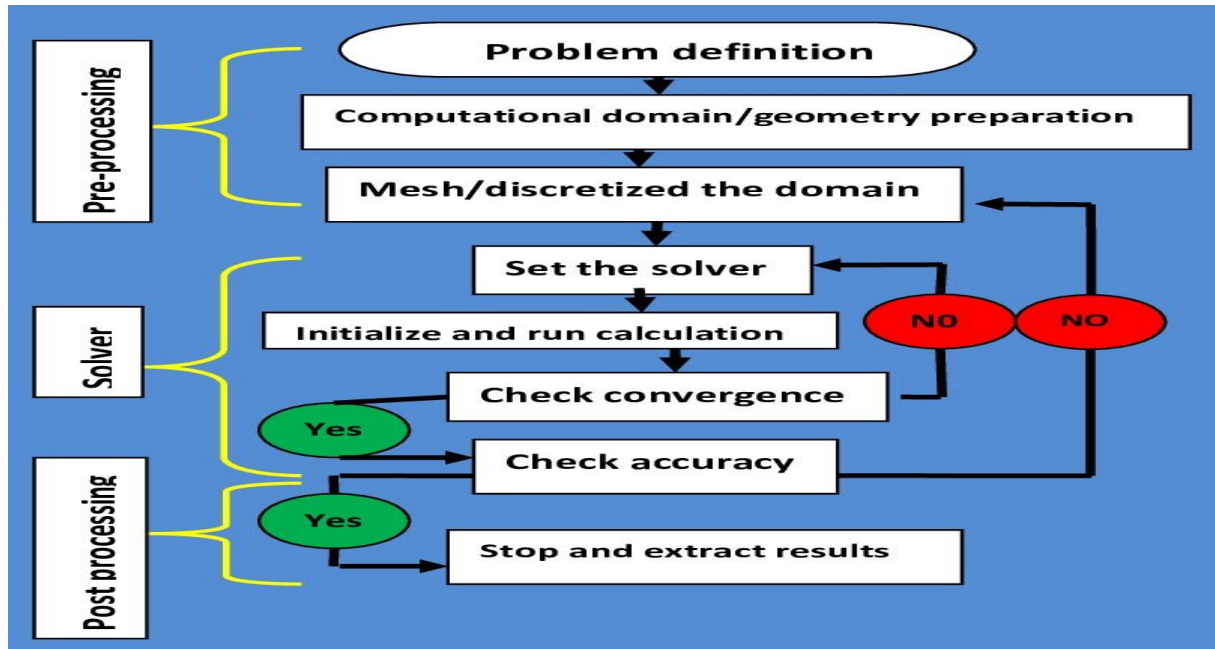


Figure 3.2Simulation procedures in ANSYS FLUENT

3.3 Governing equations for the simulation of evaporative cooling chamber

The equations of fluid flow and heat transfer are mathematical manipulation of conservation laws of fluid mechanics. These equations were used to simulate the pumice evaporative cooling chamber. These fundamental equations are briefly described below:

3.3.1 Heat and mass transfer equations

Mass transfer and energy equations are easily solved using numerical modeling for any given evaporative cooling chamber compared to analytical method (Ambaw et al., 2013). However, one must have adequate knowledge of the velocity, temperature, and relative humidity. Therefore, these parameters must be given relevant consideration when designing an evaporative storage chamber (Duret et al., 2014). Consequently, Fourier's equation for conduction (Eq. 3.1) and Fick's equation for mass diffusion (Eq. 3.2) are necessary for modelling heat and mass

transfer (T&MT) in cold storage when using the initial and final boundary conditions for zones of domain and contact surfaces for H&MT analysis (Tijskens et al, 2001).

$$\mathbf{q} = \frac{Q}{A} = -K \frac{dT}{dx} \quad (3.1)$$

where:

q is the heat flux (heat per unit area) ($W\ m^{-2}$)

Q is the heat rate (*W*)

dT/dx is the thermal gradient in the direction of the flow

A is the face area (m^2)

K is the thermal conductivity ($W\ m^{-1}K^{-1}$)

$$\frac{\partial c}{\partial t} = D \frac{\partial^2 c}{\partial x^2} \quad (3.2)$$

where:

C is the particle concentration ($kg\ m^{-3}$)

t is the time (*t*)

D is the diffusion coefficient ($m^2\ s^{-1}$)

X is the position (*m*)

Not until the introduction of computational fluid dynamics to handle engineering flow, dealing with energy, mass and momentum, boundary conditions in fluid flow was exceedingly difficult and in most instances impossible.

3.3.2 Governing equations for fluid flow simulation

The equations that govern fluid flow are presented below.

3.3.2.1 Continuity equation

The equation that explicitly defines the rate at which mass enters and leaves the system, along with its accumulation in fluid dynamics is known as the continuity equations in fluid dynamics.

The continuity equation is presented in Eq. 3.3.

$$\frac{\partial u}{\partial x} + \frac{\partial v}{\partial y} + \frac{\partial w}{\partial z} = 0 \quad (3.3)$$

where:

u, v, and w; are velocities (m s⁻¹)

3.3.2.2 Momentum Equation (x, y, and z)

The mathematical formulation that defines the conservation of momentum entering and leaving a control volume is the momentum equation. The conservation equation is presented in Eq. 3.4.

$$\rho \frac{Du}{Dt} = -\frac{dp}{dx} + \text{div}(\mu \text{grad}u) + S_{mx} \quad (3.4a)$$

$$\rho \frac{Dv}{Dt} = -\frac{dp}{dy} + \text{div}(\mu \text{grad}v) + S_{my} \quad (3.4b)$$

$$\rho \frac{Dw}{Dt} = -\frac{dp}{dz} + \text{div}(\mu \text{grad}w) + S_{mz} \quad (3.4c)$$

where:

u, v, and w; are velocities in x, y, and z (m s⁻¹)

p is the pressure (Pa)

ρ is the density (kg m^{-3})

S_{mx} , S_{my} , and S_{mz} are the source terms ($\text{m}^{-3} \text{s}^{-1}$)

μ is the viscosity ($\text{kg m}^{-1} \text{s}^{-1}$)

t is the time (s)

3.3.2.3 Energy equation

In fluid dynamics, the mathematical formulation of the statement of the conservation of energy principle is known as energy equation and is presented in Eq. 3.5.

$$\rho \frac{DE}{Dt} = -\mathbf{div}(\rho \mathbf{U}) + \left[\frac{\partial(u\tau_{xx})}{\partial x} + \frac{\partial(u\tau_{yx})}{\partial y} + \frac{\partial(u\tau_{zx})}{\partial z} + \frac{\partial(v\tau_{xy})}{\partial x} + \frac{\partial(v\tau_{yy})}{\partial y} + \frac{\partial(v\tau_{zy})}{\partial z} + \frac{\partial(w\tau_{xz})}{\partial x} + \frac{\partial(w\tau_{yz})}{\partial y} + \frac{\partial(w\tau_{zz})}{\partial z} \right] + \mathbf{div}(\mathbf{k} \cdot \mathbf{grad}T) + S_E \quad (3.5)$$

where:

\mathbf{U} is the velocity (x, y, z, t) (m s^{-1})

$u, v,$ and $w;$ are velocities in $x, y,$ and z

T is the temperature ($^{\circ}\text{C}$ or K)

p is the pressure (Pa)

ρ is the density (kg m^{-3})

H is the enthalpy (J kg^{-1})

S_E is the energy ($\text{m}^{-3} \text{s}^{-1}$)

τ_{ij} is the stress (N/m^2)

K is the thermal conductivity ($W m^{-1}K^{-1}$).

These basic questions (Eq. 3.3, 3.4, and 3.5) contain seven unknowns, therefore, two extra equations should be used to account for all the unknown variables (Tijskens et al., 2001)/

3.3.2.4 Moisture evaporation

The evaporation of moisture can be calculated using the lumped model (Nahor et al., 2005).

$$\mathbf{m} = -\frac{\partial x}{\partial t} = \mathbf{h}_m \mathbf{A}_{\text{spac}} (\rho p^v - \rho_a^v) \quad (3.6)$$

where:

m is evaporation of moisture ($kg m^{-3} s^{-1}$)

X is moisture content of product ($kgw m^{-3}$)

h_m is the mass transfer coefficient ($m s^{-1}$)

A_{spec} is the particle surface area ($m^2 m^{-3}$)

ρ_a^v is the density of water in vapour phase ($kg m^{-3}$)

ρp^v is the water vapour density at equilibrium ($kg m^{-3}$)

Or,

$$\mathbf{m} = \rho_a \frac{\partial r_a Y}{\partial t} + \mathbf{r} \mathbf{a} \rho \frac{\partial (u_i Y)}{\partial x_i} - r_a \rho_a \frac{\partial}{\partial x_j} \mathbf{D} \frac{\partial Y}{\partial x_i} \quad (3.7)$$

where:

Y is the humidity ratio ($kgw kgair^{-1}$)

r_a is the volume fraction of air (-)

3.3.2.5 The temperature in the storage chamber

Inside the storage chamber, temperature can be calculated using the model developed by Nahor et al., (2005):

$$\rho_p C_{p,p} \frac{\partial}{\partial t} (r_p T_p) = h_T A_{\text{space}} (T_a - T_p) \frac{\partial(u_i Y)}{\partial x_i} - h_{fg} m + r_p q_p \quad (3.8)$$

where:

r_p is the product volume fraction (-)

T_p is the product temperature ($^{\circ}\text{C}$)

T_a is the air temperature ($^{\circ}\text{C}$)

h_T is the heat transfer coefficient ($\text{W m}^{-2} \text{ }^{\circ}\text{C}^{-1}$)

h_{fg} is the heat of evaporation (J kg^{-1})

q_p is the product heat of respiration (W m^{-3})

$C_{p,p}$ is the specific heat capacity of product ($\text{J kg}^{-1} \text{ }^{\circ}\text{C}^{-1}$)

A_{space} is surface area of particle (m^2/m^3); m is moisture condensation ($\text{kg m}^{-3} \text{ s}^{-1}$).

1).

The inconsistency in density that occur as the result of buoyancy can be solved by treating the fluid as an ideal gas (Norton and Sun, 2006).

$$\rho = \rho_{\text{ref}}[1 - \beta(T - T_{\text{ref}})] \quad (3.9)$$

$$\rho = \frac{\rho_{\text{ref}}W_a}{RT} \quad (3.10)$$

where:

β is the thermal expansion coefficient (K^{-1})

W_a is the molecular weight of air ($kg \text{ kmol}^{-1}$).

T is the temperature (K)

T_{ref} is the reference temperature (K)

ρ is the density ($kg \text{ m}^{-3}$)

ρ_{ref} is the reference density ($kg \text{ m}^{-3}$)

R is the universal gas constant ($J \cdot K^{-1} \cdot \text{mol}^{-1}$)

The inconsistency that could arise due to the application of Navier-Stokes equations in the food industry can be incorporated into models (Norton and Sun 2006). However, most unit operations in food processing are eddy-flow (Ambaw et al., 2013; Mishra and Aharwal, 2018).

3.3.2.6 Turbulence models

In the case of turbulence modelling, the most common method is the Reynolds Average Navier-Stokes (RANS) equations (Reynolds, 1895). Therefore, standard k-epsilon ($k-\epsilon$) model is mostly used in air flow modelling (Tolesa, 2018).

Eddy viscosity (η_t) can be calculated using eddy constant (C_η) and turbulent kinetic energy (k) by varying velocities and energy degeneracy (ε) (Mishra and Aharwal, 2018).

$$\eta_t = \rho C_\eta \frac{k^2}{\varepsilon} \quad (3.11)$$

where:

η_t is the Eddy viscosity ($m^2 s^{-1}$)

C_η is the Eddy constant

k is the turbulence kinetic energy (k J)

ρ is the density ($kg\ m^{-3}$)

There are three turbulence models which includes the Low Reynolds Number (LRN) k- ε , ordinary K- ε , and Renormalization Group (RNG) k- ε (Mishra and Aharwal, 2018).

$$\frac{\partial(\rho k)}{\partial t} + \nabla(\rho u_i k) - \nabla \left[\left(\mu + \frac{\mu T}{\delta k} \right) \nabla k \right] = P + G - \rho \varepsilon \quad (3.12)$$

$$\frac{\partial(\rho \varepsilon)}{\partial t} + \nabla(\rho u_i \varepsilon) - \nabla \left[\left(\mu + \frac{\mu T}{\delta \varepsilon} \right) \nabla \varepsilon \right] = C_1 \frac{\varepsilon}{K} (P + C_3 \max(G, 0)) - C_2 \rho \frac{\varepsilon^2}{K} \quad (3.13)$$

where:

P is the shear production rate ($N\ m^{-2}\ s^{-1}$)

G is the turbulent generation rate ($N\ m^{-2}\ s^{-1}$)

k is the turbulent energy ($m^2\ s^{-2}$)

ε is the turbulence dissipation rate ($m^2\ s^{-3}$)

ρ is the density ($kg\ m^{-3}$)

μT is the turbulent viscosity ($kg\ m^{-1}\ s^{-1}$)

μ is the air/fluid viscosity ($kg\ m^{-1}\ s^{-1}$)

C_1, C_2, C_3 are model constants (-)

u_i is velocity x - direction ($m\ s^{-1}$) and

t is time (s).

3.3.2.7 Storage chamber modelling

When modelling storage conditions within an evaporative cooling chamber, the chamber can be considered as a system with multiple flows (water vapour, fluid density, latent heat of vaporization, water droplet, and air velocity) at different stages (Langlands and Henry, 2005). This analogy can be used for mass fraction and water vapour modelling using the Mishra and Aharwal model that predicted these multiple internal flows accurately (Mishra and Aharwal, 2018).

$$\frac{\partial \rho X_a}{\partial t} + \frac{\partial}{\partial x_j} \rho u_j X_a = \frac{\partial}{\partial x_i} \rho D_a \frac{\partial}{\partial x_i} X_a + r'_a \quad (3.14)$$

where:

X_a is the mass fraction water vapour ($kg\ m^{-3}\ s^{-1}$)

r'_a is the condensation or evaporation ($kg\ m^{-3}\ s^{-1}$)

U is the velocity ($m\ s^{-1}$)

ρ is the density ($kg\ m^{-3}$)

D is the diffusion term ($m^2\ s^{-1}$)

The water droplets, dispersions of particles, drying and disinfectants as the result of solid- liquid interactions can be modelled using the Lagrangian model that account for all the inconsistencies (Mishra and Aharwal, 2018).

$$m_p \frac{du_{pi}}{dt} = F_i \quad (3.15)$$

where:

m_p is the particle mass (kg),

u_{pi} is the particle velocity ($m\ s^{-1}$)

F_i is the total force of particle (N).

3.3.3 Airflow, heat, and mass transfer modelling

In evaporative cooled storage rooms, the flow can be treated as multiphase. The dimensionless parameters along with temperature and relative humidity can be solved using turbulent k- ϵ model (Tolesa 2018). The turbulent k- ϵ model is an inbuilt model that can be used to solve for the dimensionless parameters as presented below.

$$N_n = k_{c,n}(C_{n,s} - C_{n,bulk}) \quad (3.16)$$

$$Sh = \frac{k_{c,i}d_p}{D_i} = 2 + 0.6Re_d^{1/2}Sc^{1/3} \quad (3.17)$$

where:

N_n is the mass ($mol\ m^{-2}\ s^{-1}$)

$C_{n,s}$ is concentration of species ()

$C_{n,bulk}$ is concentration in the fluid bulk particle ()

Sh is the Sherwood number (dimensionless)

$k_{c,i}$ is the convective mass-transfer coefficient ($m s^{-1}$)

$k_{c,n}$ is the evaporative mass transfer coefficient ($m s^{-1}$)

Re_d is the Reynolds number

d_p is the length (m)

D_i is the diffusivity ($m^2 s^{-1}$)

Sc is the Schmidt number (dimensionless).

The heat transfer and particle heat balance were calculated using the below equations

(Andersson et al., 2012)

$$Nu = \frac{hd_p}{\lambda} = 2 + 0.6Re_d^{1/2}Pr^{1/3} \quad (3.18)$$

$$m_p C_p \frac{dT_p}{dt} = hA_p(T_{bulk} - T_p) + \frac{dm_p}{dt} h_{fg} + R\Delta H + A_p \epsilon_p \sigma (T_{surr}^4 - T_p^4) \quad (3.19)$$

where:

Nu is the Nusselt number()

h is the convective heat transfer coefficient ($W m^{-2} K^{-1}$)

d_p is the particle diameter (m)

ΔH is the reaction enthalpy (kJ)

m_p is the mass of particle (kg)

c_p is the Specific heat capacity of air ($J\ kg^{-1}\ K^{-1}$)

h_{fg} is evaporation enthalpy (kJ)

R is rate of reaction (/s)

ϵ is the porosity ()

σ is the conductivity ($S\ m^2$)

A_p is surface area of the particle (m^2)

M_p is the mass of the particle (kg)

T_{bulk} is the bulk temperature (k)

A_p is the particle area (m^2)

T_{surr}^4 is the surrounding temperature (k)

T_p is the particle temperature (k)

3.4 Energy conservation in evaporative chamber

The theory behind the energy conservation equation of cooling systems was categorized as energy transfer from produce to fluid (Nahor et al. 2005). Due to respiration heat of the produce, energy and heat configuration between fruits and vegetables interface, condensation and evaporation occurs as the temperature and energy gradient becomes the driving force (Nahor et al., 2005).

3.5 Convective cooling

The theory of heat transfer can best be described as an operation that occurs repeatedly as heat is spontaneously transferred between bodies. During storage, the unsteady-state heat transfer occurs as temperature changes. Conversely, a steady-state heat transfer occurs when temperatures do not change. This process can be categorized either as conduction, radiation, or convection. Convective cooling is a heat transfer process that occurs because of fluid motion either naturally or by the application of force (Putra et al., 2003; Singh and Paul, 2006). During forced convection, fluid movement is influenced by external force. Depending on the extent of the applied force, the flow can either be laminar or turbulent. In the case of turbulent flow, cold and hot air can be perfectly mixed with greater drop in pressure and flow rate. Therefore, forced convective cooling from any produce surface is a function of velocity magnitude. Heat transfer coefficients from produce surfaces can be empirically predicted through dimensional analysis. Equation 3.20 can be used to calculate the correlation coefficient of the forced convection cooling.

$$Nu = a \cdot (Re)^b \cdot (Pr)^c \quad (3.20)$$

where:

a, b, and c are constants

Re is the Reynolds number

Nu is the Nusselt number ()

Pr is the Prandtl number ()

However, to account for all the parameters described above, Eq. 3.21, 3.22, 3.23 and 3.24 were considered:

$$\mathbf{Re} = \rho \cdot v \cdot L / \mu \quad (3.21)$$

$$\mathbf{Gr} = \beta \cdot g \cdot \Delta T \cdot \rho^2 \cdot L^3 / \mu^2 \quad (3.22)$$

$$\mathbf{Pr} = C_p \cdot \mu / k \quad (3.23)$$

$$\mathbf{Nu} = h \cdot L / k \quad (3.24)$$

where:

Re is the Reynolds number

ρ is the fluid density (kg m^{-3})

V is the fluid velocity (m s^{-1})

L is the surface length (m)

Gr is the Grashof number ()

Nu is the Nusselt number ()

Pr is the Prandtl number ()

μ is the dynamic viscosity ($\text{kg s}^{-1}\text{m}^{-1}$)

β is the expansion coefficient (K^{-1})

g is the force of gravitation (m s^{-2})

ΔT is the surface and fluid temperature difference ($^{\circ}\text{C}$)

C_p is the heat capacity ($\text{kJ kg}^{-1}\text{C}^{-1}$)

K is the thermal conductivity ($\text{W m}^{-1}\text{C}^{-1}$)

h is the heat transfer coefficient ($\text{Wm}^{-2}\text{C}^{-1}$)

To calculate thermal resistance in a heat transfer network, Eq. 3.25 was considered.

$$\mathbf{R}_{conv} = \frac{\nabla T}{\dot{Q}/A} = \frac{1}{h} \quad (3.25)$$

where:

A is the surface area (m^2)

∇T is the change in temperature (K)

R_{conv} is the convective resistance ($\text{W}^{-1} \text{m}$)

Q is the thermal conductivity ($\text{W m}^{-1}\text{K}^{-1}$)

h is the convection coefficient (W m k^{-1})

3.6 Evapotranspiration cooling

The Penman equation is mostly used to determine the rate of evapotranspiration due to plant canopy and requires data for light intensity, temperature, humidity, wind speed and surface characteristics (Allen et al., 1998). Monteith concept is credited for introducing bulk surface resistance that describes the resistance of vapour flow through the transpiring crop and evaporating water from soil surface (Allen et al., 1998). The resistance factors are controlled by vapour pressure, solar radiation, leaf's temperature, canopy water, vegetation height, etc. These factors can be combined to get the general Penman-Monteith equation, Eq, 3.26 (Schymanski and Or, 2017).

$$E = \frac{\Delta}{\Delta\gamma} \frac{R_n}{\lambda} + \frac{\gamma}{\Delta+\gamma} F(u) D \quad (3. 26)$$

where:

Δ is the vapor pressure or temperature ($h Pa K^{-1}$)

Γ is the psychrometric coefficient ($0.67 h Pa K^{-1}$)

D is the air pressure deficit ($h.Pa$)

λ is the latent heat of vaporization ($2460 KJ kg^{-1}$)

$F(u)$ is the wind speed ($m s^{-1}$)

E is the reference evapotranspiration ($mm s^{-1}$)

γ is the psychrometric constant ($KPa K^{-1}$)

The psychrometric coefficient was calculated from Eq. 3.27:

$$\gamma = \gamma(1 + \frac{r_s}{r_a}) \quad (3.27)$$

where:

r_s and r_a are resistance factors

The time varying changes in real life situation makes it nearly impossible to get surface resistance from a field data. However, it is universally accepted that the surface resistance for water is zero but must be computed analytically for any other surfaces characterized by evapotranspiration if the resistance factors are known. Therefore, the Food and Agriculture Organization suggested the use of reference crop height of 0.12 m, with standard velocity, temperature, and relative humidity at 2 m.

CHAPTER FOUR

MATERIALS AND METHODS

4.1 Research area

The existing evaporative cooling chamber at Jomo Kenyatta University of Agriculture and Technology (JKUAT) was used for this research. JKUAT is in Juja, Kiambu County, Kenya, with an annual average temperature of 19.6 °C and an annual average rainfall of 799 mm. The geographic coordinates of JKUAT are at a longitude of 37° 01' East and latitude of 1° 11' South; with an average elevation of 1,550 m above sea level (Mahabir et al., 2017; Sow et al., 2020).

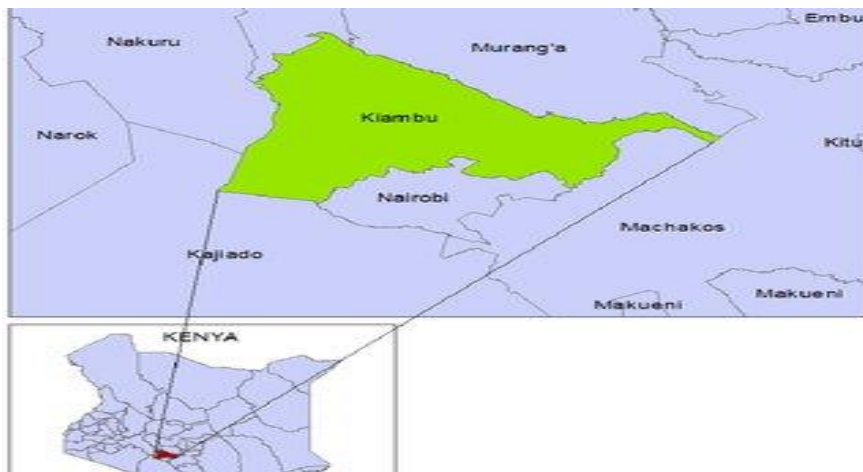


Figure 4.1 The map of Kenya showing the study area (Musa and Odera, 2015)

4.2 Experimental setup

The design of the front, rear, left, and right sides were determined using Eq. 4.1 for the four equal sides.

$$A_{\text{front}} = A_{\text{rear}} = A_{\text{left}} = A_{\text{right}} = H_c \times L_c \quad (4.1)$$

where:

A_{front} is the front side area (m²)

A_{rear} is the rear side area (m^2)

A_{left} is the left side area (m^2)

A_{right} is the right-side area (m^2)

H_c is the height of cooler (m)

L_c is the length of cooler (m)

The design of the top and floor were done using Eq. 4.2 with the top floor having equal dimensions.

$$A_{top} = A_{floor} = L_c \times W_c \quad (4.2)$$

where:

A_{top} is the top area (m^2)

A_{floor} is the floor area (m^2)

L_c is the length of the cooler (m)

W_c is the width of the cooler (m)

4.2.1 Capacity of the storage chamber

The capacity of the cooler was calculated using Eq. 4.3 and was the same as the volume of the storage space.

$$V_c = L_c \times W_c \times H_c \quad (4.3)$$

where:

V_c is the volume of the cooler (m³)

L_c is the length of the cooler (m)

W_c is the width of the cooler (m)

H_c is the height of the cooler (m)

4.2.2 Fan capacity calculation

The floor fans capacity was calculated according to Eq. 4.4 (Kumar et al., 2018).

$$\text{Fan capacity} = 0.23 \text{ m}^3/\text{min} \times \text{floor area} \quad (4.4)$$

A 10% safety factor for the fan capacity was given as Fan capacity \times 10/100

Therefore, required fan capacity was fan capacity plus factor of safety

4.2.3 The evaporative cooling chamber

The evaporative cooling chamber at JKUAT had four equal sides with a wider surface area for air circulation. The cooler contained a reservoir below it to retain water and two fans to support convective cooling and prevent condensation. The top was covered with corrugated iron sheet that was covered with soil that allows plants to grow to enhance evapotranspiration. The walls of the cooling chamber were made of porous media (pumice) and serves as a cooling pad. The main frame of the cooler was made with iron poles, supported with wire mesh (\varnothing 0.24 mm) that held the pumice. On top of the corrugated iron sheets, cowpeas were planted to support cooling through evapotranspiration (Fig. 4.2).

Plants canopy also provide cooling to the environment through the process of photosynthesis.

The storage chamber at JKUAT was design to incorporate this effect and for this purpose, the

topsoil is provided to support plants with herbaceous roots grow. The cooling effect of these crops was then transfer to the storage space to provide a conducive environment for storage.

Inside the cooler, there were two 12 V DC Denso plastic fans, model 2406KL-04W-B56, manufacture by MINEBRA Industrial Co. Limited, China. Each cooling had a speed of 9000 radian per minute (RPM) and frequency of 25 – 30 Hz, with seven blades and was mounted on the floor of the cooler to blow air upwards with the swept depth diameter of 0.0012 m. The purpose of these fans was for convective cooling and for prevention of condensation during extreme cold weather conditions. Right below these fans was a reservoir to prevent water splash. The water was later returned to the overhead tanks. There were three water tanks, all above the evaporative cooling chamber that were used through piping to supply water to evaporation walls. A 12 volts shurflo pump with capacity of $2.244 \times 10^{-4} \text{ m}^3 \text{ s}^{-1}$ and 2.7 m head (model 2088-443-144, made in Mexico) was used to pump water from the reservoir back into the overhead tank while water passing through the pumice was drained back into the reservoir. The walls of the cooler were kept constantly wet through PVC pipes with diameter 0.0127 m that were connected to the overhead tanks. These tanks were placed 2.5 m above the ground: each with a storage capacity of 0.1 m^3 .



A. Left and front view

B. Right and top view

C. The cooler outside look

Figure 4.2 Photographic views of the evaporative cooling system

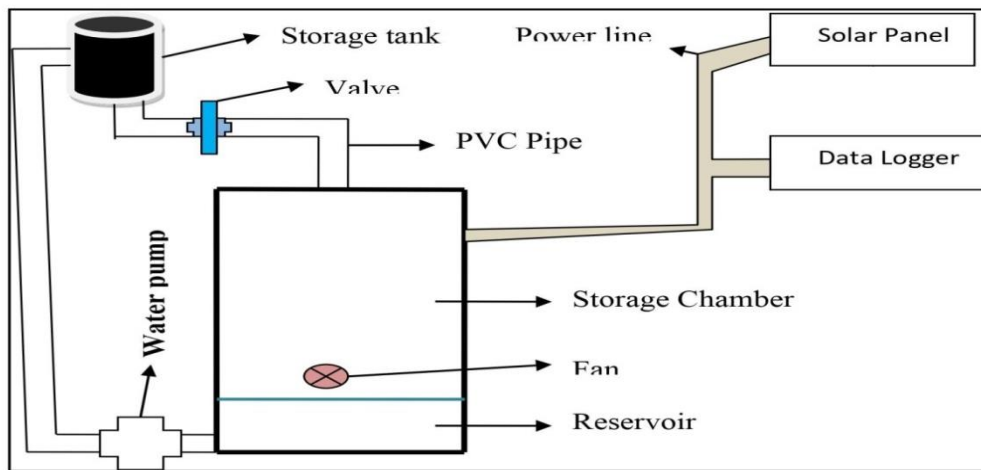


Figure 4.3 Schematic diagram of the cooling system

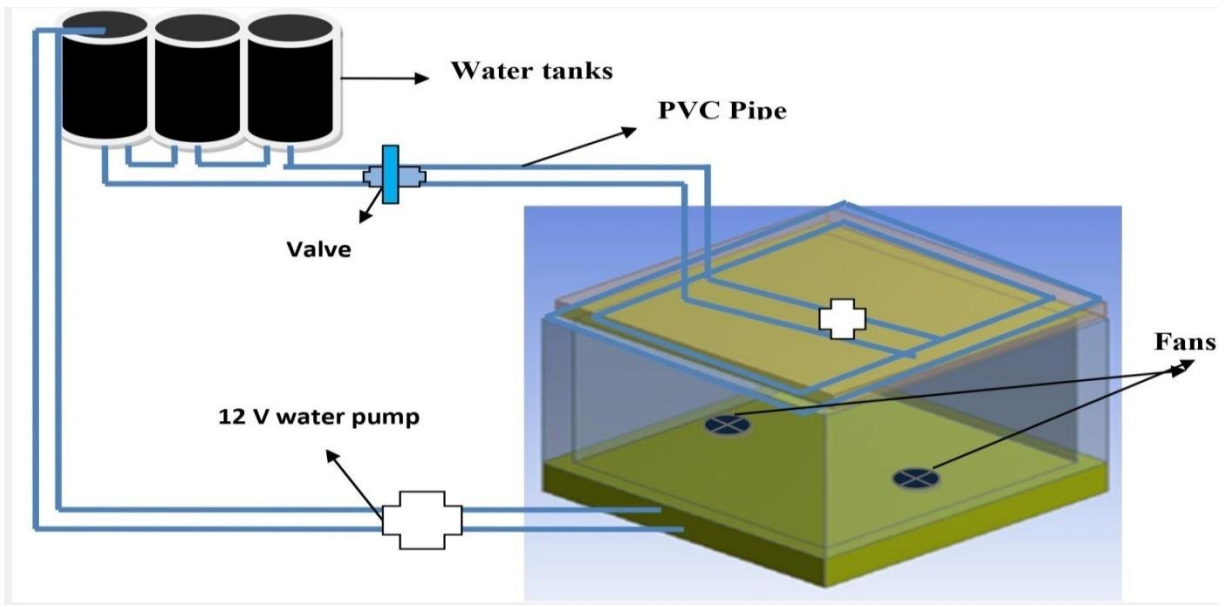


Figure 4.4 Schematic of the water distribution network

The geometrical dimensions of the cooler were 2.7 m (L) x 2.7 m (B) x 2m (H) for length, breath, and height respectively. The wall has a uniform thickness (cooling pad) of 0.15 m, including the door that was made from the same material (pumice).

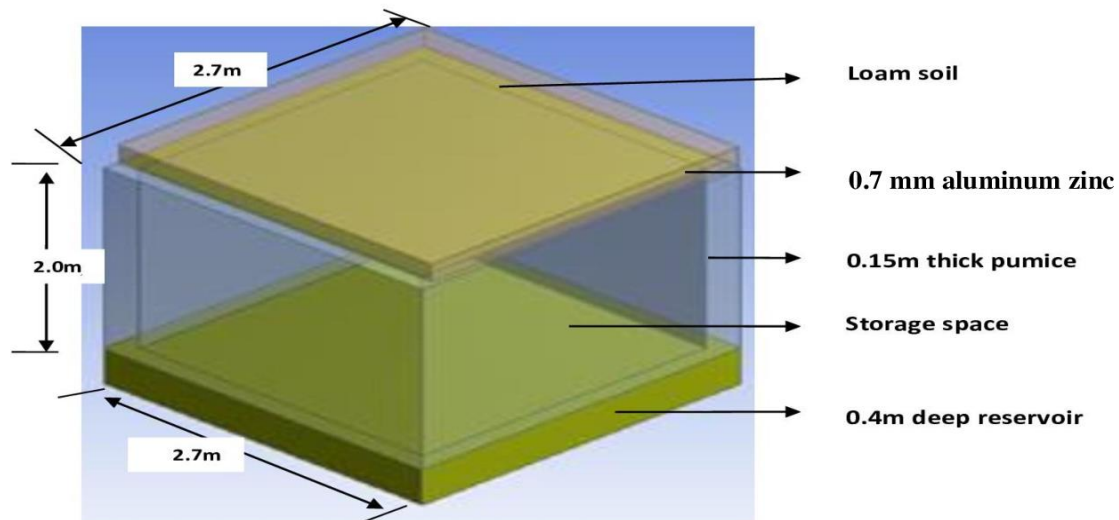


Figure 4.5 The schematics of the storage chamber in three-dimensional view

4.2.4 Design of the solar power system

The installed floor fans and water pump had the following specifications: Voltage rating of 12V, Current of 0.15A and Power rating of 1.8W. These specifications were used to select the storage battery and solar panel for the continuous running of the system during night hours. The solar panel selected had the following specifications: voltage of 17.6V, current of 7.1A and power of 125W. The 125W solar panel along with the 50 Ah storage battery were sufficient to power the Arduino nano data logger (DS3231 RTC Module), Shurflo water pump (Mode 2088-443-144, Mexican made), and 12 V DC Denso plastic fans continuously.

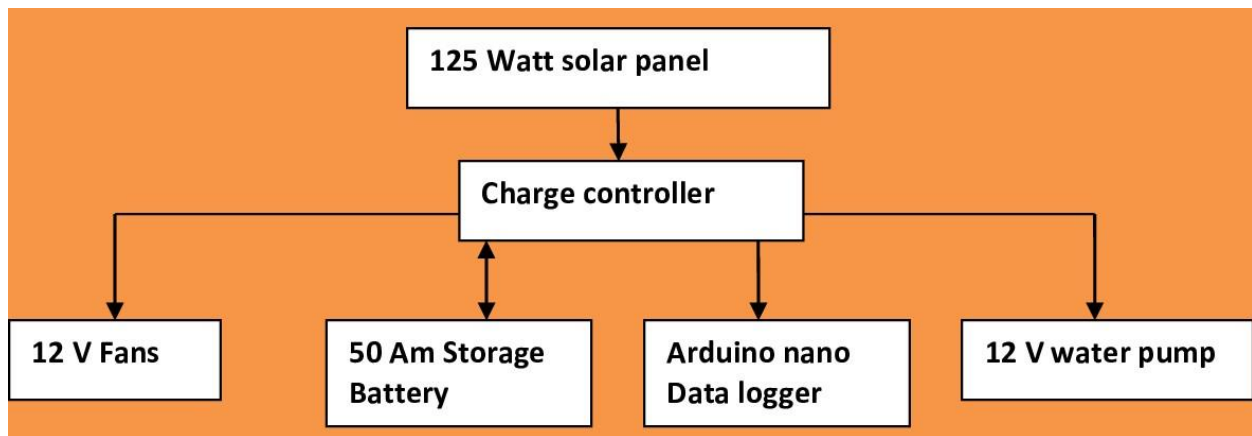


Figure 4.6Schematic of the Power distribution network

4.3 Data collection from the physical model

The experimental data was collected using an Arduino nano data logger. The hardware components of the data logger included the Arduino motherboard, SD card, and the display screen. Other accessories were temperature and relative humidity sensors, digital anemometer, and solar radiation sensor. The system was installed outside the storage chamber and the data logger automatically recorded temperature, relative humidity, solar intensity, and wind speed for every 30 seconds, average it for every 30 minutes and stored it on the SD card.

4.3.1 Solar radiation

Because temperature is driven by the amount of sunshine reaching the earth, the light intensity was one of the parameters of interest for this study. One solar radiation sensor (model; LRD Shenzhen) was positioned outside, above the storage chamber, to measure solar radiation. The LRD sensors had an operating temperature of negative 30 to positive 70 °C and calibrated using a Cr1000 data logger.

4.3.2 Wind speed

Since evaporation is a function of air velocity, the wind speed was measured to know the level of air passing through the pumice pore spaces that humidified and cooled the storage chamber. The digital anemometer (model; GM8901, Qingdao) was used to measure the outside wind with a performance rating of up to 45 m/s with an error of $\pm 3\%$. GM8901 Digital Anemometer was calibrated using a Cr1000 data logger. This model was chosen due to the constant change in wind speed and direction in Juja community, particularly during the period of the data collection. Unlike other anemometers, the GM8901 Qingdao is capable of recording zero wind velocity.

4.3.3 Temperature and relative humidity

There were ten temperature and relative humidity (T&RH) sensors (DHT11) connected to Arduino motherboard to measure the temperature and humidity. Out of the ten DHT11 sensors, nine of them were placed in the chamber to measure storage temperature and storage humidity. The nine DHT11 sensors were strategically placed at specific locations. The first one was placed in the middle of the cooler at 10cm (y-direction) from corrugated iron sheet ceiling, 120 cm (x-direction) from the walls, and 190 cm (z-direction) from the floor. Additional four sensors were

placed at the upper corners at 12cm (x-direction) from walls, 50 cm (y-direction) from the ceiling, and 150cm (z-direction) from the floor. The other four were placed at the lower end corners of the cooler at 12cm (x-direction) from the wall, 145 cm (y-direction) from corrugated iron sheet ceiling, and 55 cm (z-direction) from the floor. Lastly, one DHT11 was placed outside the storage chamber to measure ambient temperature and ambient relative humidity and was positioned above the storage chamber. The purpose of putting DHT11 sensors at different and specific locations inside the cooler was to have a better understanding of the uniformity of temperature and humidity inside the cooler. The average values from the inside were compared with the outside to know the system was reducing temperature and increasing relative humidity.

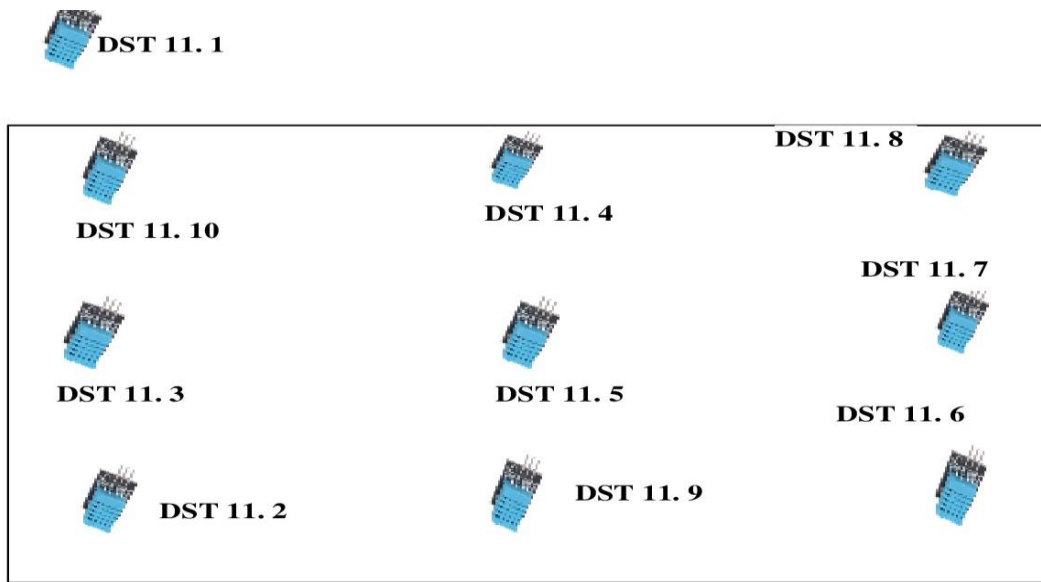


Figure 4.7A schematic diagram showing temperature and relative humidity sensors at data collection points

4.3.4 Data collection

Different set of data were collected from February 18 to April 6, 2020, for no load performance testing of the storage chamber. The cooler was not subjected to artificial influence as data was collected for seven days (February 18 to the 24, 2020) from 8:00 AM to 6:00 PM with a total

data point of 3,234 (DHT11: 1,470 for both relative humidity and temperature; GM8901 Digital Anemometer 147 wind speed data points and solar radiation Sensor 147 solar radiation data points).

The same setup and duration were followed for convective cooling (from February 25 to March 2, 2020), and evapotranspiration cooling (from March 20 to 26, 2020), thereby recording 3,234 samples each.

For evaporative cooling, data was collected for eight days (March 6 to 13, 2020) and recorded total data samples of 3,696. Finally, the three artificial influences on the cooler were operated as a single system for eleven days (March 27 to April 6, 2020) and recorded total data samples of 5,082.

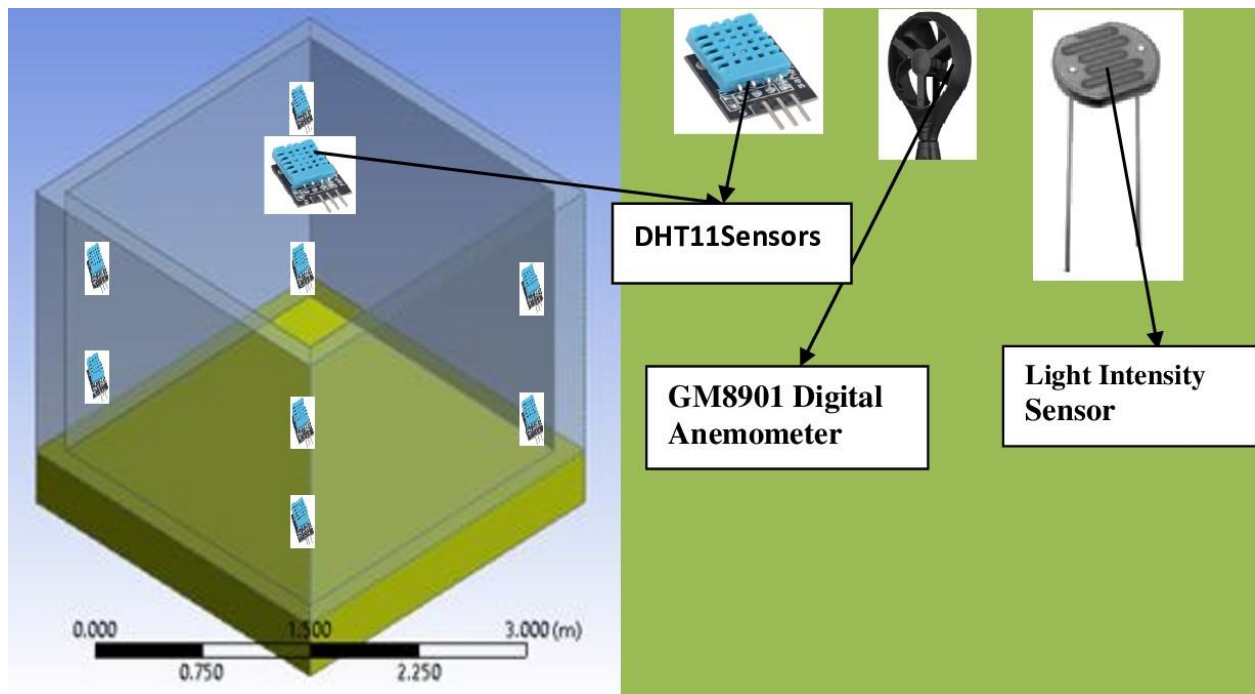


Figure 4.8Data collection points for both ambient and storage chamber

4.3.5 Saturation efficiency

The efficiency of an evaporative cooler depends on the rate of water evaporation from the

cooling pad. The evaporation is principally controlled by temperature and the degree of saturation. In this design, pumice was selected as the cooling pad with 0.15 m thickness due to its high porosity, and water retention quality. The effectiveness of the pumice(pad) was based on the cooling efficiency. The saturation efficiency (S_E) of the pumice was calculated using Eq. 4.5.

$$S_E = \frac{T_1(db) - T_2(db)}{T_1(db) - T_1(wb)} \quad (4.5)$$

where:

S_E is the saturation efficiency (%)

$T_1(db)$ is the dry bulb outdoor temperature ($^{\circ}C$)

$T_2(db)$ is the dry bulb cooler temperature ($^{\circ}C$)

$T_1(wb)$ is the wet bulb outdoor temperature ($^{\circ}C$)

4.3.6 Performance of the cooling chamber

The storage chamber performance was evaluated by comparing ambient to storage conditions. The temperature and relative humidity for each given period of data collected was plotted on a graph to visualize the differences.

4.4 Mathematical modeling

The evaporation of moisture was calculated using the lumped model (Eq.3.7). Inside storage chamber, temperature was calculated using Eq. 3.8. The inconsistencies in density due buoyancy were solved using Eq. 3.9 and 3.10

In the case of turbulence modelling, the standard k-epsilon (k-ε) model was used, and Eddy viscosity was calculated using eddy constant (Eq. 3.11). For air modelling within an evaporative cooling chamber, Eq. 3.14 was used, and the water droplet was calculated using Eq. 3.15.

In evaporatively cold rooms, the flow can be treated as multiphase. The dimensionless parameters along with temperature and relative humidity were solved by turbulent k-ε model (Eq. 3.16, 3.17, 3.18, and 3.19).

4.4.1 Heat transfer Analysis

Heat transfer analysis of the materials used for the construction of the storage chamber was estimated using Fourier's law of heat conduction.

$$\mathbf{q} = -k\nabla T \quad (4.6)$$

where:

q is the local heat flux density ($W m^{-2}$)

k is the thermal conductivity of the material ($W m^{-1}K^{-1}$)

∇T is the temperature gradient ($K m^{-1}$)

4.4.2 Computational Fluid Dynamics Simulation

4.4.2.1 Computational Fluid Dynamics Software

The student Academic ANSYS FLUENT 2019R2 was used to model the chamber. FLUENT uses advanced flow analysis software for quick simulation (Kapilane et al., 2016). FLUENT was used to simulate temperature within the evaporative cooling system. The geometry was designed using ANSYS Design Modular, a component within ANSYS WORKBENCH.

4.4.2.2 Design of the computational geometry

The geometry was generated using ANSYS DESIGN MODULER. The storage chamber had a wall thickness of 0.15 m, and a storage space of 2.4 m x 2.4 m x 2 m. Figure 4.8 shows the three-dimensional (3-D) storage chamber geometry.

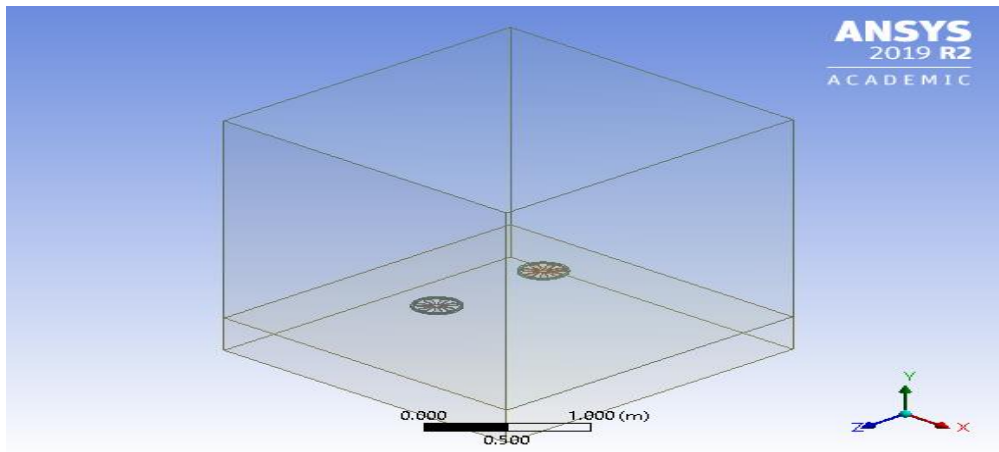


Figure 4.9 The three-dimensional geometry of the evaporative cooling chamber

4.4.2.3 Mesh generation

The computational domain was meshed with tetrahedral elements. Richardson extrapolation was used to evaluate the level of grid independency (Franke and Frank, 2008). The automatic meshing method was used to discretize the computational domain with an in-built ANSYS design modeler-meshing algorithm set to orthogonal quality and maximum skewness of 0.9. The mesh density was refined to minimum and maximum element sizes of 0.05m and 0.1m respectively. Along the wall surfaces, five inflation layers were employed, the first element was 0.05m and a growth ratio of 1.2, with the maximum of 0.1m. Mesh independence study was done to test validity and quality of discretization, and the purpose was to ensure an accurate solution regardless of the mesh size. To conduct a grid independence test, the solutions were obtained with multiple mesh sizes and their outcomes observed.

4.4.2.4 Discretization and solution scheme

To solve the mathematical equations, the computational domain was prepared and spatially discretized to very small elements that represented the control volumes. The discretized equations were integrated and solved with control volume method. The integration obtained a discretized system of equations that were solved iteratively for each control volume. The solution was initially stored at the centers of the control volumes and later at the surfaces or cell phases through interpolation methods. These interpolation methods are known as spatial discretization schemes (Versteeg and Malalasekera, 2007).

4.4.2.5 Solution schemes

The solution schemes were spatially discretized with an inbuilt ANSYS FLUENT pressure-velocity coupling algorithm and because the flow was incompressible, the SIMPLE algorithm was used for faster convergence (ANSYS 2019). The second-order upwind schemes were used to interpolate pressure, energy, and momentum. These schemes were controlled with recommended relaxation factors for convergence in a reasonable time (ANSYS 2019).

4.5 The choice of turbulence model for simulation of the storage chamber

During the trial period, six different turbulence models were tested to determine their suitability for predicting temperature and relative humidity within the storage chamber. The tested models include Standard k-epsilon ($k-\epsilon$), Realizable k- ϵ , Real Normalization Group (RNG) k- ϵ , seven equations Reynolds' stress model, the Shear-Stress-Transport (SST) k-omega ($k-\omega$), and standard k-omega ($k-\omega$) model. The seven equations Reynolds stress model had a better prediction

amongst the others; however, there was a sharp increase in computational time. Therefore, the Shear-Stress-Transport (SST) $k-\omega$ model was chosen because of its reasonable computational time and accuracy compared to the other turbulence models.

4.5.1 Model boundary conditions

The thermal and momentum boundary conditions were considered based on the experimental results for temperature and air speed (Akdemiret al., 2013). For other parameters of interest, the following assumptions were made to simplify the simulation.

1. The system was at steady-state condition
2. The flow was internal, incompressible, and multiphase flow
3. Thermo-physical properties were independent of temperature

The various boundary types and conditions that were setup are presented in Table 4.1 below.

These boundary conditions were set based on average measure values and material property.

Table 4.1 The boundary conditions and types that were used to set solver for simulation

No	Boundary type	Boundary condition
1	Storage inlet	291.59 °K
2	Storage outlet	Atmospheric pressure: 11,325 Pa
3	Pumices surfaces	Heat flux
4	Insulation layers	0.15 m thick wall (gypsum); Fans (aluminum)
5	Storage environment	308.08 K Ambient temperature; 0.6 m/s wind speed
6	Zones of domain	Liquid water zone and solid gypsum zone
7	Contact regions interfaces	Coupled walls
8	Other surfaces	No-slip conditions

4.5.2 Convergence criteria

In some cases, only two conditions of quantity imbalances and stability of monitored quantities can indicate the convergence even if the condition of residuals is not completely satisfied. However, when the imbalances or monitor quantities are not satisfied, then the solution is not yet converged. The following convergence criteria were used for this study (ANSYS, 2019):

1. The overall mass and energy conservation was achieved with mass and energy imbalances of less than one percent (1%). These imbalances measured global mass and energy conservation.
2. The residuals for momentum and continuity equations dropped to less than 10^{-3} and less than 10^{-6} for energy equation.
3. The quantities of interest reached stability as indicated by the solution monitors such as the storage outlet temperature and mass flow rate. A stable monitor is when simulation results are no longer changing with further iteration.

4.6 Solving discretized governing equations

The solving process started with the importation of the generated mesh into ANSYS FLUENT and setting up the model which turn on the inbuilt governing equations that where for the calculation. The model set-up included material and fluid set-up, boundary conditions set-up, solution methods set-up. After the appropriate set-up, the model generated the results of the parameters of interest.

4.7 Post-processing

The post processing was carried out with the importation of the solution and the model was set-up to generate contours/vectors with ANSYS inbuilt algorithms to compute data at selected locations to be display over the geometry for validation.

4.8 Validation of the results

The model was validated by comparing the model-generated data against the experimental data using student t-test to determine the significance between the two data sets.

4.9 Optimization of the storage chamber

The storage chamber was optimized with the two-equation shear stress transport equation for pad thickness variation. The simulation was done using a single variable optimization method. The average values for water flow rate, wind speed and ambient temperature were held constant due to the changes in weather conditions. The pad thickness was varied from 0.05 m to 0.2 m and evaluated to understand the effect of pad thickness on cooling efficiency. Four different pad thicknesses were considered including the current design thickness of 0.15 m. The storage chamber was later optimized based on the cooling efficiency of the pad thickness.

4.10 Data analysis

The data collected from the experimental setup and model-generated data were analyzed statistically. Analysis included generation of statistical graphs and performance of statistical tests like student t-test and regression.

Statistical parameters tested for included: Correlation coefficient (R), Coefficient of determination (R^2), Mean square error (MSE), Root mean square error (RMSE), Mean relative

error (MRE), Mean absolute error (MAE), and mean absolute percent error (MAPE) (Chicco et al., 2021). A Python programming language environment, Anaconda (Kadiyala and Kumar,2017) was used for data analysis by importing appropriate packages including: Math, pandas, Numpy, Matplotlib.pyplot, sklearn.metrics, and logistic Regression. Anaconda comes with these packages included by default for scientific analyses.

CHAPTER FIVE

RESULTS AND DISCUSSION

5.1 Performance of the storage chamber

The performance of the storage chamber was carried out with an analysis of measured data at no load, for no artificial influence on the cooler, convective cooling, evaporative cooling, evapotranspiration cooling, and combined cooling system. Figures 5.1, 5.2, 5.3, 5.4, and 5.5 presents the experimental plotted against days and time.

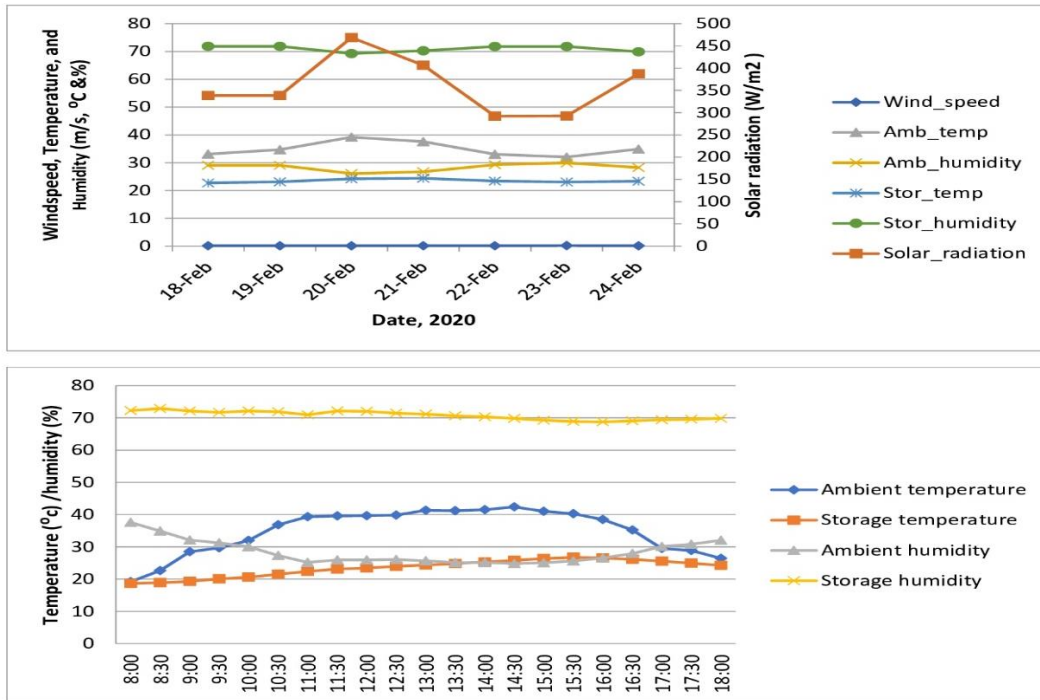


Figure 5.1 Plots showing average values from 8 AM – 6 PM daily for no cooling

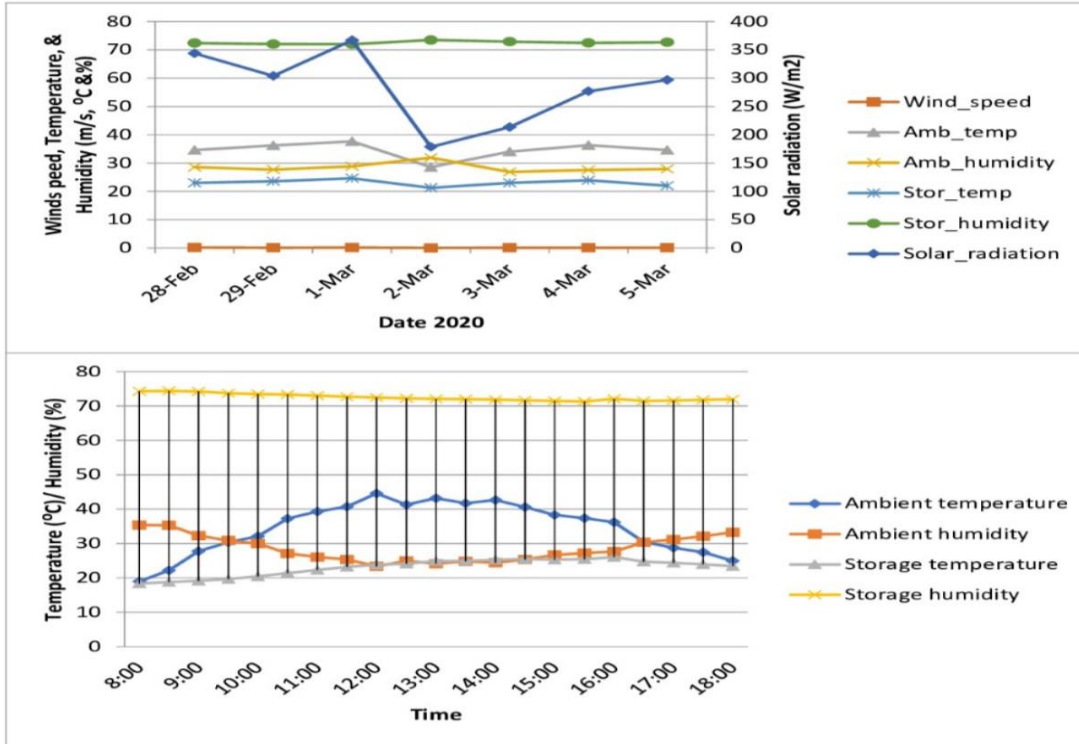


Figure 5.2 Plots showing average values from 8 AM – 6 PM daily for convective cooling

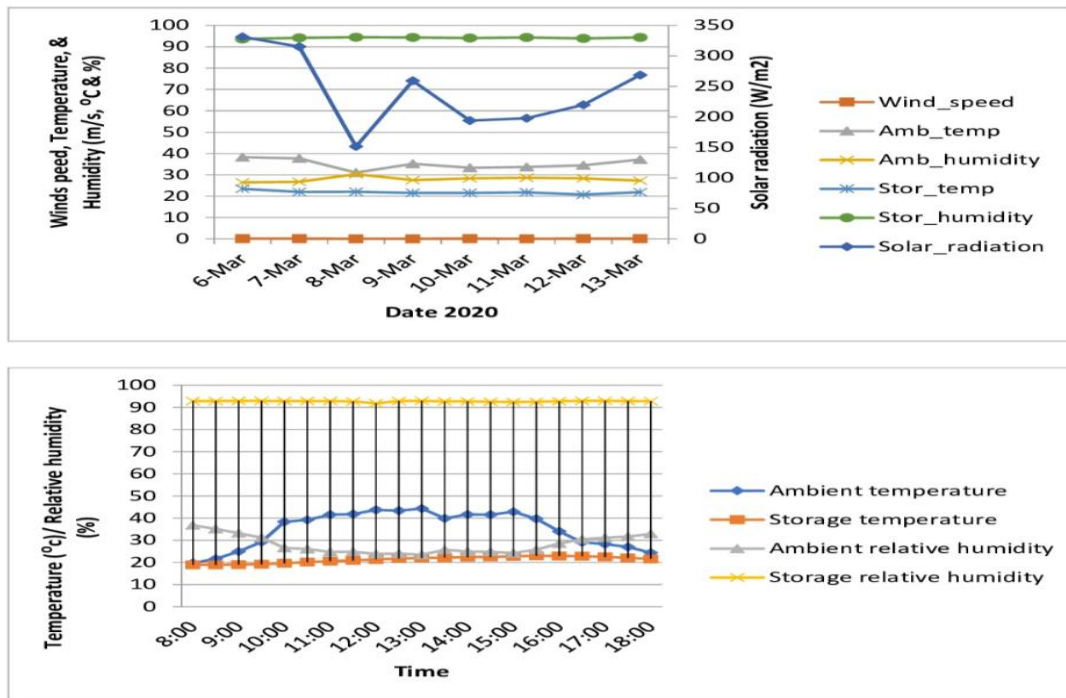


Figure 5.3 Plots showing average values from 8 AM – 6 PM daily for evaporative cooling

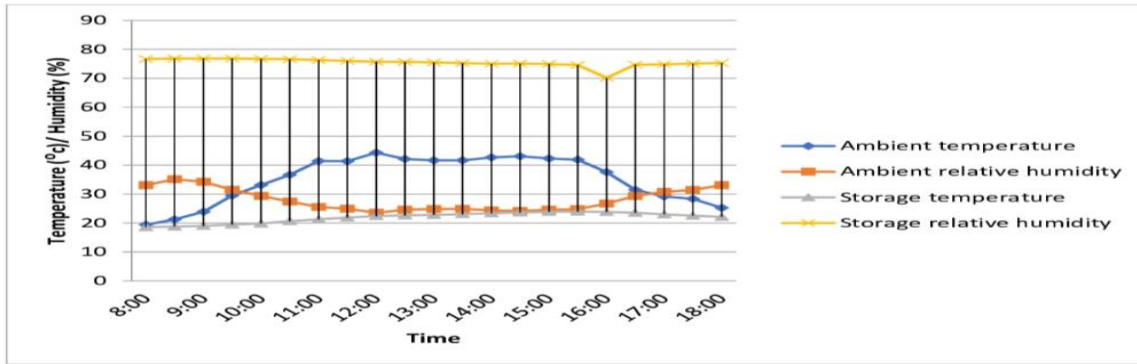
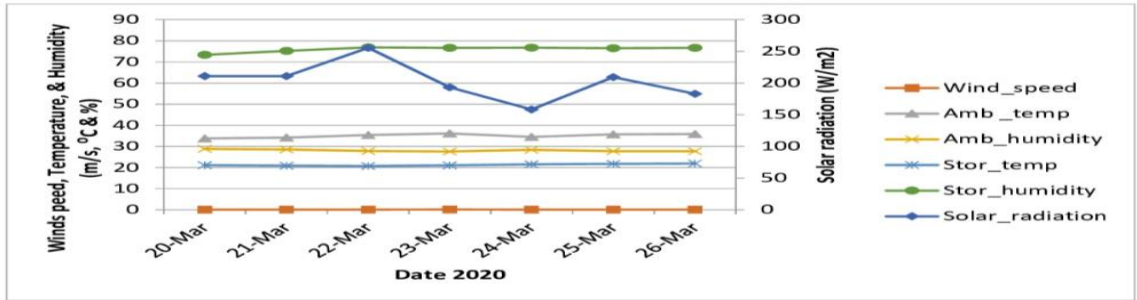


Figure 5.4 Plots showing average values from 8 AM – 6 PM daily for evapotranspiration cooling

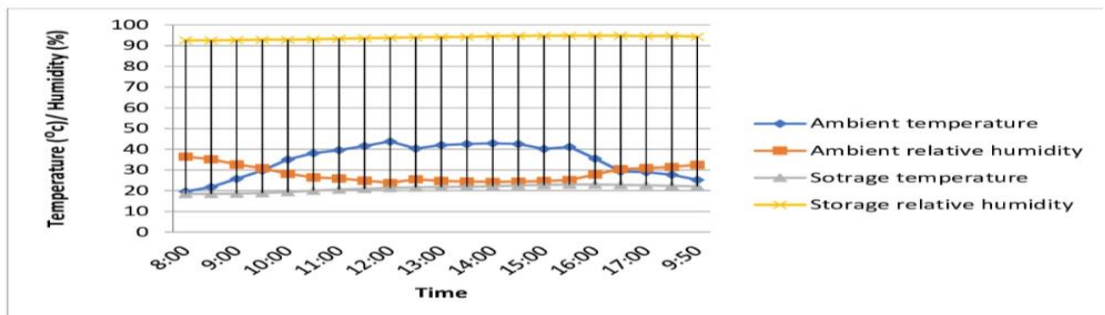
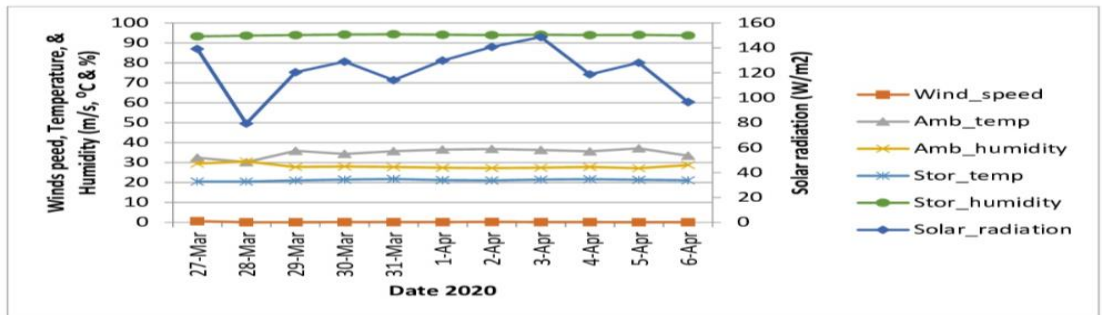


Figure 5.5 Plots showing average values from 8 AM – 6 PM daily for combined cooling system

5.1.1 The cooling chamber with natural convection

The ambient data against chamber data is presented in Fig. 5.6 for average daily temperature and average daily relative humidity as was measured in the period from February 18 – 24, 2020, between 8:00 AM to 6:00PM respectively.

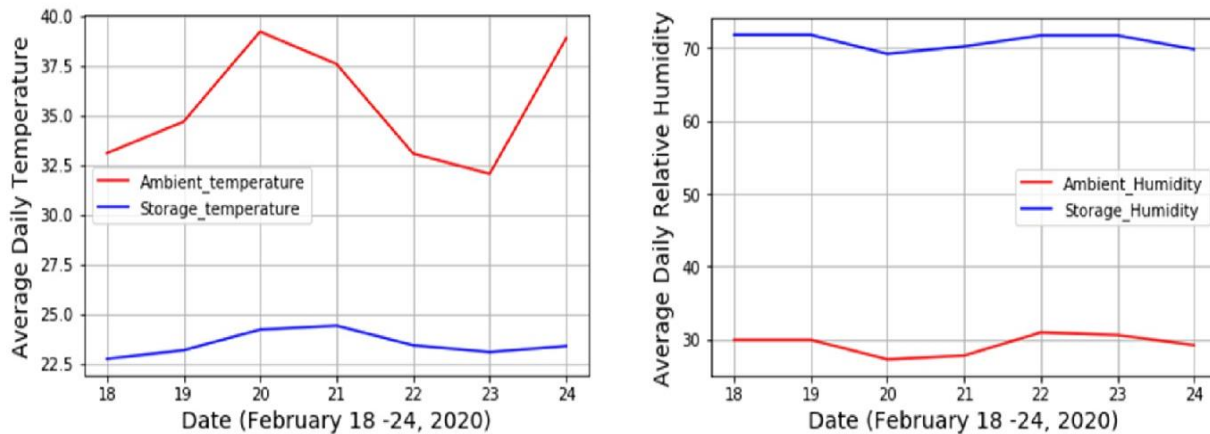


Figure 5.6Trends of daily averages of temperature and relative humidity from 8AM – 6PM

Figure 5.6 shows that during the period of data collection, the ambient temperature was quite different for each day. This difference in ambient temperature resulted in a corresponding change in ambient relative humidity. The days with higher temperature show a strong correlation with high solar radiation as show in Fig. 5.1. The average ambient temperature as shown in Fig. 5.6 was 34.93 °C and the average ambient relative humidity was 28.34%. Similarly, the storage temperature recorded from 8:00 Am to 6:00 PM ranged from 18.64 to 26.73°C and storage relative humidity ranged from 68.75 to 72.91%. The average storage temperature and relative humidity were 23.46 °C and 70.78 % respectively. The temperature and relative humidity difference were 11.47 °C and 42.44% respectively. Based on the temperature difference, the psychometric chart was used to find the wet bulb temperature (21.1 °C) that was used to calculate the saturation efficiency (Eq. 4.5). The saturation efficiency of the storage chamber without any form of cooling was 83%. Figure 5.7 presents time changes in temperature and relative humidity from 8:00 AM to 6:00PM.

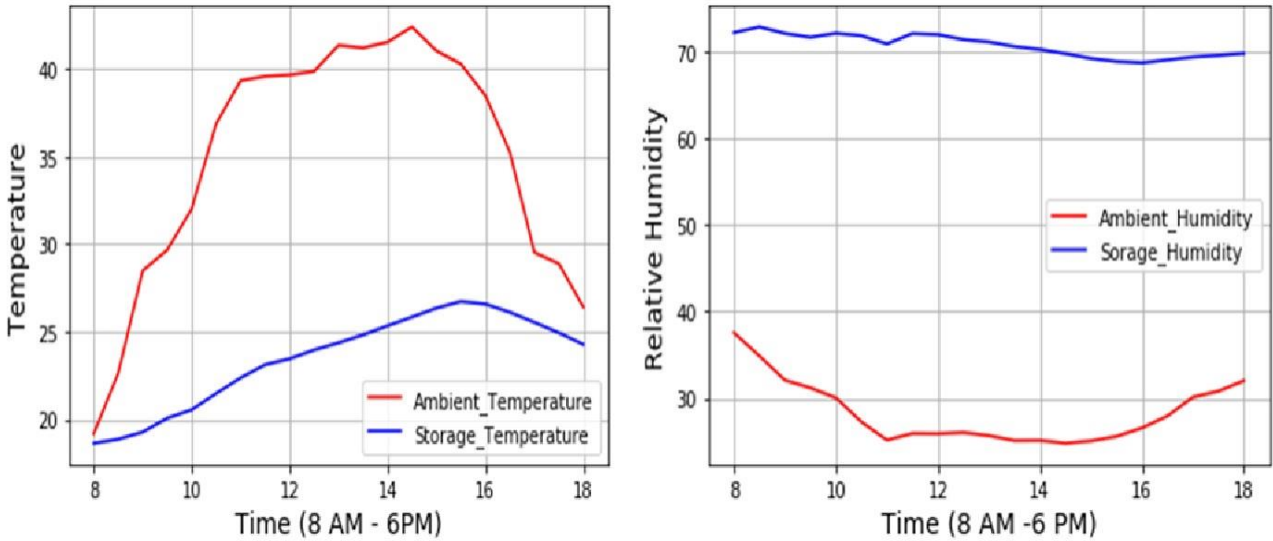


Figure 5.7Trends of hourly averagesof temperature and relative humidity from 8AM - 6PM.

Figure 5.7 above shows that an increase in ambient temperature leads to a decrease in ambient relative humidity. On the other hand, as the ambient temperature raises, the storage temperature also increased linearly with time as the storage relative humidity increases. This situation is the validation of the principle of evaporative cooling. On the temperature plot, the highest temperature was recorded around 2PM for all the days combined.

5.1.2 Performance evaluation of convective cooling applied to the cooler

The second set of data were collected when the fans were turned on as ambient and storage chamber data was recorded (Fig.5.2). There was significance difference between the ambient temperature and storage temperature on one hand and ambient relative humidity and storage relative humidity on the other hand. These differences were based on factors like, the switching on of the fans, and the weather condition. The test was carried out from February 28, 2020, to March 5, 2020. The ambient data against storage data is presented in Fig. 5.8 for average daily temperature and average daily relative humidity from 8:00 AM to 6:00PM respectively.

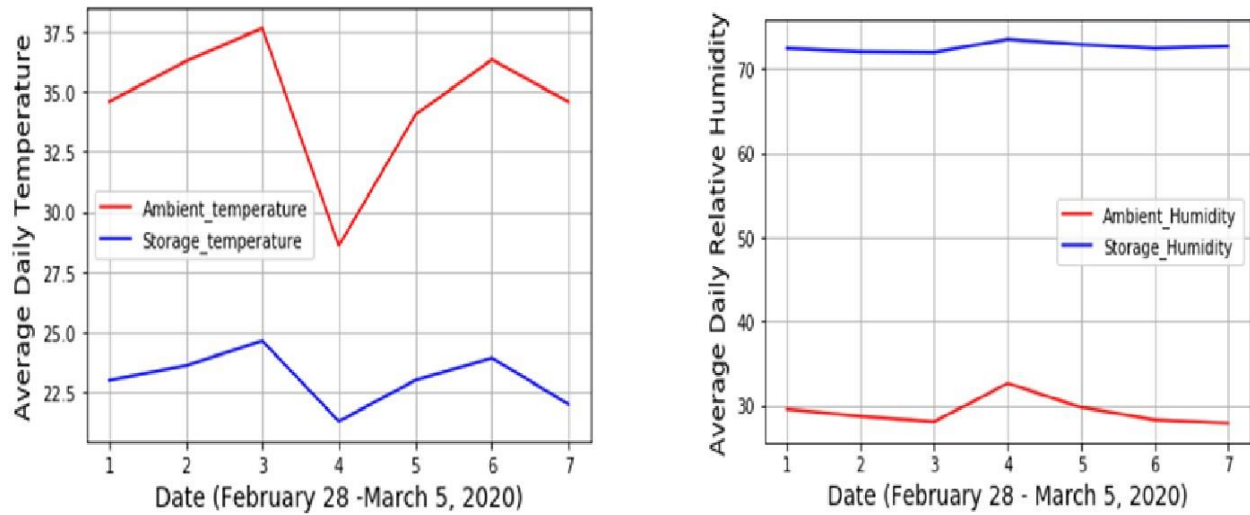


Figure 5.8 Trends of daily averages temperature and relative humidity for convective cooling

Figure 5.8 shows that ambient temperature was quite different for each day. This difference in ambient temperature resulted in a corresponding change in ambient relative humidity, thereby affecting the storage condition. The days with higher temperature show a strong correlation with high solar radiation. The average ambient temperature as shown in Fig. 5.8 was 34.58 °C and the average ambient relative humidity was 28.46%. Similarly, the storage temperature recorded at thirty minutes interval from 8:00 AM to 6:00 PM ranged from 18.37 to 26.06 °C and storage relative humidity ranged from 71.31 to 74.39%. The average storage temperature and relative humidity for the time mention were 23.1 °C and 72.52 % respectively. A further 0.36 °C decreased in temperature and an increase 1.74% in relative humidity was because of fans. The average temperature and relative humidity difference were 11.48 °C and 44.06% respectively. The wet bulb temperature was determined from the psychrometric chart (21.1°C) and the saturation efficiency was 85%. Figure 5.9 presents time changes in temperature and relative humidity from 8:00 AM to 6:00PM.

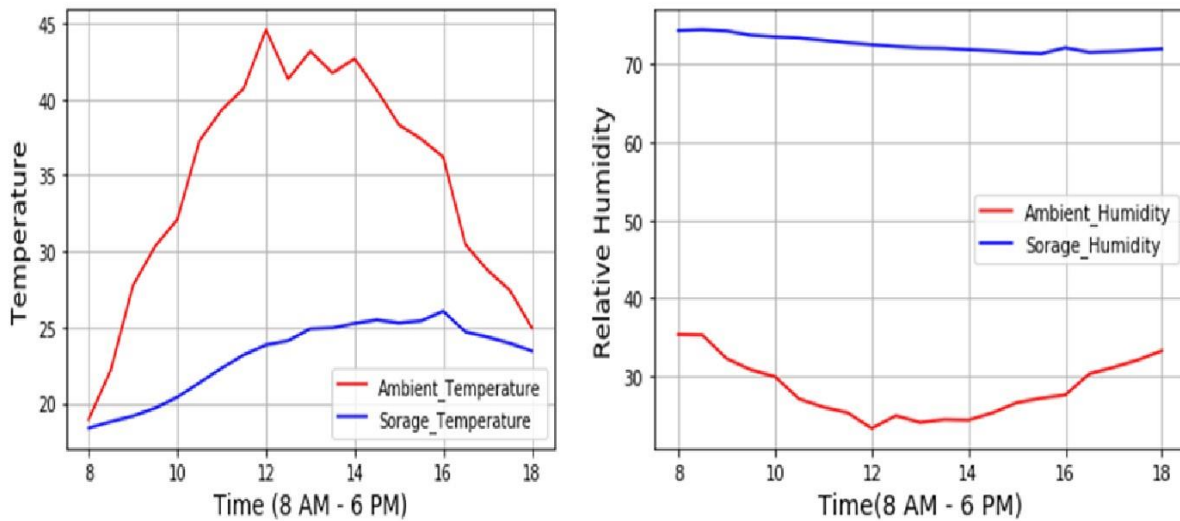


Figure 5.9 Trends of hourly averages of temperature and relative humidity for convective cooling

Unlike Fig. 5.7, the highest hourly temperature was recorded around 12:00 mid-day while the highest storage temperature was above 26 °C around 4PM for Fig. 5.4. The researcher observed that at 4PM, the sun light was directly facing the door of the storage chamber thereby sending direct sunlight into the storage chamber through the little openings around the door of the chamber. Fig. 5.9 also shows that an increase in ambient temperature leads to a decrease in ambient relative humidity. On the other hand, as the ambient temperature raises, the storage temperature also increased linearly with time especially during the morning hours and as it decreases, the storage temperature decreases while storage relative humidity increases. This situation is the validation of the principle of evaporative cooling.

5.1.3 Performance evaluation of the cooling chamber with evaporative cooling applied

The third set of data was collected when water was been applied along the walls of the storage chamber as ambient and storage data was recorded (Fig. 5.3). There was significance difference

between the ambient temperature and storage temperature on one hand and ambient relative humidity and storage relative humidity on the other hand. The experiment was carried out from March 6 - 13, 2020. The ambient data against storage data is presented in Fig. 5.10 for average daily temperature and average daily relative humidity from 8:00 AM to 6:00PM respectively.

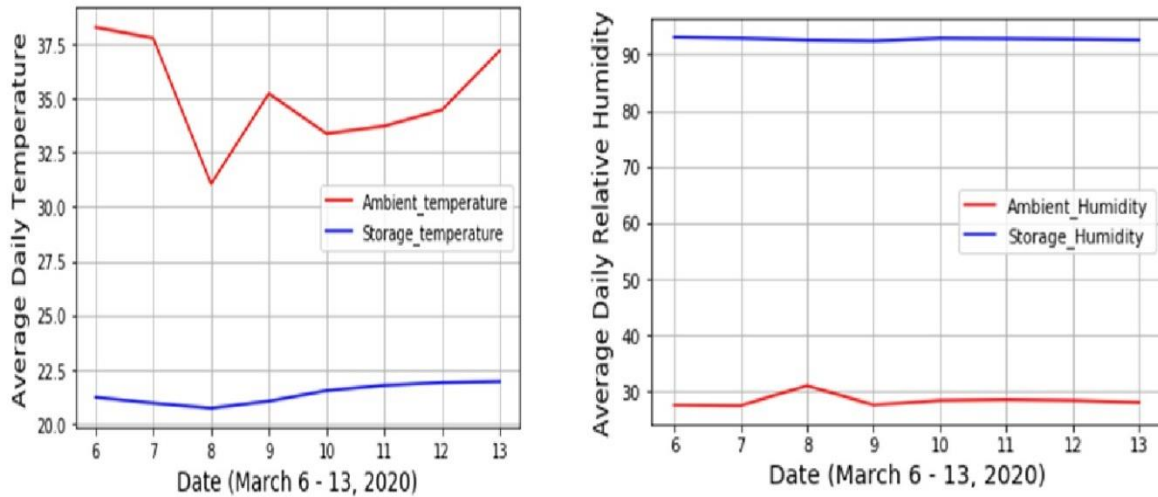


Figure 5.10 Trends of daily averages of temperature and relative humidity for evaporative cooling

Figure 5.10 shows that ambient temperature was quite different for each day. This difference in ambient temperature resulted in a corresponding change in ambient relative humidity (RH), thereby affecting the storage condition. The days with higher temperature saw a strong correlation with high solar radiation. The average ambient temperature as shown in Fig. 5.10 was 35.06 °C and the average ambient RH was 28.09%. Similarly, the storage temperature recorded from 8:00 Am to 6:00 PM ranged between 20 to 22.5°C and storage RH ranged from 91.78 to 92.94%. The average storage temperature and RH were 21.29 °C and 92.78 % respectively. A further 2.17 °C decreased in temperature and an increase 22% in relative humidity was due to evaporative cooling. The average temperature and RH difference were 13.77 °C and 64.69% respectively. The wet bulb temperature was determined from the psychrometric chart (21.1°C) and

the saturation efficiency was 98.6%. Figure 5.11 presents time changes in temperature and relative humidity from 8:00 AM to 6:00PM.

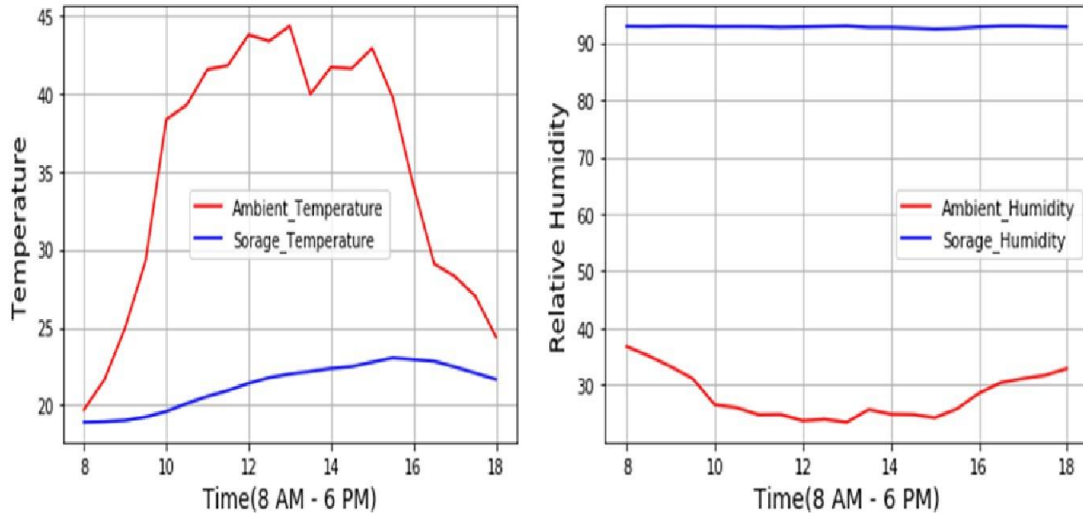


Figure 5.11 Trends of hourly averages of temperature and relative humidity for evaporative cooling

Unlike Fig. 5.9, the highest hourly temperature was recorded around 1PM (44 °C) and the lowest at 8AM. The highest storage temperature was above 23 °C around 3:30PM from Fig. 5.11. The researcher observed that around this time, the sun light was directly facing the door of the storage chamber thereby sending direct sunlight into the storage chamber through the little openings around the door of the chamber. Fig. 5.11 also shows that an increase in ambient temperature leads to a decrease in ambient RH. On the other hand, as the ambient temperature raises, the storage temperature also increased linearly with time especially during the morning hours and as it decreases, the storage temperature decreases while storage RH increases. This situation is the validation of the principle of evaporative cooling.

5.1.4 Performance evaluation of evapotranspiration cooling

The fourth set of data was collected when cowpeas were used as the source of evapotranspiration which were planted on top of the roof as ambient and storage data recorded (Fig. 5.4). There was significance difference between the ambient temperature and storage temperature on one hand and ambient relative humidity (RH) and storage RH on the other hand. However, there was a dropped in RH compared to evaporative cooling (EC). The test was carried out from March 20 - 26, 2020. The ambient data against storage data is presented in Fig. 5.12 for average daily temperature and average daily RH from 8:00 AM to 6:00PM respectively.

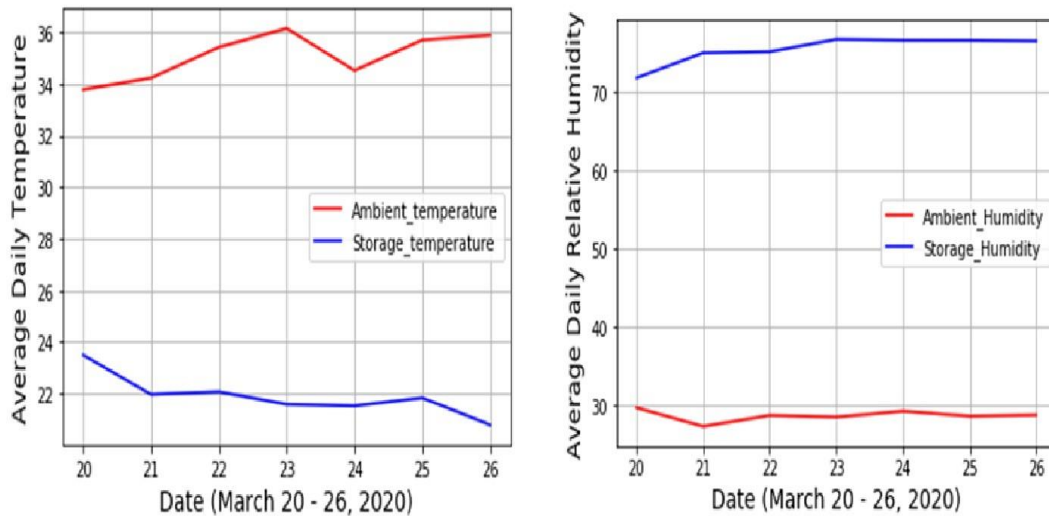


Figure 5.12 Trends of daily averages for temperature and relative humidity for evapotranspiration cooling

Figure 5.12 shows that ambient temperature was similar and varied between 33 and 37 °C from 8AM – 6PM during the period. This difference in ambient temperature resulted in a corresponding change in ambient RH, thereby affecting the storage condition. The days with higher temperature saw a strong correlation with high solar radiation. The average ambient temperature as shown in Fig. 5.12 was 35.14 °C and the average ambient RH was 27.99%. Similarly, the storage temperature recorded from 8:00 Am to 6:00 PM ranged from 18.6 to 23.94

°C and storage RH ranged from 74.16 to 76.87%. The average storage temperature and RH were 21.89 °C and 75.61 % respectively. A further 1.78 °C decreased in temperature and an increase 5.18% in RH was due to evapotranspiration cooling.

The average temperature and RH difference were 13.25 °C and 47.62% respectively. The wet bulb temperature was determined from the psychrometric chart (21.1°C) and the saturation efficiency was 94%. The data collection started nine days after the cowpeas were planted, at which time the crops average height was 0.3m and continued for seven days. By the end of the data collection, the crops average height was 0.8m. Figure 5.13 presents time changes in temperature and RH from 8:00 AM to 6:00PM.

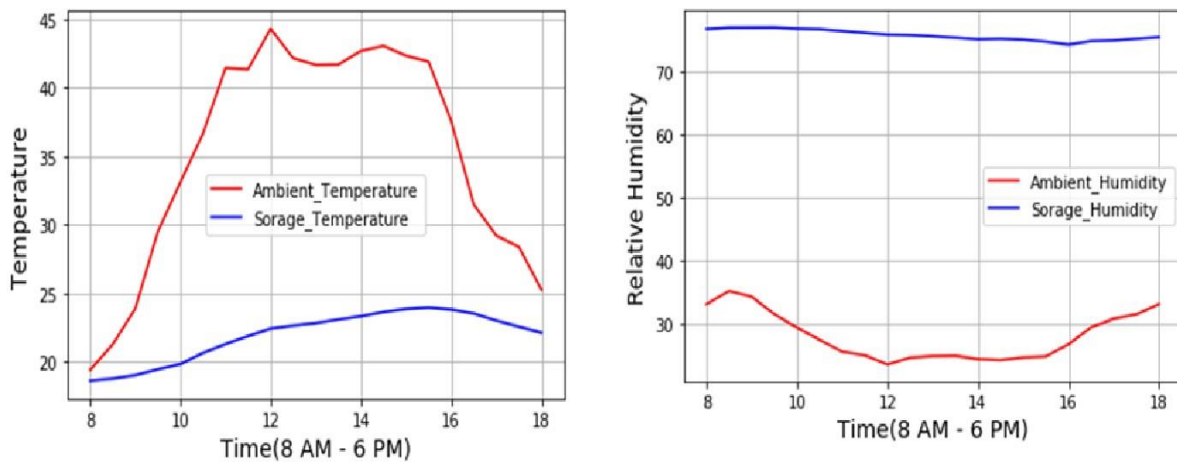


Figure 5.13 Trends of hourly averages of temperature and relative humidity for evapotranspiration cooling

Unlike Fig. 5.11, the highest hourly temperature was recorded around 12 noon (44 °C) and the lowest at 8AM. The highest storage temperature was above 23 °C around 3:30PM from Fig. 5.13. The researcher observed that around this time, the sun light was directly facing the door of the storage chamber thereby sending direct sunlight into the storage chamber through the little openings around the door of the chamber. Fig. 5.13 also shows that an increase in ambient

temperature leads to a decrease in ambient RH. On the other hand, as the ambient temperature raises, the storage temperature also increased linearly with time especially during the morning hours and as it decreases, the storage temperature decreases while storage relative humidity increases. This situation is the validation of the principle of EC and the relationship between temperature and RH (temperature raise leads to a decrease in relative humidity).

5.1.5 Performance evaluation of the cooling chamber with combined cooling

The final performance test for the no load storage chamber was conducted as a single system comprising of the previously discuss cooling methods. The data was collected when convective cooling, evaporative cooling, and evapotranspiration cooling where operated as a single unit data recorded (Fig. 5.5). There was significance difference between the ambient temperature and storage temperature on one hand and ambient relative humidity (RH) and storage RH on the other hand. The test was carried out from March 27 – April 6, 2020, from 8AM -6PM daily. The result of ambient data plotted against storage data is presented in Fig. 5.14 for average daily temperature and average daily RH from 8:00 AM to 6:00PM respectively.

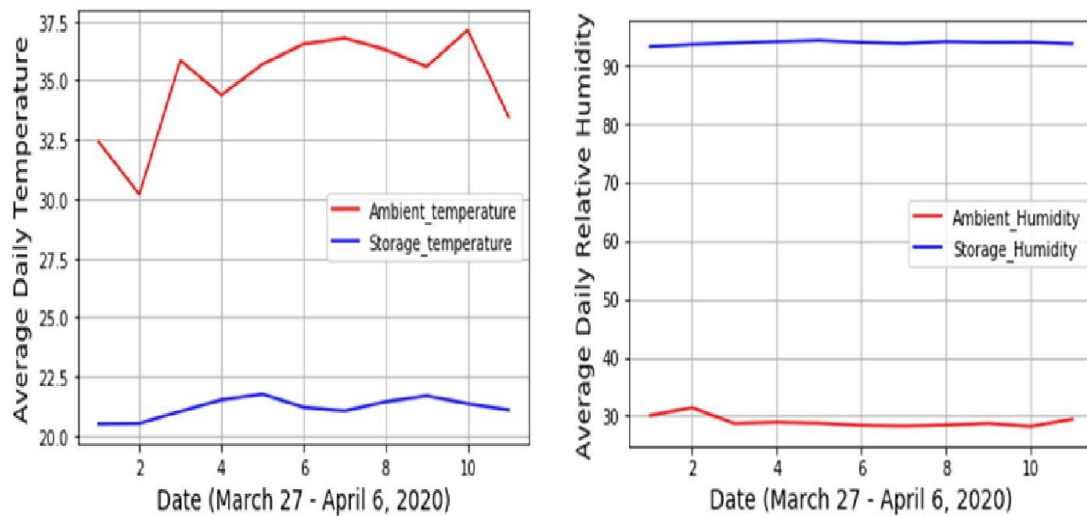


Figure 5.14 Trends of daily averages for temperature and relative humidity for combined cooling

Figure 5.14 shows that ambient temperature was quite different for each day and varied between 30 and 38 °C during the period. This difference in ambient temperature resulted in a corresponding change in ambient RH, thereby affecting the storage condition. The days with higher temperature saw a strong correlation with high solar radiation. The average ambient temperature as shown in Fig. 5.14 was 34.9 °C and the average ambient RH was 28.13%. Similarly, the storage temperature recorded from 8:00 Am to 6:00 PM each day ranged between 18.44 to 22.99 °C and storage RH ranged from 92.55 to 94.88%. The average storage temperature and relative humidity(T&RH) were 21.19 °C and 93.95 % respectively. A further 2.27 °C decreased in temperature and an increase 23.17% in relative humidity was due to the combined cooling. The average T&RH difference were 13.74 °C and 65.8% respectively. The wet bulb temperature was determined from the psychometric chart (21.1°C) and the saturation efficiency was 99%. Figure 5.15 presents time changes in T&RH from 8:00 AM to 6:00PM.

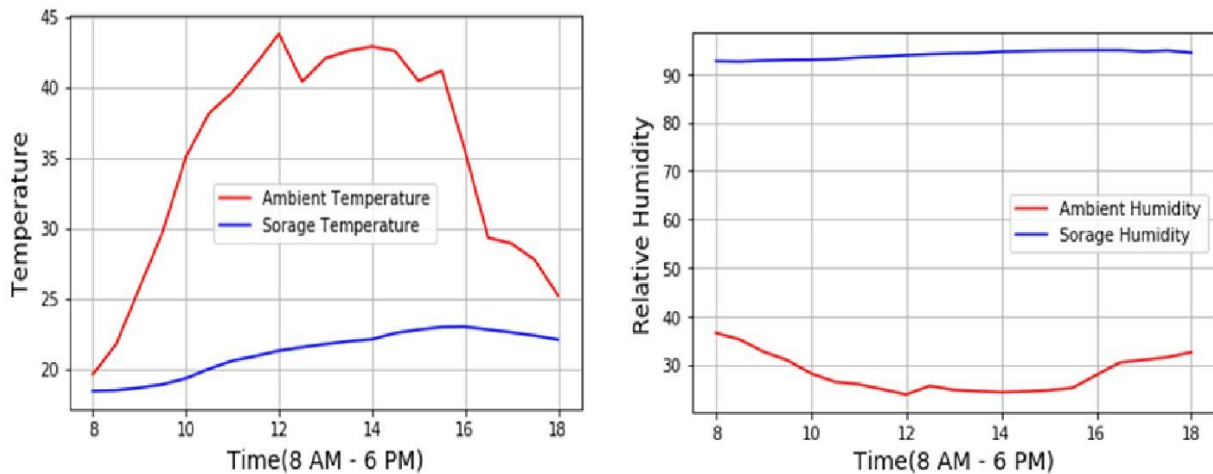


Figure 5.15 Trends of hourly averages of temperature and relative humidity for combined cooling

Figure 5.15 shows that the highest hourly ambient temperature was recorded around 12 noon (44 °C) and the lowest at 8AM. The highest storage temperature was above 23 °C around 4PM as shown in Fig. 5.15. The researcher observed that around this time, the sun light was directly facing the door of the storage chamber thereby sending direct sunlight into the storage chamber through the little openings around the door of the chamber. Fig. 5.15 also shows that an increase in ambient temperature leads to a decrease in ambient RH. On the other hand, as the ambient temperature raises, the storage temperature also increased linearly with time especially during the morning hours and as it decreases, the storage temperature decreases while storage relative humidity increases. This situation is the validation of the principle of evaporative cooling and the relationship between T&RH (temperature raise leads to a decrease in relative humidity).

5.1.6 Comparisons between the cooling methods

The performance evaluation of the cooling system was conducted by comparing storage chamber temperature and relative humidity (T&RH) conditions. The average daily storage T&RH within the pumice cooling chamber without the application of any cooling method were 23.46 °C and 70.78% respectively. The difference between ambient and storage temperature was 11.47 °C. The relative humidity (RH) was increase by 42.44% within the storage space compared to ambient RH. These differences in T&RH were because the storage chamber is a closed space with pumice walls forming the boundary between the ambient and storage space. Pumice is a light weighted fine grain volcanic rock categorized under sedimentary rock that contains pore spaces with good water retention quality. Therefore, pumice padding can humidify the hot ambient air and cools it before conveying it to the storage space. This test was necessary as to determine the cooling efficiency of pumice before endeavoring to evaluate the efficiency of the

different cooling methods. The result was used as the basis to measure the effect of each cooling method.

In the case of convective cooling, the storage T&RH difference between indirect cooling and when the fans were turn on was reported as 0.54 °C decrease and a 1.74% increase respectively. There was no significant change in storage conditions between no cooling and convective cooling. Therefore, the researcher recommends that the cooler must not be operated to store fruits and vegetables under the current design when supported with only convective cooling. This is because most fruits and vegetables are better preserved under at temperatures lower than 22 °C and RH above 85%.

As the chamber was operated on the principle of evaporation, the fans were turn off and water was supplied to the pumice. The storage T&RH difference between no cooling and evaporative cooling were 1.65 °C decrease and 21.95% increase respectively. This was a material difference compared to no cooling and convective cooling for both T&RH. Therefore, the researcher recommends that the storage chamber be operated as an evaporative cooler on a general level. However, it will be necessary to switch on the fans during extremely cold season to prevent condensation or freezing inside the chamber.

Similar difference for temperature was reported for evapotranspiration, but the storage RH was almost the same as convective cooling method. Therefore, in terms of temperature reduction, evapotranspiration was better than convective cooling. However, both methods did not meet the minimum benchmark of relative humidity for fruits and vegetables storage.

The differences in storage T&RH between no cooling method and combined systems were 2.45 °C decrease and 23.8% increase respectively. The combined cooling system presented a better storage condition for fruits and vegetables that can be used to meet its purpose in regions with

hot and dry climate. However, running the system as a single unit will increase the cost of operation. Giving the differences reported for both T&RH between evaporative cooling and combined system, and based on the cost benefit analysis, the researcher recommend evaporative cooling in general. The combined cooling system can be adapted for only special kind of fruits and vegetables storage.

Figure 5.16 presents all experimental data and further clarifies the explanations provided on Fig. 5.6 to 5.15

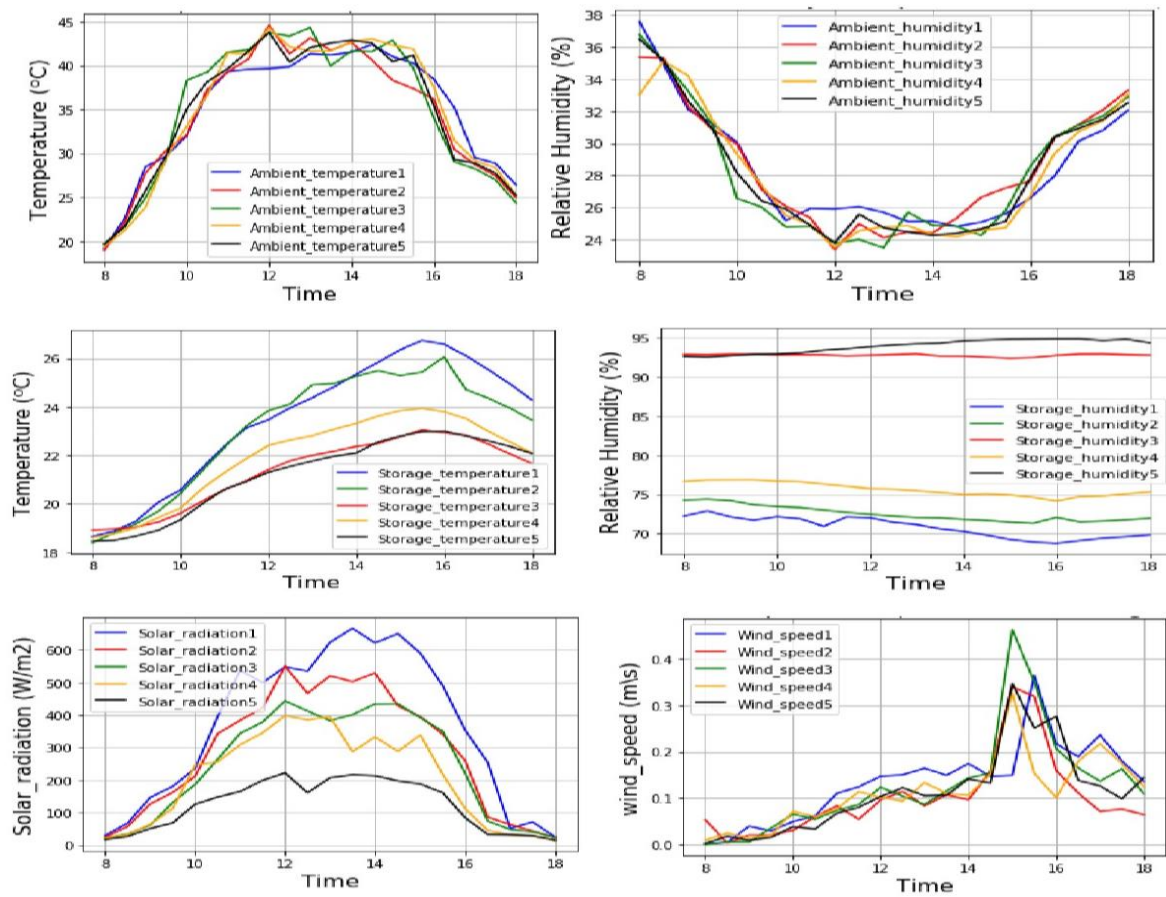


Figure 5.16 Trends of hourly changes for each measure variable in all instances.

5.2 Computational fluid dynamics modelling

5.2.1 The domain mesh

The automatic meshing method used in discretization of the geometry with the in-build ANSYS design modeler-meshing algorithm and set orthogonal quality and maximum skewness of 0.9 resulted into a refined mesh density consisting of 501,358 elements and 389,244 nodes. The minimum and maximum element size was 0.05m and 0.1m respectively.

5.2.2 The result mesh independence study

Mesh independence study was done to test validity and quality of discretization. This test was to ensure that the solution is accurate regardless of the mesh size. Six different mesh sizes were tested for temperature and mass flow rate with the first initial solution ran with 0.1m minimum and 0.2m maximum, which gave 97,638 elements and 25,298 nodes; then refined for the next solutions to 0.09m, 0.07m, 0.06m, 0.05m and 0.04m for minimum element sizes. Table 5.2 shows the simulation results for different mesh sizes used for the independent test before selecting 0.05 m. The simulation time was 4 to 8 hours, with over 3000 iterations before the solution converged on a HP Window 10 Pro LAPTOP-SCJFUG9 with processing capacity of AMD A8-7410 APU 2.20 GHZ and 64-bit operating system, X64-based HP Processor.

Table 5.1 Mesh independence test and results

No	Minimum element size (m)	Maximum element size (m)	Number of Nodes	Number of Elements	Mass (g/s)	Temperature (°C)
1	0.1	0.2	25,298	97,638	8.229	19.76
2	0.09	0.16	30,590	119,532	8.230	19.74
3	0.07	0.14	41,080	161,669	8.232	19.70
4	0.06	0.12	58,251	232,420	8.236	19.68
5	0.05	0.1	389,244	501,358	8.239	19.66
6	0.04	0.08	459,351	511,876	8.239	19.66

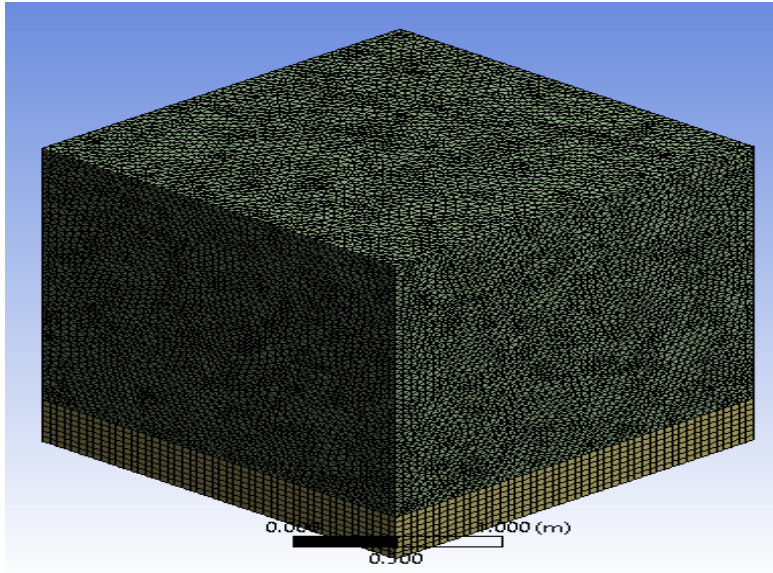


Figure 5.17 Mesh section of the computational model

5.3 Temperature predictions

This subsection presents the results from the modelled storage chamber. The result shows that the storage space temperature varied from 18.37 °C (291.52 °K) to 24.29 °C (297.44 °K) depending on the probe location and time. This result shows that the model output is much lower than the ambient temperature and with acceptable prediction of the storage temperature. Figure 5.18 shows the time average contours of temperature distribution across the storage space. The time average variation of temperature was mainly because of different boundary conditions that were considered during the model setup. The materials of paramount concern were given boundary conditions based on experimental data while others were set at no-slip condition. Because of the different material surfaces separating the storage space from either side of the cooler, these variations were on-avoidable.

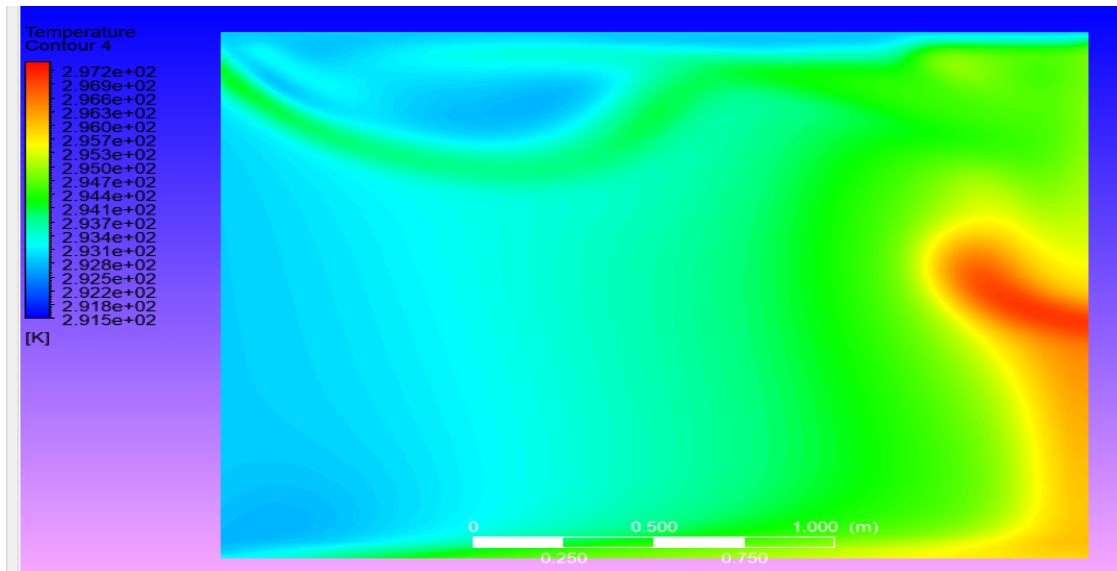


Figure 5.18 Predicted model temperature profile for steady state condition

5.4 Model validation

The validation of the model was conducted by comparing the experimental temperatures with the predicted temperatures, including measurement uncertainty. Table 5.2 shows experimental being compared with the modelling results. In general, the model shows a good level of prediction for air temperature distribution in the space.

Table 5.2 Experimental temperature and predicted temperature at 30 minutes interval from 8am to 6pm

Time	Average Ambient temperature	Average Storage temperature					Model predicted temperature
		Natural cooling	Convection	Evaporation	Transpiration	Combined technologies	
08:00	19.37	18.64	18.37	18.91	18.6	18.44	18.37
08:30	21.89	18.87	18.8	18.95	18.75	18.48	18.67
09:00	26.15	19.28	19.17	19.03	19	18.66	18.96
09:30	29.69	20.07	19.69	19.24	19.43	18.9	19.26
10:00	34.11	20.55	20.41	19.6	19.81	19.33	20.55
10:30	37.63	21.48	21.36	20.11	20.62	20	20.85

11:00	40.24	22.37	22.31	20.56	21.27	20.58	21.15
11:30	41.01	23.12	23.2	20.94	21.86	20.91	21.44
12:00	43.21	23.46	23.84	21.4	22.4	21.29	22.01
12:30	41.41	23.96	24.12	21.77	22.62	21.54	22.52
13:00	42.5	24.37	24.9	22	22.8	21.76	22.89
13:30	41.42	24.82	24.96	22.17	23.07	21.96	23.1
14:00	42.28	25.34	25.26	22.36	23.31	22.1	23.61
14:30	42.04	25.84	25.49	22.48	23.62	22.54	22.75
15:00	40.95	26.35	25.29	22.76	23.84	22.78	23.14
15:30	40.09	26.73	25.43	23.04	23.94	22.97	22.93
16:00	36.36	26.58	26.06	22.93	23.8	22.99	22.51
16:30	31.21	26.11	24.7	22.82	23.51	22.79	22.57
17:00	28.93	25.54	24.36	22.46	22.99	22.59	22.9
17:30	27.89	24.94	23.95	22.06	22.54	22.36	21.63
18:00	25.24	24.28	23.45	21.66	22.1	22.08	21.33

5.4.1 Natural cooling Vs.Model temperature

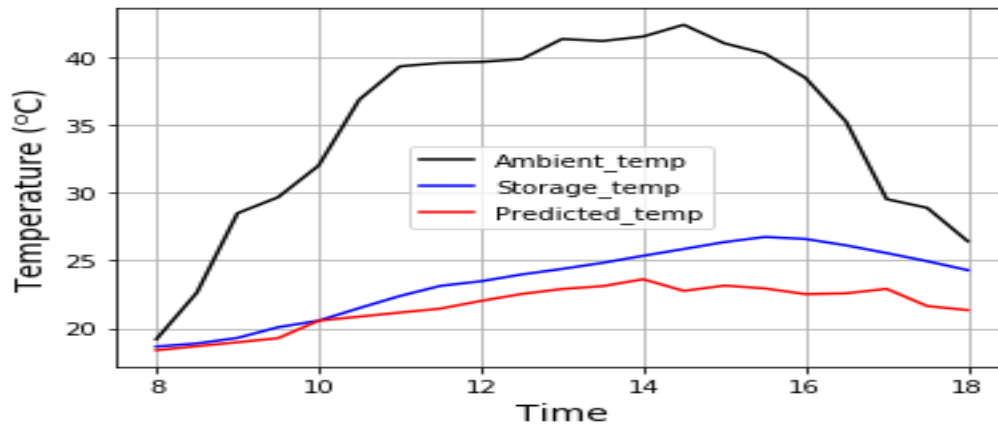


Figure 5.19 Comparison of ambient temperature, storage temperature, and model predicted temperature for no cooling

From the comparison between storage temperature for natural cooling method and model predicted temperature, the coefficient of determination, mean square error, root mean square error, and correlation were 0.88, 5.14, 2.34, and 0.86 respectively.

5.4.2 Convection cooling Vs.Model temperature

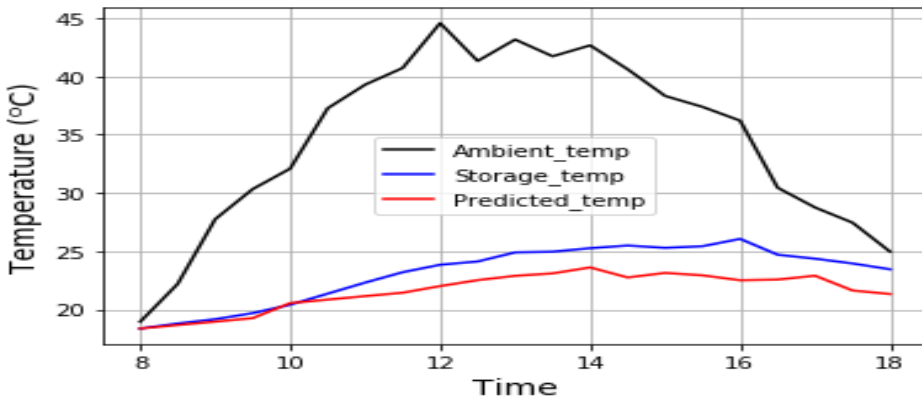


Figure 5.20 Comparison of ambient temperature, storage temperature, and model predicted temperature for convection cooling

From the comparison between storage temperature for convective cooling method and model predicted temperature, the coefficient of determination, mean square error, root mean square error, and correlation were 0.89, 3.3, 1.8, and 0.94 respectively.

5.4.3 Evaporative cooling Vs.Model temperature

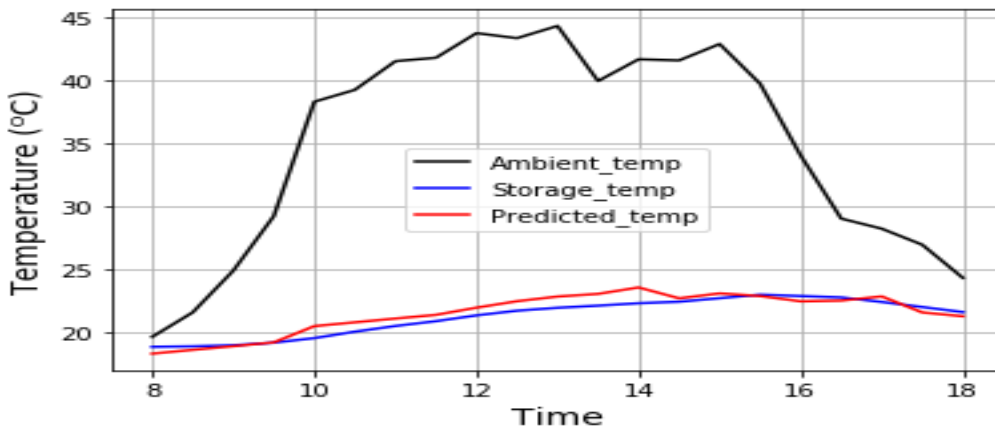


Figure 5.21 Comparison for ambient temperature, storage temperature, and model predicted temperature for evaporative cooling

From the comparison between storage temperature for evaporative cooling method and model predicted temperature, the coefficient of determination, mean square error, root mean square error, and correlation were 0.89, 0.36, 0.6, and 0.9 respectively.

5.4.4 Evapotranspiration cooling Vs. Model temperature

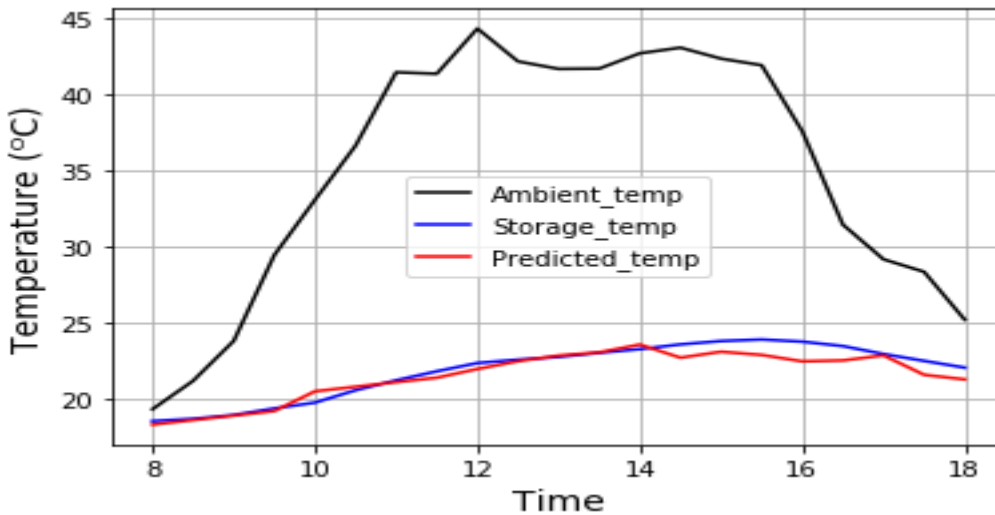


Figure 5.22 Comparison for ambient temperature, storage temperature, and model predicted temperature for evapotranspiration cooling

From the comparison between storage temperature for evapotranspiration cooling method and model predicted temperature, the coefficient of determination, mean square error, root mean square error, and correlation were 0.9, 0.35, 0.6, and 0.9 respectively.

5.4.5 Combined cooling Vs Model Temperature

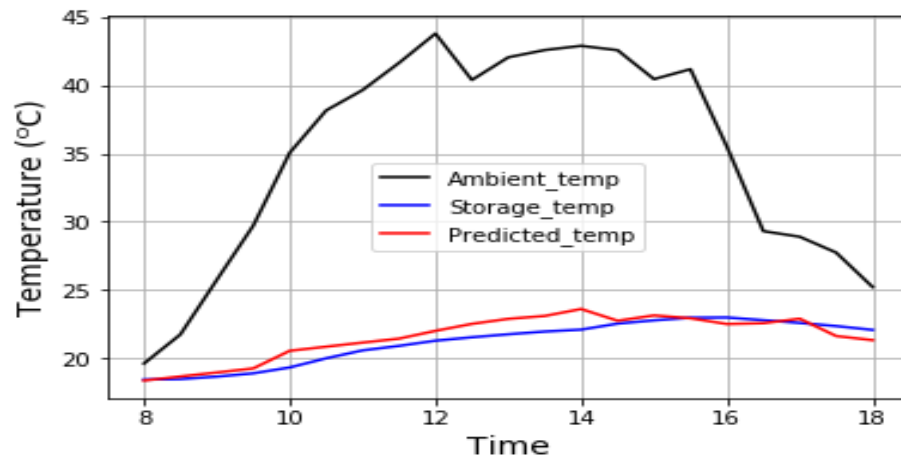


Figure 5.23 Comparison for ambient temperature, storage temperature, and model predicted temperature for combined cooling technologies

From the comparison between storage temperature for combined cooling method and model predicted temperature, the coefficient of determination, mean square error, root mean square error, and correlation were 0.85, 0.5, 0.7, and 0.8 respectively.

5.5 Storage optimization

The result of the simulation shows the pad thickness of 0.2m improved the cooling efficiency by 2% above the current design. Table 5.3 present the summary of the optimized evaporative cooling chamber based on cooling efficiency using the CFD model. The optimum point based on the single variable (pad thickness) optimization was 200mm. The dependent variable was the predicted temperature as all other parameters were held constant (water flow rate, velocity, and ambient temperature).

Table 5.3 Storage optimization based on pad thickness

No	Cooling pad (pumice) thickness (mm)	Water flow rate (l/min)	Air velocity (m/s)	Ambient temperatures (°C)	Predicted temperatures (°C)	Cooling efficiency (%)
1	50	1.75	0.6	34.93	23.1	71
2	100	1.75	0.6	34.93	21.89	80
3	150	1.75	0.6	34.93	21.19	83
4	200	1.75	0.6	34.93	20.29	85
5	250	1.75	0.6	34.93	20.29	85

5.5.1 Optimum pumice pad thickness

Figure 5.24 shows the changes in temperature inside the storage as result of change in pad thickness. The optimum point on the graph occurred at pad thickness of 200 mm that resulted to a storage temperature of 20.29 °C. When the pad thickness was increased to 250 mm, the model predicted was the same as the 200 mm pad thickness. The researcher conclusion on the optimum pad thickness was based on the single variable optimization method.

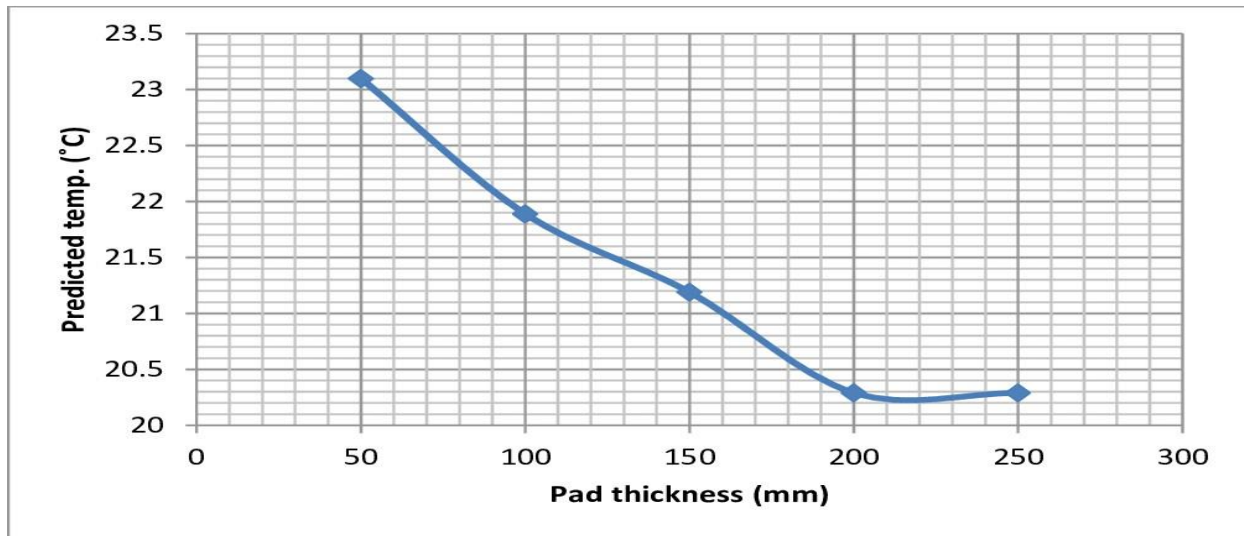


Figure 5. 24The plot showing the optimum pad thickness

CHAPTER SIX

CONCLUSIONS AND RECOMMENDATIONS

6.1 Conclusion

The primary objective of this study was to evaluate the performance of the evaporative cooling (EC) system and provide both energy savings and better thermal control in the storage space with an optimized computational fluid dynamics (CFD) model. The experimental investigation carried out on the storage chamber provided a clearer understanding on the temperature and relative humidity (T&RH) distribution at different times of the day. The storage T&RH were driven by ambient conditions.

The performance evaluation of the cooling system was conducted by comparing storage chamber T&RH conditions. The average daily storage T&RH within the pumice cooling chamber without the application of any cooling method were 23.46 °C and 70.78% respectively. The difference between ambient and storage temperature was 11.47 °C. The storage relative humidity (RH) was increase by 42.44% compared to ambient RH. In the case of convective cooling, the storage T&RH difference between no cooling and when fans were turn on was 0.54 °C lower and a 1.74% increase respectively.

The storage temperature and relative humidity difference between natural cooling and EC were 1.65 °C lower and 21.95% higher respectively. This was a material difference compared to no cooling and convective cooling for both T&RH.

Similar difference for temperature was reported for evapotranspiration, but the storage RH was almost the same as convective cooling method. Therefore, in terms of temperature reduction, evapotranspiration was better than convective cooling. However, both methods did not meet the minimum benchmark of RH for fruits and vegetables storage.

The differences in storage T&RH between no cooling method and combined systems were 2.45 °C lower and 23.8% increase respectively. The combined cooling system presented a better storage condition for fruits and vegetables that can be used to meet its purpose in regions with hot and dry climate. However, running the system as a single unit will increase the cost of operation. The combined cooling system can be adapted for only special kind of fruits and vegetables storage.

Findings of this study show that the evaporative cooling chamber can effectively be used by local farmers in Kenya to reduce postharvest losses (PHL). However, prospective users should consider suitability of the storage chamber for specific use as the cooler is not appropriate for the storage of fruits and vegetables that are to be stored under temperature below 15 °C. Therefore, to promote the usage of this technology, there must be awareness on benefits and suitability, identify specific end user, increased availability of appropriate designed types, and affordability in regions with average daily temperature above 25 °C across Kenya.

The integrated CFD model is a powerful tool that can be used to design an optimum energy efficient air distribution system without compromising food quality. The three-dimensional Computational Fluid Dynamics (CFD) was developed and predicted the storage temperature with minimum error. The model was optimized using a single variable optimization method by changing the pad thickness. The optimum point based on pad thickness optimization was 200mm. The experimental results and the model predicted temperature show a strong correlation, with a high coefficient of determination and a low root mean square error. These results implied that the model was reliable in predicting the storage temperature. The prototype requirements from this study show that the alternate material should have a good water retention and circulation quality like pumice.

6.2 Recommendations

The researcher recommends that the storage chamber be operated as an evaporative cooler on a general level because of cost benefits analysis. However, it will be necessary to switch on the fans during extremely cold season to prevent condensation or freezing inside the chamber. The researcher also recommends that the cooler must not be operated to store fruits and vegetables under the current design when supported with only convective cooling or evapotranspiration cooling only. This is because most fruits and vegetables are better preserved under at temperatures lower than 22 °C and relative humidity above 85%.

6.3 Future work

Future work needs to be done to arrive at an ideal air distribution system in terms of material selection, cost reduction and ease of retrofit for rollout to fresh produce storage facilities. Alternative materials that can provide similar storage temperature and relative humidity need to be identified. In addition, the design and development of an air distribution prototype that can be installed in the monitored storage facility can be look at in future.

References

- Ahmed, E. M., Abaas, O., Ahmed, M., & Ismail, M. R. (2011). Performance evaluation of three different types of local evaporative cooling pads in greenhouses in Sudan. *Saudi journal of biological sciences*, 18(1), 45-51
- Akdemir, S., Ozturk, S., Edis, F. O., & Bal, E. (2013). CFD Modelling of two different cold stores ambient factors. *IERI Procedia*, 5, 28-40.
- Allen, R. G., Pereira, L. S., Raes, D., & Smith, M. (1998). Crop evapotranspiration-Guidelines for computing crop water requirements-FAO Irrigation and drainage paper 56. *Fao, Rome*, 300(9), D05109.
- Allouche, Y., Varga, S., Bouden, C., & Oliveira, A. C. (2017). Dynamic simulation of an integrated solar-driven ejector-based air conditioning system with PCM cold storage. *Applied energy*, 190, 600-611.
- Al-Sulaiman, F. (2002). Evaluation of the performance of local fibers in evaporative cooling. *Energy conversion and management*, 43(16), 2267-2273.
- Alves, J. L. F., da Silva, J. C. G., da Silva Filho, V. F., Alves, R. F., de Araujo Galdino, W. V., & De Sena, R. F. (2019). Kinetics and thermodynamics parameters evaluation of pyrolysis of invasive aquatic macrophytes to determine their bioenergy potentials. *Biomass and bioenergy*, 121, 28-40.
- Ambaw, A., Delele, M. A., Defraeye, T., Ho, Q. T., Opara, L. U., Nicolăi, B. M., & Verboven, P. (2013). The use of CFD to characterize and design post-harvest storage facilities: Past, present and future. *Computers and Electronics in Agriculture*, 93, 184-194.
- Andersson, M., Yuan, J., & Sundén, B. (2012). SOFC modeling considering electrochemical reactions at the active three phase boundaries. *International journal of heat and mass transfer*, 55(4), 773-788
- Ansys, H. F. S. S. "High frequency electromagnetic field simulation." *Retrieved from* (2019)
- Arah, I. K., Kumah, E. K., Anku, E. K., & Amaglo, H. (2015). An overview of post-harvest losses in tomato production in Africa: causes and possible prevention strategies. *Journal of Biology, Agriculture and Healthcare*, 5(16), 78-88.
- Balogun, A. A., & Ariahu, C. C. (2020). Quality Evaluation of African Eggplant Stored in Evaporative Coolers. *Asian Food Science Journal*, 23-33.
- Balogun, A. A., Ariahu, C. C., & Ikya, J. K. (2019). Quality evaluation of fresh tomato stored in evaporative coolers. *Asian Food Science Journal*, 1-8.
- Bergougnoux, V. (2014) The history of tomato from domestication to biopharming Biotechnology advances, 32(1), 170-189
- Boyd, C. E. (2019). *Water quality: an introduction*. Springer Nature.

- Bradford, K. J., Dahal, P., Van Asbrouck, J., Kunusoth, K., Bello, P., Thompson, J., & Wu, F. (2018) The dry chain: Reducing postharvest losses and improving food safety in humid climates. *Trends in Food Science & Technology*, 71, 84-93.
- Carrier, O., Shahidzadeh-Bonn, N., Zargar, R., Aytouna, M., Habibi, M., Eggers, J., & Bonn, D. (2016). Evaporation of water: evaporation rate and collective effects. *Journal of Fluid Mechanics*, 798, 774-786.
- Cheng, W. L., Chen, H., Hu, L., & Zhang, W. W. (2015). Effect of droplet flash evaporation on vacuum flash evaporation cooling: modeling. *International Journal of Heat and Mass Transfer*, 84, 149-157.
- Chicco, D., Warrens, M. J., & Jurman, G. (2021). The coefficient of determination R-squared is more informative than SMAPE, MAE, MAPE, MSE and RMSE in regression analysis evaluation. *PeerJ Computer Science*, 7, e623.
- de Oliveira Alves Sena, E., de Oliveira Silva, P. S., de Araujo Couto, H. G. S., Gonçalves Júnior, D. H., de Aragão Batista, M. C., Nogueira Matos, P., ... & Gutierrez Carnellosi, M. A. (2019). Hydrocooling on the shelf-life quality of cashew apples. *Postharvest biology and technology*.
- Defraeye, T. (2014) Advanced computational modelling for drying processes—A review *Applied Energy*, 131, 323-344
- Dhakulkar, K. T., Hinge, M. V., Kolhe, M. S., Chaudhari, M. R., & Mahalle, M. S. (2018). An experimental analysis of direct evaporative cooler by changing its cooling pads. *International Research Journal of Engineering and Technology (IRJET)*, 5(5), 292-299.
- Dhande, D. Y., & Pande, D. W. (2018). Multiphase flow analysis of hydrodynamic journal bearing using CFD coupled fluid structure interaction considering cavitation. *Journal of King Saud University-Engineering Sciences*, 30(4), 345-354
- Ding T, Alves W A L, Araújo S A, Santana J C C, Ling J G, Chen J C, et al. Simulation approach for optimal design of vacuum cooling on broccoli by simulated annealing technique. *International Journal of Agricultural and Biological Engineering*, 2014; 7(5): 111–115.
- Doğramacı, P. A., & Aydın, D. (2020). Comparative experimental investigation of novel organic materials for direct evaporative cooling applications in hot-dry climate. *Journal of Building Engineering*, 30, 101240.
- Duan, L. B., Zhao, X. R., Liu, J. M., Geng, W. C., Xie, H. Y., & Sun, H. N. (2012). Effect of annealing ambient on the structural, optical and electrical properties of (Mg, Al)-codoped ZnO thin films. *Physica Scripta*, 85(3), 035709
- Duan, Z., Zhan, C., Zhao, X., & Dong, X. (2016). Experimental study of a counter-flow regenerative evaporative cooler. *Building and Environment*, 104, 47-58.

- Duret, S., Hoang, H. M., Flick, D., & Laguerre, O. (2014). Experimental characterization of airflow, heat and mass transfer in a cold room filled with food products. *International journal of refrigeration*, 46, 17-25.
- Elsisi, S. F., Taha, A. T., & Omar, M. N. (2020). Cucumber Hydrocooling Treatment and its Relationship to Quality Properties during Cold Storage. *Journal of Soil Sciences and Agricultural Engineering*, 11(9), 521-528.
- El-Ramady, H. R., Domokos-Szabolcsy, É., Abdalla, N. A., Taha, H. S., & Fári, M. (2015). Postharvest management of fruits and vegetables storage. In *Sustainable agriculture reviews* (pp. 65-152). Springer, Cham.
- França, C. F., Ribeiro, W. S., Silva, F. C., Costa, L. C., Rêgo, E. R., & Finger, F. L. (2015). Hydrocooling on postharvest conservation of butter lettuce. *Horticultura brasileira*, 33, 383-387.
- Franke, J., & Frank, W. (2008) Application of generalized Richardson extrapolation to the computation of the flow across an asymmetric street intersection *Journal of Wind Engineering and Industrial Aerodynamics*, 96(10-11), 1616-1628
- Getahun, S., Ambaw, A., Delele, M., Meyer, C. J., & Opara, U. L. (2017). Analysis of airflow and heat transfer inside fruit packed refrigerated shipping container: Part I–Model development and validation. *Journal of food engineering*, 203, 58-68.
- Goldstein, E. A., Raman, A. P., & Fan, S. (2017). Sub-ambient non-evaporative fluid cooling with the sky. *Nature Energy*, 2(9), 1-7.
- Griggs, D., Stafford-Smith, M., Gaffney, O., Rockström, J., Öhman, M. C., Shyamsundar, P., ...& Noble, I. (2013). Sustainable development goals for people and planet. *Nature*, 495(7441), 305-307.
- Gunhan, T. U. N. C. A. Y., Demir, V. E. D. A. T., & Yagcioglu, A. K. (2007). Evaluation of the suitability of some local materials as cooling pads. *Biosystems engineering*, 96(3), 369-377.
- Hasan, A. (2012). Going below the wet-bulb temperature by indirect evaporative cooling: analysis using a modified ϵ -NTU method *Applied energy*, 89(1), 237-245.
- Islam, M. P., Morimoto, T., & Hatou, K (2013) Dynamic optimization of inside temperature of Zero Energy Cool Chamber for storing fruits and vegetables using neural networks and genetic algorithms. *Computers and electronics in agriculture*, 95, 98-107
- James, A., & Zikankuba, V. (2017) Postharvest management of fruits and vegetable: A potential for reducing poverty, hidden hunger and malnutrition in sub-Saharan Africa. *Cogent Food & Agriculture*, 3(1), 1312052. <https://doi.org/10.1080/23311932.2017.1312052>
- Kadiyala, A., & Kumar, A. (2017). Applications of python to evaluate environmental data science problems. *Environmental Progress & Sustainable Energy*, 36(6), 1580-1586.

- Kajishima, T., & Taira, K. (2017). Numerical simulation of turbulent flows. In *Computational Fluid Dynamics* (pp. 207-235) Springer, Cham
- Kapilan, N., Gowda, M. M., & Manjunath, H. N. (2016) Computational Fluid Dynamics Analysis of an Evaporative Cooling System *Strojnickýčasopis-Journal of Mechanical Engineering*, 66(2), 117-124
- Karithi, E. M. (2016). *Evaluation of the efficacy of coolbot™ cold storage technology to preserve quality and extend shelf life of mango fruits* (Doctoral dissertation, University of Nairobi)
- Khond, V. W. (2011). Experimental investigation of desert cooler performance using four different cooling pad materials. *American journal of scientific and industrial research*, 2(3), 418-421.
- .Kipruto, K. M. (2017). Effect of near infrared reflection and evaporative cooling on quality of mangoes *Agricultural Engineering International: CIGR Journal*, 19(1), 162-168
- Kitinoja, L. (2013) Use of cold chains for reducing food losses in developing countries. *Population*, 6(1.23), 5-60
- Krishnakumar, K., & Goldberg, D. E. (1992) Control system optimization using genetic algorithms *Journal of Guidance, Control, and Dynamics*, 15(3), 735-740
- Kitinoja, L., & Kader, A. A. (2015) Measuring postharvest losses of fresh fruits and vegetables in developing countries *Postharvest Education Foundation*, 1-26
- Kituu, G. M., Korir, M. K., Mutwiwa, U., & Sila, D. N. (2014). Development of a computer model simulation for predicting the performance of a near infrared reflecting charcoal cooler for on farm storage of mangoes
- Kumar, D., & Kalita, P. (2017) Reducing postharvest losses during storage of grain crops to strengthen food security in developing countries *Foods*, 6(1), 8
- Kumar, R., Chandra, S., Samsher, B. S., Kumar, R., & Kumar, A. A. (2018). Zero energy cool chamber for food commodities: Need of eco-friendly storage facility for farmers: A review. *Journal of Pharmacognosy and Phytochemistry*, 7(5), 2293-2301
- Langlands, T. A. M., & Henry, B. I. (2005). The accuracy and stability of an implicit solution method for the fractional diffusion equation. *Journal of Computational Physics*, 205(2), 719-736.
- Liberty, J. T., Ugwuishiwu, B. O., Pukuma, S. A., & Odo, C. E. (2013) Principles and application of evaporative cooling systems for fruits and vegetables preservation *International Journal of Current Engineering and Technology*, 3(3), 1000-1006
- Liu, H., Zhou, Q., Liu, Y., Wang, P., & Wang, D. (2015) Experimental study on cooling performance of air conditioning system with dual independent evaporative condenser *International journal of refrigeration*, 55, 85-92.

- Luo, Y., Yang, H., Lu, L., & Qi, R. (2014) A review of the mathematical models for predicting the heat and mass transfer process in the liquid desiccant dehumidifier *Renewable and Sustainable Energy Reviews*, 31, 587-599
- Mahabir, R., Stefanidis, A., Croitoru, A., Crooks, A. T., & Agouris, P. (2017) Authoritative and volunteered geographical information in a developing country: A comparative case study of road datasets in Nairobi, Kenya. *ISPRS International Journal of Geo-Information*, 6(1) 24
- Manyozo, F. N., Ambuko, J., Hutchinson, M. J., & Kamanula, J. F. (2018) Effectiveness of evaporative cooling technologies to preserve the postharvest quality of tomato *International Journal of Agronomy and Agricultural Research*, 13, 114-127.
- Menter, F. R. (1994). Two-equation eddy-viscosity turbulence models for engineering applications. *AIAA journal*, 32(8), 1598-1605.
- Mishra, P., & Aharwal, K. R. (2018, August) A review on selection of turbulence model for CFD analysis of air flow within a cold storage In IOP Conference Series: Materials Science and Engineering (Vol. 402, No. 1, p. 012145) IOP Publishing
- Misra, D., & Ghosh, S. (2018). Evaporative cooling technologies for greenhouses: a comprehensive review. *Agricultural Engineering International: CIGR Journal*, 20(1), 1-15.
- Montazeri, H., Blocken, B., & Hensen, J. L. M. (2015) Evaporative cooling by water spray systems: CFD simulation, experimental validation and sensitivity analysis. *Building and environment*, 83, 129-141
- Mordi, J. I., & Olorunda, A. O. (2003) Effect of evaporative cooler environment on the visual qualities and storage life of fresh tomatoes *Journal of food science and technology (Mysore)*, 40(6), 587-591
- Munang, R. T., Thiaw, I., & Rivington, M. (2011). Ecosystem management: Tomorrow's approach to enhancing food security under a changing climate. *Sustainability*, 3(7), 937-954.
- Musa, M. K., & Odera, P. A. (2015). Land use land cover changes and their effects on agricultural land a case study of Kiambu County Kenya.
- Nahor, H. B., Hoang, M. L., Verboven, P., Baelmans, M., & Nicolai, B. M. (2005) CFD model of the airflow, heat and mass transfer in cool stores *International Journal of Refrigeration*, 28(3), 368-380.
- Norton, T., & Sun, D. W. (2006). Computational fluid dynamics (CFD)—an effective and efficient design and analysis tool for the food industry: a review. *Trends in Food Science & Technology*, 17(11), 600-620.
- Putra, N., Roetzel, W., & Das, S. K. (2003). Natural convection of nano-fluids. *Heat and mass transfer*, 39(8), 775-784.

- Ridolfi, C., Hoffman, V., & Baral, S. (2018). *Post-harvest losses: Global scale, solutions, and relevance to Ghana*. Intl Food Policy Res Inst.
- Reynolds, O. (1895). IV. On the dynamical theory of incompressible viscous fluids and the determination of the criterion. *Philosophical transactions of the royal society of london.(a.)*, (186), 123-164.
- Rosegrant, M. W., Magalhaes, E., Valmonte-Santos, R. A., & Mason-D'Croz, D. (2018) Returns to investment in reducing postharvest food losses and increasing agricultural productivity growth Prioritizing development: A cost benefit analysis of the United Nations' sustainable development goals, 322-338
- Roy, S. K., & Pal, R. K. (1989, September) A low cost zero energy cool chamber for short term storage of mango. In III International Mango Symposium 291 (pp. 519-524).
- Schymanski, S. J., & Or, D. (2017). Leaf-scale experiments reveal an important omission in the Penman–Monteith equation. *Hydrology and Earth System Sciences*, 21(2), 685-706.
- Sena, E. D. O. A., da Silva, P. S. O., de Aragão Batista, M. C., Sargent, S. A., de Oliveira Junior, L. F. G., Pagani, A. A. C., & Carnelossi, M. A. G. (2019). Calcium application via hydrocooling and edible coating for the conservation and quality of cashew apples *Scientia Horticulturae* 256, 108531.
- Shahali, P., Rahmati, M., Alavi, S. R., & Sedaghat, A. (2016). Experimental study on improving operating conditions of wet cooling towers using various rib numbers of packing. *International journal of refrigeration*, 65, 80-91.
- She, X., Cong, L., Nie, B., Leng, G., Peng, H., Chen, Y & Luo, Y. (2018). Energy-efficient and-economic technologies for air conditioning with vapor compression refrigeration: A comprehensive review. *Applied Energy*, 232, 157-186.
- She, X., Wu, J., Xu, H., Zhong, J., Wang, Y., Song, Y. & Vajtai, R. (2017) High Efficiency Photocatalytic Water Splitting Using 2D α -Fe₂O₃/g-C₃N₄ Z-Scheme Catalysts *Advanced Energy Materials*, 7(17), 1700025
- Singh, A. K., & Paul, T. (2006). Transient natural convection between two vertical walls heated/cooled asymmetrically. *International Journal of Applied Mechanics and Engineering*, 11(1), 143-154.
- Singh, K., & Das, R. (2017). Simultaneous optimization of performance parameters and energy consumption in induced draft cooling towers. *Chemical Engineering Research and Design*, 123, 1-13.
- Singh, S., Khemariya, P., Rai, A., Rai, A. C., Koley, T. K., & Singh, B. (2016). Carnauba wax-based edible coating enhances shelf-life and retain quality of eggplant (*Solanum melongena*) fruits. *LWT*, 74, 420-426.

- Sohani, A., Sayyaadi, H., & Hoseinpoori, S. (2016). Modeling and multi-objective optimization of an M-cycle cross-flow indirect evaporative cooler using the GMDH type neural network *International Journal of Refrigeration*, 69, 186-204.
- Sow, I., Murimi, E., & Mutwiwa, U. (2020). Evaporative Cooler Climate Prediction using Artificial Neural Network. *JOURNAL OF SUSTAINABLE RESEARCH IN ENGINEERING*, 5(3), 113-127.
- Sultan, M., Miyazaki, T., & Koyama, S. (2018) Optimization of adsorption isotherm types for desiccant air-conditioning applications. *Renewable Energy*, 121, 441-450.
- Taira, K., Brunton, S. L., Dawson, S. T., Rowley, C. W., Colonius, T., McKeon, B. J., ...& Ukeiley, L. S. (2017). Modal analysis of fluid flows: An overview. *Aiaa Journal*, 55(12), 4013-4041.
- Tijsskens, L. M. M., Greiner, R., Biekman, E. S. A., & Konietzny, U. (2001). Modeling the effect of temperature and pH on activity of enzymes: the case of phytases *Biotechnology and bioengineering*, 72(3), 323-330.
- Tolesa, G. N. (2018a). Modelling of micro-environment inside evaporatively and coolbot cooled stores using computational fluid dynamics models and changes in quality of stored tomatoes (Doctoral dissertation, University of KwaZulu-Natal Pietermaritzburg South Africa).
- Tolesa, G. N., & Workneh, T. S. (2017b). Influence of storage environment, maturity stage and pre-storage disinfection treatments on tomato fruit quality during winter in KwaZulu-Natal, South Africa. *Journal of food science and technology*, 54(10), 3230-3242
- Tolesa, G. N., & Workneh, T. S. (2017, September) Effects of evaporative cooling and CoolBot air conditioning on changes in the environmental conditions inside the cooling chamber In *VII International Conference on Managing Quality in Chains (MQUIC2017) and II International Symposium on Ornamentals in 1201* (pp. 281-288)
- Vala, K. V., Kumpavat, M. T., & Nema, A. (2016). Comparative performance evaluation of evaporative cooling local pad materials with commercial pads. *International Journal of Engineering Trends and Technology*, 39(4), 198-203.
- Vala, K. V., Makwana, M., & Sagarika N. (2019) Validation of Evaporative Cooling System using CFD Analysis *Int. J. Curr. Microbiol App. Sci*, 8(3), 393-399
- Vala, K. V., Saiyed, F., & Joshi, D. C. (2014) Evaporative cooled storage structures: an Indian scenario. *Trends in Post Harvest Technology*, 2(3), 22-32
- Versteeg, H. K., & Malalasekera, W. (2007) An introduction to computational fluid dynamics: the finite volume method. Pearson education
- Yadav, A. S., & Bhagoria, J. L. (2013). Heat transfer and fluid flow analysis of solar air heater: A review of CFD approach. *Renewable and Sustainable Energy Reviews*, 23, 60-79.

- Yanhua, L., Enli, L., Rahman, M. M., Yu, W., Jiaming, G., &Jie, Z. (2017). Numerical simulation of temperature and relative humidity in zero energy cool Chamber International Journal of Agricultural and Biological Engineering, 10(3), 185-193.
- Zhang, L., Dang, C., &Hihara, E. (2010) Performance analysis of a no-frost hybrid air conditioning system with integrated liquid desiccant dehumidification International journal of refrigeration, 33(1), 116-124